ÇUKUROVA UNIVERSITY
INSTITUTE OF NATURAL AND APPLIED SCIENCES

PhD THESIS

Hamed KAGHAZCHI

FINITE ELEMENT INVESTIGATION OF THE EFFECT OF CONDUCTIVITY CHANGES IN ISCHEMIC HEART TISSUE ON ELECTROCARDIOGRAPHY

DEPARTMENT OF ELECTRICAL AND ELECTRONICS ENGINEERING

ADANA-2019

ÇUKUROVA UNIVERSITY
INSTITUTE OF NATURAL AND APPLIED SCIENCES

FINITE ELEMENT INVESTIGATION OF THE EFFECT OF CONDUCTIVITY CHANGES IN ISCHEMIC HEART TISSUE ON ELECTROCARDIOGRAPHY

Hamed KAGHAZCHI

PhD THESIS

DEPARTMENT OF ELECTRICAL AND ELECTRONICS ENGINEERING

We certify that the thesis titled above was reviewed and approved for the award of degree of the Doctor of Philosophy by the board of jury on 10/06/2019.

…….	……	……..……....
Assoc. Prof. Dr. M. Kerem ÜN	Prof. Dr. Ulus ÇEVİK	Assoc. Prof. Dr. Ahmet ÇALIK
SUPERVISOR	MEMBER	MEMBER
……	……	
Asst. Prof. Dr. Ahmet AYDIN	Asst. Prof. Dr. Emine AVŞAR AYDIN	
MEMBER	MEMBER	

This PhD Thesis is written at the Department of Electrical and Electronics Engineering of Institute of Natural And Applied Sciences of Çukurova University.
Registration Number:

Prof. Dr. Mustafa GÖK
Director
Institute of Natural and Applied Sciences

Note: The usage of the presented specific declerations, tables, figures, and photographs either in this thesis or in any other reference without citiation is subject to "The law of Arts and Intellectual Products" number of 5846 of Turkish Republic.

ABSTRACT

PhD THESIS

FINITE ELEMENT INVESTIGATION OF THE EFFECT OF CONDUCTIVITY CHANGES IN ISCHEMIC HEART TISSUE ON ELECTROCARDIOGRAPHY

Hamed KAGHAZCHI

ÇUKUROVA UNIVERSITY
INSTITUTE OF NATURAL AND APPLIED SCIENCES
DEPARTMENT OF ELECTRICAL AND ELECTRONICS ENGINEERING

Supervisor : Assoc. Prof. Dr. Mustafa Kerem ÜN
Year: 2019, Pages: 125
Jury : Assoc. Prof. Dr. Mustafa Kerem ÜN
: Prof. Dr. Ulus ÇEVİK
: Assoc. Prof. Dr. Ahmet ÇALIK
: Asst. Prof. Dr. Ahmet AYDIN
: Asst. Prof. Dr. Emine AVŞAR AYDIN

Electrocardiography (ECG) is a common diagnostic tool based on reading potentials on human torso and make deductions about the heart health. Many quasi-static numerical studies exist in the literature that tackle forward and inverse problem of ECG. While the abnormal transmembrane potential of the ischemic tissue is taken into account in these studies, the decreased conductivity due to this pathology has been largely ignored. In the first part of this study, we have investigated numerically the effect of ischemic conductivities on the torso potentials, and the effect of these torso potentials on the solution of the inverse problem. To achieve this objective, a finite element code has been written to solve the bidomain problem on realistic two-dimesinal torso geometries, and a related optimization code is written that uses the finite element code. Our results show that the ischemic conductivity has a noticable effect on the torso potentials but makes a small difference when locating the ischemic region in the inverse problem. In the second part of this thesis work, a novel iterative scheme for the solution of the inverse problem has been developed. The method is based on the parameterization of the location of the ischemic regions, where the parameters are determined using sensitivity analysis and finite element optimization. It has been observed that the method succesfully locates the ischemic region.

Keywords: Bidomain model, Finite Element, Forward problem, Inverse problem, Ischemia, Conductivity, Optimization, Sensitivity Analysis

ÖZ

DOKTORA TEZİ

KALBIN İSKEMIK BÖLGELERINDEKI İLETKENLIK DEĞIŞIKLIĞININ ELEKTROKARDIOGRAFI ÜZERINE ETKILERININ SONLU ELEMANLAR YÖNTEMIYLE ARAŞTIRILMASI

Hamed KAGHAZCHI

ÇUKUROVA ÜNİVERSİTESİ
FEN BİLİMLERİ ENSTİTÜSÜ
ELEKTRİK - ELEKTRONİK MÜHENDİSLİĞİ ANABİLİM DALI

Danışman : Doç. Dr. Mustafa Kerem ÜN
Yıl: 2019, Sayfa: 125
Jüri : Doç. Dr. Mustafa Kerem ÜN
: Prof. Dr. Ulus ÇEVİK
: Doç. Dr. Ahmet ÇALIK
: Dr. Öğr. Üyesi Ahmet AYDIN
: Dr. Öğr. Üyesi Emine AVŞAR AYDIN

Elektrokardiyografi (EKG), insan vücudu üstünde ölçülen elektrik potansiyellerinden kalp sağlığı hakkında çıkarımda bulunulan yaygın bir tanı yöntemidir. Literatürde EKG'nin ileri ve ters problemlerini hesaplamalı yöntemlerle çözen pek çok yarı-statik çalışma mevcuttur. Bu çalışmalarda iskemik dokudaki abnormal membran potansiyeli dikkate alınırken, dokunun bu patolojiyle azalan iletkenliği büyük ölçüde gözardı edilmiştir. Bu çalışmanın ilk kısmında iletkenliğin ileri problemde ölçülen torso potansiyelleri üstündeki ve bu şekilde oluşan torso potansiyellerinin ters problemin çözümü üstündeki etkisini incelenmiştir. Bu hedef doğrultusunda, iki-bölgeli kalp problemini iki-boyutlu gerçekçi torso geometrileri üzerinde çözen bir sonlu elemanlar programı ve bu programı kullanan bir optimizasyon kodu yazılmıştır. Sonuçlarımız iskemik iletkenliğin torso potansiyelleri üstünde gözle görülür bir etkisi olduğunu, iskemik bölgeyi bulma amacıyla ters problem çözülürken ise minimal bir etkisinin olduğunu göstermiştir. Tezin ikinci kısmında, ters problemi çözmek üzere özgün iteratif bir yöntem geliştirilmiştir. Yöntem, iskemik bölgenin konumunun parametrizasyonuna dayanmakta, parametreler hassasiyet analizi ve sonlu elemanlarla optimizasyonu ile belirlenmektedir. Yöntemin iskemik bölgeyi başarıya bulduğu gözlemlenmiştir.

Anahtar Kelimeler: İki bölgeli model, sonlu elemanlar, ileri problem, ters problem, iskemi, iletkenlik, optimizasyon, hassasiyet analizi

EXTENDED SUMMARY

Mathematically modelling the electrical activity of the heart is an attempt to describe continuum-based modelling of cardiac electrical activity from the cell level to the body surface which is called the forward problem, and modelling of cardiac electrical activity from the body surface to the cell level is called the inverse problem.

The application of numerical and computational techniques to interpret, simulate and ultimately elucidate the physiological function of complex whole-organ systems such as the heart has developed rapidly within the last two decades.

The heart is a muscullar organ that acts as a variable speed biomechanical pump. The electrical excitation of the heart is intimately linked with other processes that together constitute the heart beat. The electrical currents that initiate the contraction of the heart also spread through the other tissues of the body. This electrical activity can be recorded on the body surface and provides a non-invasive measures of cardiac electrical function. This was first demonstrated by Waller more than 100 years ago. Waller published the first human recording in 1887 and introduced the term *elecctrocardiography* or ECG.

Electrocardiography (ECG) is a commonly used diagnostic method that is based on reading electrical potentials on human torso and make deductions about the health of the heart. Despite the fact that it is the most frequently used diagnostic technique, there are cases where ECG monitoring remains inadequate. Ischemia (where perfusion of the heart tissue is compromised), injury (advanced form of ischemia) and necrosis (tissue death), depending also on the size and location of the pathology on the heart, may get unnoticed in ECG monitoring.

Due to its clinical significance, the electrical activity of the heart has been the subject of engineering simulation studies as well. The main objective of these studies is to predict the effect of certain heart-related parameters on the ECG outcome. A large number of studies exist in the literature where the torso potentials are mathematically determined from the mycordium or pericardium potentials. This

type of simulation performed on the heart-torso geometry is accomplished by numerically solving the partial differential equations (PDE) of the electrostatic medium on the torso geometry, and of the electrostatic medium or the so-called bidomain model, a more advanced model, on the heart geometry. Recent literature shows that the bidomain model is the preferred model for the heart and the finite element method is the preferred method for solving the related PDE's numerically. In the current literature, the transmembrane potential in the tissue is usually taken as a source term and the extracellular potential is computed in quasi-static applications of bidomain model. To model ischemic tissue, transmembrane potentials corresponding to such tissues are imposed as source in the problem. However, although tissue conductivities change significantly under ischemic, injury and necrotic conditions, this factor has never been taken into account in forward-ECG studies.

The heart requires a continuous supply of oxygen due to its high energy need. Coronary artery occlusion causes an almost immediate loss of function and a relatively rapid death of affected myocytes. Ischemia is caused by insufficient oxygen supply to the heart muscle due to reduced blood flow to the tissue. It is a relatively common heart condition which reflects itself with a shifted transmembrane potential (TMP) and reduced conductivity of the affected tissue. While several numerical studies covered ischemia within a forward analysis, they have simulated ischemia by imposing the diseased TMP to the tissue but largely ignored the decreased conductivity associated with this pathology.

The first objective in this study is to investigate numerically the effect of changing conductivies due to presence of ischemia, injury and necrosis on the outcome of the forward-ECG problem (hence the ECG readings). To achieve this objective, a finite element code has been written to solve the bidomain problem on realistic thorax geometries. The program has been designed in such a way that it allow different conductivity values to be assigned to different points of the problem domain. That way, the pathological tissue has been represented not only by inducing

the pathological membrane potential but also the pathological conductivity values to the problem and a more realistic model for ischemic heart has been obtained. A comparison of the outcome of this model has been done with the outcome of the model where ischemia is represented only with imposed transmembrane potentials, and conclusions have been drawn.

We have solved the forward problem in two different configuration.

The first one involves estimating the torso potentials from known epicardial potentials. The problem is solved first by assuming a homogeneous torso model with an average conductivity assigned to the entire torso without distinguishing different tissues. Then, the same problem is solved with an inhomogeneous torso model where different tissue are distinguished by assigning them the appropriate conductivities. The testing of the code has been accomplished by comparing its results with those obtained from COMSOL package.

In the second configuration, the torso model includes the heart and its blood-filled chambers, and inhomogeneity is taken into account by distinguishing different types of tissues. To fulfill one of the main objectives of this dissertation work, examples are run with ischemic (unhealthy) and healthy conductivity values to assess the effect of ischemic conductivity on the torso potentials. Furthermore, the effect of anisotropic conductivity has been also evaluated by comparing the results of anisotropic conductivity with those obtained with isotropic conductivity.

The second objective of this study is to investigate the effect of conductivity change in determining the epicardial potentials and the localization of ischemic region in the heart in the inverse problem of ECG. The inverse problem of ECG can involve either the reconstruction of epicardial potentials or reconstruction of TMP from a given set of torso potentials, both of which lead to ill-posed systems and handled with regularization methods.

As commonly done in the testing of solution methods for inverse problems, we have created pseudo-experimental data by running the forward analysis. Forward analysis gives us torso potentials from epicardial potential data (or TMP data) that

are consistent with each other. In the inverse analysis, input and output of the forward analysis change roles. The torso potentials calculated in the forward analysis constitutes the input of the inverse problem and the objective is to reconstruct the underlying epicardial potentials (or TMP distribution) as output. The reconstruction of TMP allows us to locate the ischemic region due to its altered TMP. The ischemic conductivity is indirectly involved in this analysis, when torso potentials used in the inverse analysis is created by taking the ischemic conductivity into account in the forward analysis.

As the third objective, we would like to propose a new novel iterative scheme to tackle the inverse problem in order locate the ischemic region in the heart. Sensitivity based FE optimization scheme is started with an initial estimate of ischemic region that is far from its actual location. In a convergent, scheme, as the parameters evolve iteratively, the ischemic region will approach its actual location.

In many engineering problems, the optimal configuration of a medium is found though an iterative process where the parameters to be optimized gradually approach their optimal values. This method is often applied in the material property estimation or topology optimization in mechanical structures.

To apply it to the inverse problem of ECG (i.e. to the localization of the ischemic region), TMP distribution should be parameterized and optimization should be applied with respect to these parameters. The defined function takes a value of 0 mV everywhere except a rectangular region where it smoothly decreases to -30 mV. This region signifies the ischemic region in the heart. The size and the location of this ischemic region depends continuously on the parameter of the function.

Capturing the exact geometry of the ischemic region is not a concern in this method since we assume a priori its shape to be rectangular. If part of the rectangular region falls beyond the limits of the heart boundary during optimization iteration, the algorithm disregard that part. Hence, it is possible that the converged ischemic region may be a truncated rectangle. Furthermore, the patch of identified ischemic elements in the irregular FE mesh will look like a polygon rather than a rectangle.

GENİŞLETİLMİŞ ÖZET

Kalbin elektriksel aktivitesinin matematiksel olarak modellenmesinde, kalp elektriksel aktivitesinin hücre seviyesinden vücut yüzeyine doğru modellennesine ileri problem, elektriksel aktivitenin vücut yüzeyinden hücre seviyesine modellenmesine ise geri problem denir.

Kalp gibi karmaşık ve bütünlüklü organ sistemlerinin fizyolojik fonksiyonunu yorumlamak, simule etmek ve nihayetinde açıklamak için sayısal ve hesaplamalı tekniklerin uygulanması son yirmi yılda hızla gelişmiştir. Kalp, değişken hızlı mekanik bir pompa görevi gören kaslı bir organdır. Kalbin elektriksel uyarılması, birlikte kalp atışını oluşturan diğer işlemlerle yakından bağlantılıdır. Kalbin kasılmasını başlatan elektrik akımları vücudun diğer dokularına da yayılır. Bu elektriksel aktivite, vücut yüzeyinde kaydedilebilir ve kalbin elektriksel işleyişinin invazif olmayan bir şekilde ölçümünü sağlar. Bu ilk defa Waller tarafından 100 yıldan daha uzun bir süre önce ortaya konulmuştur. Waller, insan üstünde yapılan ilk kaydı 1887'de yayınlamış ve elektrokardiyografi terimini önermiştir.

Elektrokardiografi (EKG), gövde (torso) üstünde elektrik potansiyellerini okuyarak kalp ile ilgili çıkarımda bulunulan yaygın bir teşhis yöntemidir. Kalp rahatsızlıklarının teşhisinde halen en sık başvurulan teşhis yöntemi olmasına rağmen, EKG'nin yetersiz kaldığı vakalar vardır. İskemi (dokuya yeterince kan gitmemesi), bunun ileri halleri olan hasarlanma ("injury") ve nekroz (doku ölümü, "necrosis"), lezyonun büyüklüğü ve kalpteki yerine bağlı olarak standart EKG'de fark edilemeyebilir.

Kalbin elektriksel sisteminin davranışı, klinik önemi dolayısıyla uzun yıllardır mühendislik simülasyonu çalışmalarına da konu olmuştur. Bu çalışmaların temel amacı, kalple ilgili parametrelerin EKG üzerine etkilerini önceden tahmin edebilmektir. Kalp yüzeyinde (perikardiyum) veya dokusunda (miyokardiyum) oluşan elektrik potansiyellerinden, torso üstünde EKG ile ölçülen potansiyelleri

matematiksel olarak belirlemeye yönelik literatürde pek çok çalışma vardır. Kalp-torso geometrisi üstünde gerçekleştirilen bu tarz bir simülasyon, genelde torsoda elektrostatik, kalpte ise elektrostatik veya daha ileri bir model olan iki bölgeli modelin ("bidomain model") kısmi diferansiyel denklemlerini nümerik olarak çözerek gerçekleştirilmektedir. Yakın zamandaki literatürde, kalp için, elektrostatik yerine iki bölgeli modelin, nümerik yöntem olarak ise (sonlu farklar ve sınır elemanları yöntemi yerine) sonlu elemanlar yönteminin tercih edildiği görülmektedir.

Literatürde, yarı-statik iki bölgeli model uygulamalarında genelde dokudaki membran potansiyeli kaynak ("source") olarak alınıp hücredışı potansiyel hesaplanır. İskemik dokuyu modellemek için ise iskemik dokuya özgü membran potansiyel değerleri kaynak olarak alınır. Ancak, iskemi, yaralanma ve nekrozda dokunun iletkenliğinde önemli ölçüde değişiklik olmasına rağmen bu durum ileri problem çözümlerinde şimdiye dek gözardı edilmiştir.

Kalp, yüksek enerji ihtiyacı nedeniyle sürekli bir oksijen kaynağı gerektirir. Koroner arter tıkanıklığı hemen hemen bir fonksiyon kaybına ve etkilenen miyositlerin nispeten hızlı bir şekilde ölmesine neden olur. İskemi, dokuya kan akışının azalmasından dolayı kalp kasının yeterince oksijen alamamasından kaynaklanır. İskemi kendini, etkilenen dokuda kaymış bir transmembran potansiyeli (TMP) ve iletkenliğinin azalması ile yansıtan nispeten yaygın bir kalp rahatsızlığıdır. Yapılan birkaç sayısal ileri analiz çalışmasında, iskemi modellernirken dokuya hastalıklı TMP empoze edilmiş ama bu patoloji ile ilişkili olarak azalan iletkenlik göz ardı edilmiştir.

Bu projedeki birinci amacımız, iskemik, hasarlı ve nekrozlu dokuda, bu patolojilerle birlikte değişen iletkenliklerin ileri elektrokardiografi probleminin çözümüne (yani EKG okumalarına) etkisini nümerik olarak araştırmaktır. Bu amaca ulaşmak üzere, iki bölgeli model problemini gerçekçi toraks geometriler üstünde çözen bir sonlu elemanlar programı kodlanmıştır. Program, problem uzayının istenilen bölgesine farklı iletkenlik değerleri atanmasına izin verecek şekilde

tasarlanmıştır. Bu şekilde hastalıklı dokunun, sadece membran potansiyeli değerleri ile oynanarak değil, aynı zamanda malzeme özelliklerindeki değişimler çerçevesinde de simülasyonu sağlanmış ve hastalığın daha gerçekçi bir modeli oluşturulmuştur. Analiz sonuçları, sağlıklı dokunun ve sadece membran potansiyeli ile simüle edilen hastalıklı dokunun vereceği sonuçlarla karşılaştırılmış ve çıkarımlarda bulunulmuştur.

Çalışmada, ileri problemi iki farklı konfigürasyonda çözdük. Birincisi, gövde potansiyellerini bilinen epikardiyal potansiyellerden tahmin etmeyi içermektedir. Problem ilk önce, farklı dokular ayırt edilmeden tüm gövdeye atanan ortalama bir iletkenliğe sahip homojen bir gövde modeli varsayılarak çözülmüştür. Daha sonra aynı problem, farklı dokulara uygun iletkenliklerin atanmasıyla ayırt edildiği homojen olmayan bir gövde modeli ile çözülmüştür. Sonuçlar COMSOL paketinden elde edilen sonuçlarla karşılaştırılmıştır.

İkinci yapılandırmada gövde modeli, kalbi ve kan dolu odacıklarını içerir ve homojen olmama durumu, farklı doku türlerini ayırt ederek dikkate alınır. Bu tez çalışmasının ana amaçlarından birini yerine getirmek için örnekler, iskemik iletkenliğin gövde potansiyelleri üzerindeki etkisini değerlendirmek üzere iskemik (sağlıksız) ve sağlıklı iletkenlik değerleri ile çalıştırılmıştır. Ayrıca, anizotropik iletkenliğin etkisi, anizotropik iletkenliğin sonuçları, izotropik iletkenlik ile elde edilenlerle karşılaştırılarak değerlendirilmiştir.

Bu çalışmanın ikinci amacı, iletkenlik değişiminin epikardiyal potansiyelleri belirlemede etkisini ve kalpteki iskemik bölgenin lokalizasyonunu EKG'nin ters problemini kullanarak araştırmaktır. EKG'nin ters problemi, belirli bir gövde potansiyeli verisinden, epikardiyal potansiyellerin veya TMP'nin regularizasyon yöntemleriyle bulunmasını içerir ve her iki durumda da kötü koşullanmış sistemlere yol açar.

Ters problemler için önerilen çözüm yöntemlerini test ederken sıklıkla yapıldığı gibi, ileri analizleri çalıştırarak yapay deneysel veriler oluşturduk. İleri analiz bize, epikardiyal potansiyel verileriyle (veya TMP verileriyle) tutarlı olan

torso potansiyelleri verir. Ters analizde ise ileri analizin girdi ve çıktıları rol değiştirir. İleri analizde hesaplanan gövde potansiyelleri ters problemin girdisini oluşturur ve amaç, epikardiyal potansiyelleri (veya TMP dağılımı) çıktı olarak yakalayabilmektir. TMP'nin bulunması, değişen TMP değeri nedeniyle iskemik bölgeyi tespit etmemizi sağlar. İskemik iletkenlik, ters analizde kullanılan gövde potansiyelleri, ileri analizde iskemik iletkenlik dikkate alınarak oluşturulduğundan, bu analize dolaylı bir etkide bulunmaktadır.

Üçüncü hedef olarak, kalpteki iskemik bölgenin yerini belirlemek için ters problemi çözen yeni bir yöntem önerdik. Hassasiyet analizine dayalı FE optimizasyon yaklaşımı, asıl konumundan uzak olan iskemik bölgenin iterasyona ilk tahmini olafrak verilmesiyle başlar. Yakınsama varsa, parametreler yinelemeli olarak değiştikçe, iskemik bölge gerçek konumuna yaklaşır.

Birçok mühendislik probleminde, bir ortamın optimal konfigürasyonu, optimize edilecek parametrelerin kademeli olarak optimal değerlerine yaklaştırıldığı yinelemeli bir süreçte bulunur. Bu yöntem genellikle mekanik yapılarda malzeme özelliği tahmini veya topoloji optimizasyonunda uygulanır.

Bu yöntemi ECG'nin ters problemine (yani iskemik bölgenin lokalizasyonuna) uygulamak için, TMP dağılımı parametrelendirilmeli ve bu parametrelere göre optimizasyon uygulanmalıdır. Tanımlanan fonksiyon, düzgün bir şekilde -30 mV değerine düştüğü dikdörtgen bir bölge dışında her yerde 0 mV'luk bir değer alır. Bu bölge, kalpteki iskemik bölgeyi gösterir. Bu iskemik bölgenin büyüklüğü ve yeri, fonksiyon parametrelerine sürekli olarak bağlıdır.

İskemik bölgenin tam geometrisini yakalamak gibi bir kaygı bu yöntemde söz konusu değildir, çünkü bögenin şeklini dikdörtgen olarak kabul ediyoruz. Dikdörtgen bölgenin bir kısmı, optimizasyon yinelemesi sırasında kalp sınırının sınırlarının dışına çıkarsa, algoritma bu kısmı dikkate almaz. Bu nedenle, yakınsama ile belirlenmiş iskemik bölgenin kesik bir dikdörtgen olması da mümkündür. Ayrıca, regüler olmayan bir FE kafesinde tanımlanmış iskemik bölgenin elemanları dikdörtgen değil bir çokgen(poligon) gibi görünecektir.

ACKNOWLEDGEMENTS

I would like to express my heartfelt thanks to Assoc. Prof. Dr. Mustafa Kerem ÜN for his supervision, guidance, encouragements, extremely useful suggestions and continuous confidence in me throughout this thesis. It has been a great honor to have Assoc. Prof. Dr. Mustafa Kerem ÜN as supervisor.

I would like to thank to Prof. Dr. Ulus ÇEVİK, Assoc. Prof. Dr.Ahmet ÇALIK, Asst. Prof. Dr. Ahmet AYDIN, Asst. Prof. Dr. Emine AVŞAR AYDIN for accepting to be the member of examining committee for my thesis.

Special thanks go out to my uncle Mr. Mostafa KAGHAZCHI, who has always given me support and help during my studies.

Finally, I would like to express my deepest gratitude to my wife, Vafa MİRZAYEVA for her patience, encouragement and continuous morale support.

CONTENTS **PAGES**

ABSTRACT....I
ÖZ.... II
EXTENDED SUMMARY.... III
GENİŞLETİLMİŞ ÖZET VII
ACKNOWLEDGEMENTS.... XI
CONTENTS.... XII
LIST OF FIGURES XVIII
LIST OF ABBREVIATIONS AND SYMBOLS XXIV
1.INTRODUCTION 1
1.1.Prologue 1
1.2.Objective and Thesis Layout 3
2.PHYSIOLOGICAL AND CLINCIAL BACKGROUND 5
2.1.Anatomy of The Heart.... 5
2.2.Electrophysiology of the Heart.... 6
2.3.The Cardiac Action Potential 10
2.4.Electrocardiogram 14
2.5.The Ischemic Heart 21
3.FINITE ELEMENT METHOD 23
3.1.Introduction 23
3.2.The Finite Element Formulation 24
4.FORWARD PROBLEM OF ELECTROCARDIOGRAPHY 29
4.1.Introduction 29
4.2.Electrostatic Modelling of a Conductive Medium 29
4.3.Electrostatic Modelling of the Torso 31
4.4.Finite Element Formulation of the Torso Problem.... 34
4.5.Bidomain Model of the Heart.... 38
4.6.Finite Element Formulation of the Bidomain Heart 42

4.7.Material Properties of Heart Tissue 44
4.8.Geometric Model 47
4.9.Modelling of ischemic region 48
4.10.Programming of the Forward Problem of Electrocardiography 49
5.INVERSE PROBLEM OF ELECTROCARDIOGRAPHY 51
5.1.Introduction 51
5.2.Reconstruction of Epicardial Potential 52
5.3.Reconstruction of Transmembrane Potential 54
5.4.Regularization Methods 56
5.4.1.Pseudo-Inverse Matrix 58
5.4.2.The Singular Value Decomposition 58
5.4.3.Truncated Singular Value Decomposition 61
5.4.4.Tikhonov Regularization 61
5.4.5.Mean Value Regularization 63
5.4.6.Choice of Regularization Parameter 64
6.AN ITERATIVE OPTIMIZATION METHOD FOR THE INVERSE PROBLEM 67
6.1.Introduction 67
6.2.Finite Element Optimization Based on Sensitivity Analysis 67
6.2.1.Objective Function Minimization 69
6.3.Programming of the Inverse Problem of Electrocardiography 72
7.RESULTS 75
7.1.Introduction 75
7.2.Forward Problem Examples 75
7.2.1.Results of the Homogeneous Torso Model 76
7.2.2.Results of the Inhomogeneous Torso Model 79
7.2.3.Results of Inhomogeneous Torso, Isotropic, and Anisotropic Heart 80
7.3.Inverse Problem Examples 86
7.3.1.Reconstruction of Epicardial Potential 86

7.3.2.Reconstruction of Transmembrane Potentials 89
7.3.3.Results of Finite Element Optimization..... 103
8.DISCUSSION AND CONCLUSION 109
8.1.Discussion and Conclusion 109
8.2.Future Research..... 112
REFERENCES 113
CURRICULUM VITAE..... 125

LIST OF TABLES **PAGES**

Table 2.1. Conduction velocities in different regions of the heart (Andrew Pullan, Cheng, and Buist 2005) 8
Table 2.2. Intracellular (i) and extracellular (e) concentrations of Na^+, K^+ and Ca^{2+}. (Andrew Pullan, Cheng, and Buist 2005). 11
Table 4.1. Healthy intracellular and extracellular conductivities (Ruud et al. 2009) 46
Table 4.2. Ischemic intracellular and extracellular conductivities (Ruud et al. 2009) 47
Table 4.3. Conductivity values corresponding to organs in the model. 47

LIST OF FIGURES **PAGE**

Figure 2.1. Depiction of heart anatomy (Dmytro F. 2008) 6
Figure 2.2. Electrical Conduction System of the Heart (Burger and Kälz n.d.). 7
Figure 2.3. Cardiac fiber structure 9
Figure 2.4. Fiber and sheet structure of the left ventricle a transmural block from ventricular wall illustrating (1) change of muscle fiber direction across the wall and (2) organization of muscle fibers into sheets. Vectors a, b, c define the three principal directions within the heart, a: fiber axis, b: sheet axis, c: sheet normal 10
Figure 2.5. A typical action potential from a cardiac muscle cell (Johnson 2003)..... 13
Figure 2.6. The electric circuit representing the cell membrane..... 14
Figure 2.7.Action potential curves in different tissues of the heart. The segments of the ECG curve defined by each cardiac tissue are shown with corresponding colors (Farina 2008b). 15
Figure 2.8. Connection of electrodes to the body. 16
Figure 2.9. The Einthoven triangle, with leads I, II, and III and the projection of the heart vector on the leads. 17
Figure 2.10.(a), (b), (c) Connections of electrodes for the three augmented limb leads. (d) Standard and augmented lead-vector directions in the frontal plane..... 18
Figure 2.11.(a) Pericardial leads and their direction of lead vectors in the transverse plane. 19
Figure 2.12. Normal 12-lead electrocardiogram. 19
Figure 2.13. An idealized ECG signal from a modern ECG recording device. 20

Figure 2.14.Electrophysiology of myocardial ischemia. (A): typical action potentials of an ischemic myocardial cell and a healthy one. (B): extracellular potentials measured from a live ischemic canine heart at the plateau phase, shown in a longitudinal cross section view. 22
Figure 3.1. (a) A two-dimensional finite element mesh with vertex nodes and (b) an element with its node numbers indicated. 25
Figure 3.2. Linear shape function of the *j*th node in two-dimesion. 25
Figure 3.3. Triangular elements: (a) 3-node linear, (b) 6-node quadratic, (c) 10-node cubic (Grandin 1986b). 28
Figure 4.1. Schematic depiction of the heart domain H, surroundied by the torso domain T. ∂T and ∂H denote the outer boundary of the torso and the heart-torso interface, respectively (Barth, Keyes, and Roose 2007). 34
Figure 4.2. Boundary condition for k^{th} element of a mesh 38
Figure 4.3. Schematic representation of bidomain model with circuit elements. 40
Figure 4.4.Two-dimensional geometric model of the torso (Geneser et al. 2006) 48
Figure 5.1. Number of singular values σ versus error norm for a given α. The optimal σ value is indicated with a dot. 65
Figure 5.2. α versus error norm for a given number of singular values σ. The optimal value is indicated with a dot. 65
Figure 5.3. Transmembrane potential function. 68
Figure 5.4. Optimization Algorithm Scheme. 73
Figure 6.1. Inhomogeneous torso model with epicardial potential nodes shown with blue nodes and torso potential nodes shown with red nodes. 76
Figure 6.2. Potentials enforced at 24 epicardial nodes in the forward problem simulations (Taken from(Wang 2012)). 77

Figure 6.3. Potentials (mV) in homogeneous torso model. The mesh has 4299 nodes and 8154 elements. 78
Figure 6.4. Torso surface potentials that is obtained from homogeneous torso model. 78
Figure 6.5. Potentials (mV) in inhomogeneous torso model. The mesh has 6128 nodes and 11871 elements. 79
Figure 6.6. Torso surface potentials that is obtained from inhomogeneous torso model. 80
Figure 6.7.Inhomogeneous torso model, isotropic heart conductivity and ischemic region on the top of left ventricle (Ischemia 1). The mesh has 3181 nodes and 6252 elements. 81
Figure 6.8. Change of torso potentials with isotropic heart tissue, healthy, and unhealthy conductivities. (Ischemia 1) 82
Figure 6.9. Change of torso potentials with anisotropic heart tissue, healthy, and unhealthy conductivities (Ischemia 1). 82
Figure 6.10.Inhomogeneous torso model, isotropic heart conductivity and ischemic region on the right hand side of left ventricle (Ischmeia 2). The mesh has 4641 nodes and 9172 elements 83
Figure 6.11.Change of torso with isotropic heart tissue, healthy, and unhealthy conductivities (Ischemia 2) 83
Figure6.12.Change of torso potentials with anisotropic heart tissue, healthy, and unhealthy conductivities (Ischemia 2). 84
Figure6.13.Inhomogeneous torso model, isotropic heart conductivity and ischemic region on the left hand side of right ventricle (Ischemia 3). The mesh has 2863 nodes and 5616 elements 84
Figure 6.14.Change of torso potentials with isotropic heart tissue, healthy, and unhealthy conductivities (Ischemia 3). 85
Figure 6.15.Change of torso potentials with anisotropic heart tissue, healthy, and unhealthy conductivities (Ischemia 3). 85

Figure 6.16.Reconstructed epicardial potentials obtained by TSVD regularization method. 87
Figure 6.17.Reconstructed epicardial potentials obtained by Tikhonov zero order regularization method. 87
Figure 6.18.Reconstructed epicardial potentials obtained by Tikhonov first order regularization method. 88
Figure 6.19.Reconstructed epicardial potentials obtained by Tikhonov mean value regularization method. 88
Figure 6.20.Comparison of different approaches in the reconstruction of the epicardial potentials. 89
Figure6.21.Localizing the ischemic region with healthy and unhealthy conductivities using TSVD regularization (Ischemia 1). 90
Figure6.22.Localizing the ischemic region with healthy and unhealthy conductivities using zero order Tikhonov regularization (Ischemia 1) 91
Figure6.23.Localizing the ischemic region with healthy and unhealthy conductivities using first order Tikhonov regularization (Ischemia 1) 91
Figure6.24.Localizing the ischemic region with healthy and unhealthy conductivities using Mean value regularization (Ischemia 1). 92
Figure6.25.Localizing the ischemic region with healthy and unhealthy conductivities using TSVD regularization (Ischemia 2). 92
Figure6.26.Localizing the ischemic region with healthy and unhealthy conductivities using Zero order Tikhonov regularization (Ischemia 2) 93
Figure6.27.Localizing the ischemic region with healthy and unhealthy conductivities using First order Tikhonov regularization (Ischemia 2) 93

Figure6.28.Localizing the ischemic region with healthy and unhealthy conductivities using Mean value regularization (Ischemia 2). 94
Figure6.29.Localizing the ischemic region with healthy and unhealthy conductivities using TSVD regularization (Ischemia 3). 94
Figure6.30.Localizing the ischemic region with healthy and unhealthy conductivities using Zero order Tikhonov regularization (Ischemia 3)..... 95
Figure6.31.Localizing the ischemic region with healthy and unhealthy conductivities using First order Tikhonov regularization (Ischemia 3)..... 95
Figure6.32.Localizing the ischemic region with healthy and unhealthy conductivities using Mean value regularization (Ischemia 3). 96
Figure6.33.Localizing the ischemic region with healthy and unhealthy conductivities using TSVD regularization (Ischemia 1). 97
Figure6.34.Localizing the ischemic region with healthy and unhealthy conductivities using Zero order Tikhonov regularization (Ischemia 1)..... 98
Figure6.35.Localizing the ischemic region with healthy and unhealthy conductivities using First order Tikhonov regularization (Ischemia 1)..... 98
Figure6.36.Localizing the ischemic region with healthy and unhealthy conductivities using Mean value regularization (Ischemia 1). 99
Figure6.37.Localizing the ischemic region with healthy and unhealthy conductivities using TSVD regularization (Ischemia 2). 99
Figure6.38.Localizing the ischemic region with healthy and unhealthy conductivities using Zero order Tikhonov regularization (Ischemia 2)..... 100

Figure6.39.Localizing the ischemic region with healthy and unhealthy conductivities using First order Tikhonov regularization (Ischemia 2)..... 100
Figure6.40.Localizing the ischemic region with healthy and unhealthy conductivities using Mean value regularization (Ischemia 2). 101
Figure6.41.Localizing the ischemic region with healthy and unhealthy conductivities using TSVD regularization (Ischemia 3). 101
Figure6.42.Localizing the ischemic region with healthy and unhealthy conductivities using Zero order Tikhonov regularization (Ischemia 3)..... 102
Figure6.43.Localizing the ischemic region with healthy and unhealthy conductivities using First order Tikhonov regularization (Ischemia 3)..... 102
Figure6.44.Localizing the ischemic region with healthy and unhealthy conductivities using Mean value regularization (Ischemia 3). 103
Figure6.45.Localizing the isotropic ischemic region using FE optimization (Ischemia 1). 104
Figure6.46.Localizing the isotropic ischemic region using FE optimization (Ischemia 2). 105
Figure6.47.Localizing the isotropic ischemic region using FE optimization (Ischemia 3). 105
Figure6.48.Localizing the anisotropic ischemic region using FE optimization (Ischemia 1). 106
Figure6.49.Localizing the anisotropic ischemic region using FE optimization (Ischemia 2). 107
Figure6.50.Localizing the anisotropic ischemic region using FE optimization (Ischemia 3). 107

LIST OF ABBREVIATIONS AND SYMBOLS

ECG	:	Electrocardiography
FEM	:	Finite Element Method
FE		Finite Element
RA	:	Right Atria
LA	:	Left Atria
RV	:	Right Ventricle
LV	:	Left Ventricle
SA	:	Sinoatrial node
AV	:	Atrioventricular node
LL	:	Left Leg
LA	:	Left Arm
RA	:	Right Arm
TMP	:	Transmembrane Potential
SVD	:	Singular Value Decomposition
TSVD	:	Truncated Singular Value Decomposition
GHM		Generalized Helicoid Model
FE		Finite Element
R	:	Gas Constant
F	:	Faraday Constant
T	:	Absolute Temperature
Z_x	:	Valance of Ion
E_x	:	Nernst Potential of Ion
V_m	:	Transmembrane Potential
Φ_i	:	Intracellular Potential
Φ_e	:	Extracellular Potential
I_{Na}	:	Sodium Current

I_{Ca}	:	Calcium Current
I_K	:	Potassium Current
g_x	:	Conductance of Ion Channel
C_m	:	Membrane Capacitance
I_m	:	Total Membrane Current
N_i	:	Shape Function
$\mathbf{J(x)}$	:	Jacobian Matrix
$\mathbf{K}$	:	Stiffness Matrix
$\mathbf{f}$	:	Load Vector
E	:	Electric Field
B	:	Magnetic Field
J	:	Current Density
σ	:	Conductivity
σ_T	:	Torso Conductivity
∂T	:	Torso Surface
∂H	:	Heart Surface
w	:	Weighting Function
Φ_T	:	Torso Potantial
σ_i	:	Interacellular Conductivity of Heart
σ_e	:	Extracellular Conductivity of Heart
σ^*	:	Conductivity Tensor
$\mathbf{A}$	:	Orthogonal Rotation Matrix
$\theta(x,y)$	:	Orientation Function
u_H	:	Heart Potential
T	:	Torso Domain
H	:	Heart Domain
Ω	:	Whole Body Surface
$\mathbf{A}^\dagger$	:	Pseudoinverse Matrix

1. INTRODUCTION

1.1. Prologue

The electrical activity of the heart can be modeled using mathematical approaches at different levels. At cellular level, membrane potential models are proposed for different cell types in the heart. The application of computational techniques to simulate the heart electromechanics has evolved rapidly within the last two decades. The predictive power of such methods has provided the researchers with a vast knowledge about the functioning mechanism of the heart (Andrew Pullan, Cheng, and Buist 2005).

The heart is the organ which is responsible for pumping blood through the vascular system of the body. From an engineering point of view, it is a mechanical pump which is controled by a sophisticated electrical system. Electrical impulses generated at *sinoatrial node* of the heart propogate through a set of specialized cells in a controlled manner which allows the contraction of heart muscles in an effective and timely manner (Andrew Pullan, Cheng, and Buist 2005).

Many health problems associated with the heart are related to the disturbances occuring in the electrical activity of the heart. As a result, different heart problems can be diagnosed with *electrocardiogram*, or *ECG*, which is a relatively simple noninvasive tool to monitor the heart's electrical activity. In fact, ECG can be utilized to diagnose a variety of conditions including infarctions, arrhythmias caused by conduction system problems and ischemic heart disease (Barth, Keyes, and Roose 2007).

Mathematical models of electrical excitation of the heart provide different opportunities to researchers. Calculation of the body potentials (including those measured on torso with ECG) induced by a cardiac source is referred to as the *forward problem of electrocardiography* (Gulrajani 1998a), (Andrew Pullan, Cheng, and Buist 2005). By solving the forward problem, one can predict what kind of effect certain pathologies may have on the torso potentials (i.e. on the ECG readings).

Furthermore, the forward problem enables the analysis of rare or hypothetical patholgies with respect to their reflection on the ECG potentials.

To deduce information about the heart condition (e.g. location of electrical source in the heart, locating the pathological tissue etc.) from the body potentials constitutes the *inverse problem of the electrocardiography*. Clinicians "solve" this problem everyday by observing the ECG readings of their patients, but the formal solution of this problem is less than simple (Smith and Barr 2001). Inverse problem is mathematically more chalenging to solve since they are generally ill-conditioned and require some sort optimization to find the "best solution" among the pool of candidate solutions.

Both forward and inverse problems of ECG are known for several decades. Before the development of the *Bidomain Model* by Tung(Tung 1978), they have been formulated as electrostatic forward and inverse problems. It is safe to say that analytical solutions to the forward problem have been in existence for centuries since they invole the solution of the well-known *Laplace* or *Poisson* partial differential equation (PDE) on simple geometries (cylinders, spheres etc.). Analytical solutions to the inverse problem of ECG have been derived in that setting involve usually concentric or eccentric circles or spheres to model torso under different conditions (Barr, Ramsey, and Spach 1977),(Rudy and Oster 1997), (Rudy, Plonsey, and Liebman 1979), (Franzone and Magenes 1979), (Rudy and Plonsey 1980), (Iakovidis and Martin 1992),(P. R. Johnston and Gulrajani 1997), (Smith and Barr 2001),. The ill-posedness of the inverse problem has been demonstrated on the analytical solutions (Iakovidis and Martin 1991).

After the availability of computers for large scale simulation, both forward problems and inverse problems, especially in the bidomain setting, have been tackled using numerical methods such as finite element (Lopez-Perez, Sebastian, and Ferrero 2015), finite difference (Berenfeld and Abboud 1996), (Clayton and Panfilov 2008), (S. Pezzuto, J.Hake 2010), (Tveito et al. 2017), boundary element (Wach et al. 1997), (Fischer et al. 2000), (Stenroos and Haueisen 2008), (Guofa Shou et al. 2008),

(Jamison et al. 2011), (Darrell J. Swenson et al. 2011) finite volume (Bendahmane, Bürger, and Ruiz-Baier 2010), and coupled finite element-boundary element methods(Pullan 1996), (Fischer et al. 2000).

The finite element method (FEM) offers several advantages over the other methods such the ability to model over arbitrary geometries, incorporate anisotropies and inhomogeneities and be open to adaptive algorithms, and is still very popular in the comtemporary research.

Ischemia is caused by insufficient oxygen supply to the heart muscle due to reduced blood flow to the tissue. It is a relatively common heart condition which reflects itself with a shifted transmembrane potential (TMP) and reduced conductivity of the affected tissue.

Ischemia has been a main focus in the numerical study of heart conduction. In FEM, presence of ischemia is simulated by imposing an abnormal TMP potential to the tissue. Yet, the fact that the conductivity of the ischemic tissue also changes has been only recently recognized and taken into account in numerical studies (B. M. Johnston et al. 2018), (Brett M. Burton et al. 2018).

With the advancement in the capacity of computers, many biological phenomena can nowadays be modelled numerically with more details than before. We have used the FEM in this research to evaluate the effect of conductivity changes due to ischemia on the torso ECG readings, an issue that has been largely ignored sofar.

1.2. Objective and Thesis Layout

The first objective of this thesis is to investigate the effect of conductivity change in ischemic heart tissue on torso potentials. To achieve that, a custom-made finite element (FE) code has been written to solve the forward problem of ECG with ischemic conductivities imposed on the ischemic region of the heart.

Next, we have examined whether the torso potentials produced with ischemic conductivities make a better input data in locating the ischemic region in the inverse problem.

The clinical relevance of the inverse problem of ECG is unquestionable and our second objective is to propose and test a new novel iterative scheme to tackle the inverse problem in order locate the ischemic region in the heart.

Chapter 2 briefly reviews the anatomy and physiology of the heart and presents some basic concepts of heart bioelectricity.

The FEM formulation utilized in this research is described in detail in Chapter 3.

Chapter 4 describes the forward problem of electrocardiography and introduces the bidomail model for cardiac tissue.

Chapter 5 presents the inverse problem of elecctrocardiography. The reconstruction epicardial potentials and TMPs from torso potentials are described here, the latter allowing us to locate the ischemic area in the heart. Regularization methods are also described in this chapter.

We present the new iterative method to solve the inverse problem in Chapter 6. The sensitivity-based FE optimization scheme is described in detail.

The results of the example problems are presented in Chapter 7.

A thorough evaluation of the results and the related discussion, along with future research directions are given in Chapter 8.

2. PHYSIOLOGICAL AND CLINCIAL BACKGROUND

2.1. Anatomy of The Heart

The human heart is one of the most important organs in the human body. It is responsible for delivering oxygen and nutrient to all parts of the body by circulating the blood in the vascular system. (Kahle et al. 2004).

The heart consists of four main chambers (Fig. 2.1): two upper, smaller thin-walled chambers, called the right and left atria (RA and LA), and two lower, larger thicker-walled chambers, called the right and left ventricles (RV and LV). The ventricles have to fulfil the major part of the pumping action of the heart and thus have to generate much higher pressures. As a consequence, the ventricles have ticker walls than the atria, especially the left ventricle, whose wall is approximately three times thicker than the wall of right ventricle (Katz 2011).

The atria are separated from the ventricles by the *cardiac skeleton*, which is a non-conducting layer of connective tissue. At the base formed mainly by the left atrium, the major blood vessels of the heart, namely the aorta, the superior and inferior vena cava, the pulmonary artery and pulmonary vein enter and leave the upper part of the heart. The bottom of the ventricles is called the apex of the heart (Ottesen, Olufsen, and Larsen 2004).

The heart muscle, the *myocardium*, is the muscle tissue bordered by the inner surface (*endocardium*) and the outer surface (*epicardium*). It consists primarily of heart muscle cells, also known as *cardiac myocytes*. A wall of muscular tissue, referred to as the *septum*, divides the heart into a left and a right half, each of which involves one atrium and one ventricle. The right half of the heart pumps blood to the lungs (pulmonary circulation) and the left half perfuses the entire body with blood (systemic circulation) (Kahle et al. 2004),(Ottesen, Olufsen, and Larsen 2004).

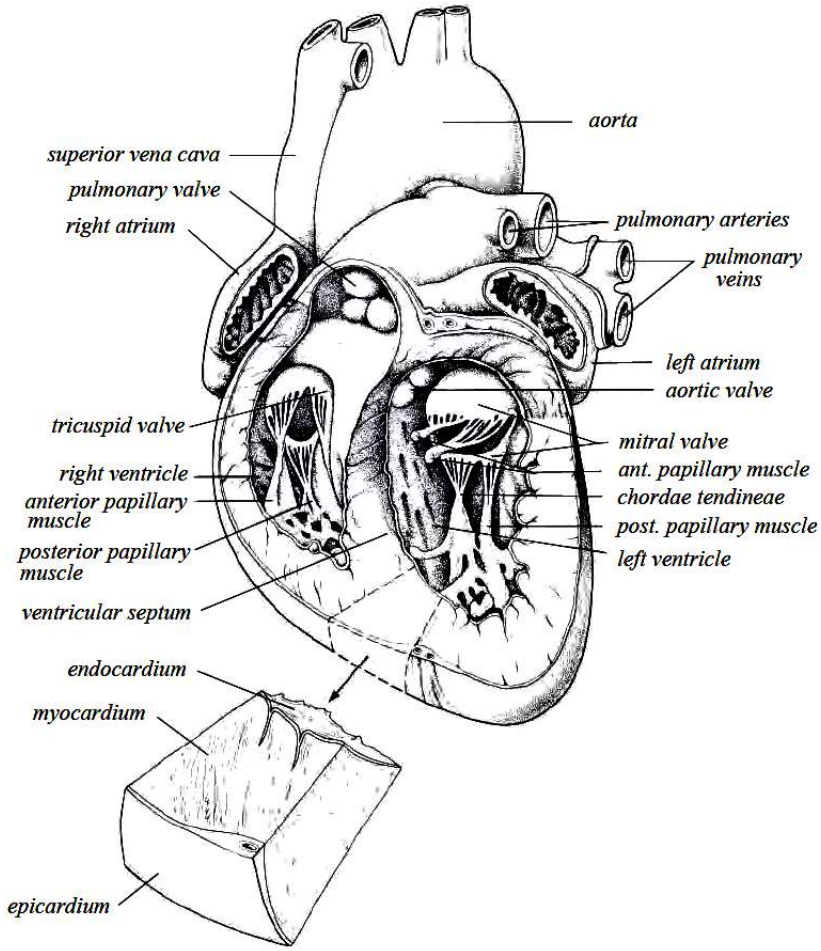


Figure 2.1. Depiction of heart anatomy (Dmytro F. 2008)

2.2. Electrophysiology of the Heart

The electrical impulses are initiated and conducted through the cardiac conduction system in such a way that the heart contracts in a coordinated and rhythmic manner to fulfill its function as a pump (Fig. 2.2). The impulse is generated at the *sinoatrial* (SA) *node* (Iaizzo 2009).

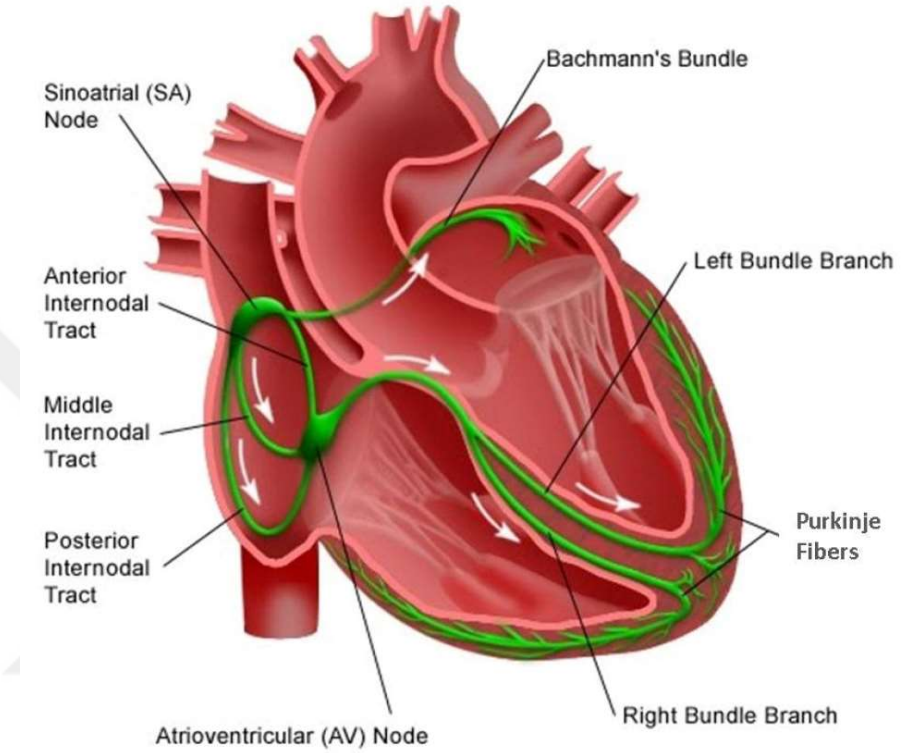


Figure 2.2. Electrical Conduction System of the Heart (Burger and Kälz n.d.).

The SA node consists of specialized cells, also known as pacemaker cells, which spontaneously creates electrical impulses at a rate of about 60-100 times per minute even in the absence of any neural stimulation. Each electrical impulse then moves through the walls of both atria to the atrioventricular (AV) node. Since the atria and the ventricles are electrically isolated from each other, the AV node presents the only connection between the two where electrical impulses are transmitted from the atria into the ventricles. The AV node slightly delays incoming impulses before they are transmitted to the ventricles to ensure that the atrial contraction is complete before ventricular contraction begins. After passing through the AV node, the electrical impulse rapidly moves down to the *bundle of His*, which bifurcates into the right and left bundle branches. They transmit the impulse from

the AV node along the septum to the right and left ventricles, respectively. The bundle branches finally end in an extensive network of tiny fibers, *the Purkinje fibers*, situated in the left and right ventricle. These specialized fibers rapidly transmits the electrical impulse to the entire ventricular myocardium. This coordinated spread of electrical impulse causes the ventricles to contract and pump blood to the body (Macfarlane et al. 2010), (Marieb and Hoehn 2013).

To ensure a coordinated contraction, the conduction velocity of the impulse varies in different regions of the heart (Table 2.1).

Table 2.1. Conduction velocities in different regions of the heart (Andrew Pullan, Cheng, and Buist 2005)

SA node	< 0.01 m/s
Atrial muscle	1 – 1.2 m/s
AV node	0.02 – 0.05 m/s
His bundle	1.2 – 2 m/s
Bundle branches	1.50- 4 m/s
Purkinje fibers	1.50- 4 m/s
Ventricular muscle	0.3 – 0.5 m/s

The human heart muscle, the myocardium, consists of a few billions of myocytes. Cardiac myocytes have roughly a cylindrical shape with an average length of 50-100 µm and an average diameter of 10-25 µm. The actual shape, size and alignment of the myocytes depend on their location and function in the heart. For instance, atrial myocytes are smaller than ventricular myocytes (Glass and Mcculloch 1987),(Marieb and Hoehn 2013).

The cell membrane of cardiac myocytes separates the interior of the cell, the *intracellular space*, from the surrounding medium, the *extracellular space*. Individual cardiac myocytes are connected to each other end-to-end and/or side to side by so-called *intercalated discs*. Intercalated discs connect the intracellular

spaces of neighboring cells, through which ions and small molecules can readily pass from one cell to the other without crossing the cell membrane. These cell-to-cell junctions allow the rapid propagation of electrical impulses from one cell to the other during contraction. In the ventricular myocardium, these gap junctions are mostly found at the longitudinal end of the cells and fewer along the transverse direction (Fig. 2.3). Hence, electrical conduction in the longitudinal fiber direction is approximately three times faster than in transverse direction. This implies that the electrical conductivity within the heart is *anisotropic*, i.e. direction-dependent. Furthermore, the anisotropy is stronger in the intracellular space compared to the extracellular space (Glass and Mcculloch 1987), (Volume, Sirovich, and Marsden n.d.),(J. G. Stinstra et al. 2005),(J. G. Stinstra et al. 2005).

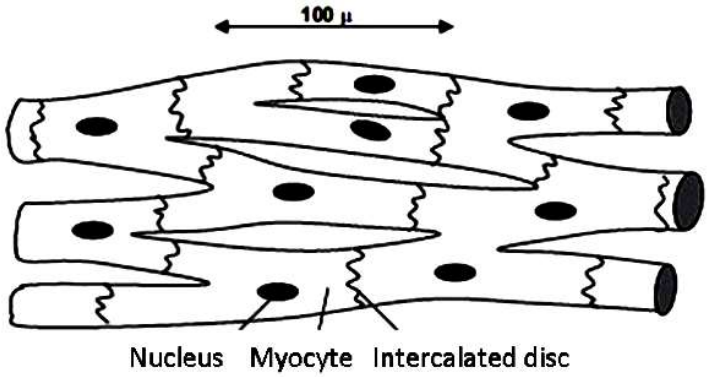


Figure 2.3. Cardiac fiber structure (Veneroni 2006).

The fibers are in turn arranged into muscle layers (sheets). Hence, in order to describe the anisotropy of conductivity, it is possible to define three principal directions at any point within the myocardium (Fig. 2.4). The first one is along the fiber direction (fiber axis), the second one is perpendicular to the fiber axis lying in the sheet plane (sheet axis), and the third one is normal to the sheet plane (sheet normal) (Fox 2006),(Sherwood 2012).

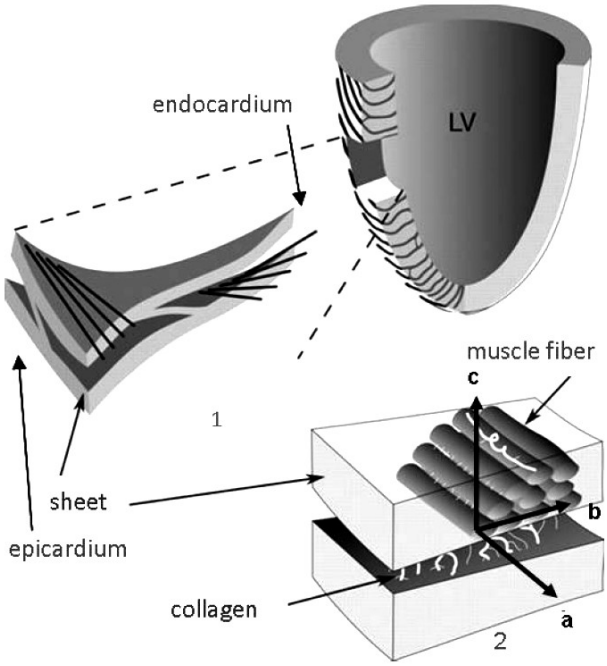


Figure 2.4. Fiber and sheet structure of the left ventricle a transmural block from ventricular wall illustrating (1) change of muscle fiber direction across the wall and (2) organization of muscle fibers into sheets. Vectors **a**, **b**, **c** define the three principal directions within the heart, **a**: fiber axis, **b**: sheet axis, **c**: sheet normal (Andrew Pullan, Cheng, and Buist 2005).

2.3. The Cardiac Action Potential

Cardiac muscle cells, like any other cell in the body, is encapsulated with a cell membrane which is made of phospholipids. Phospholipids form long molecules with one end being hydrophilic and the other hydrophobic. The cell membrane is a barrier, formed by two layers of phospholipid molecules (a *bilipid layer*) separating the inside of the cell, the intracellular space, from the outside of the cell, the extracellular space.

The cell membrane contain specialized proteins that form locally small pores in the membrane. These pores are generally called *ion channels* since they are ion specific, i.e. allow the passage of specific ions under appropriate conditions. The

specificity of these ion channels is the reason behind the potential difference across the cell membrane. The main ions that are responsible for this TMP are Na^+, K^+ and Ca^{2+}. The protein called *Sodium-Potassium ATPase* maintain a low Na^+ and high K^+ concentration in the extracellular space. Similarly, Ca^{2+}-specific ion channels keep a low Ca^{2+} concentration inside the cell (Table 2.2) (Andrew Pullan, Cheng, and Buist 2005),(Macfarlane et al. 2010).

Table 2.2. Intracellular (i) and extracellular (e) concentrations of Na^+, K^+ and Ca^{2+}. (Andrew Pullan, Cheng, and Buist 2005).

Ion	**Concentration (mM)**
$[Na^+]_i$	10
$[Na^+]_e$	140
$[K^+]_i$	145
$[K^+]_e$	5.4
$[Ca^{2+}]_i$	0.00012
$[Ca^{2+}]_e$	1.8

The concentration difference causes a chemical potential while the ion build-up forms an electrostatic potential across the cell membrane. The potential at which the chemical and electrostatic forces acting on a specific ion are in equilibrium is called the *reversal potential*. The potential difference across the cell membrane due to the ion x is called the *Nernst potential*, given by:

$$E_x = \frac{RT}{Z_x F} \ln\left(\frac{[X]_e}{[X]_i}\right) \tag{2.1}$$

where $[X]_i$ and $[X]_e$ are the intracellular and extracellular concentrations of the ion x, respectively. In the above equation, T is the absolute temperature, R is the universal gas constant (8.314 J $mol^{-1}K^{-1}$), Z_x is the valence of the ion and F is Faraday's constant (96.485 C mol^{-1}). Using the values listed in Table 2.1 with Eq. 2.1 results

to the following Nernst potentials for various ions at body temperature (37 ºC): E_{Na} = 70 mV, E_K = -88 mV, E_{Ca} = 128 mV (Andrew Pullan, Cheng, and Buist 2005).

The potential due to the presence of multiple monovalent ions is calculated with the *Goldman equation*. It is usually given by:

$$V = -\frac{RT}{F}\ln\left(\frac{P_k[K^+]_i + P_{Na}[Na^+]_i + P_{Cl}[Cl^+]_o}{P_k[K^+]_o + P_{Na}[Na^+]_o + P_{Cl}[Cl^+]_i}\right) \tag{2.2}$$

where P_{Na}, P_K, and P_{Cl} are the membrane permeability of Na^+, K^+, and Cl^- ions, respectively (Ottesen, Olufsen, and Larsen 2004).

The potential difference that exists across the cell membrane, i.e. the TMP, equals:

$$V_m = \Phi_i - \Phi_e \tag{2.3}$$

where Φ_i and Φ_e are the potentials in the intracellular and extracellular space, respectively. Typically, the permeability of the cell membrane is larger to K^+, since it is a smaller ion and can easily leak across the cell membrane. Hence, the equilibrium potential of around -90 mV, called the *resting potential*, for the cardiac cell is close to the Nernst potential E_K of this ion (Andrew Pullan, Cheng, and Buist 2005).

Small perturbations in the resting potential does not create a response in the tissue. On the other hand, a sufficiently large biochemical stimulus activates ion channels and shifts the TMP to different levels, called the *action potential*.

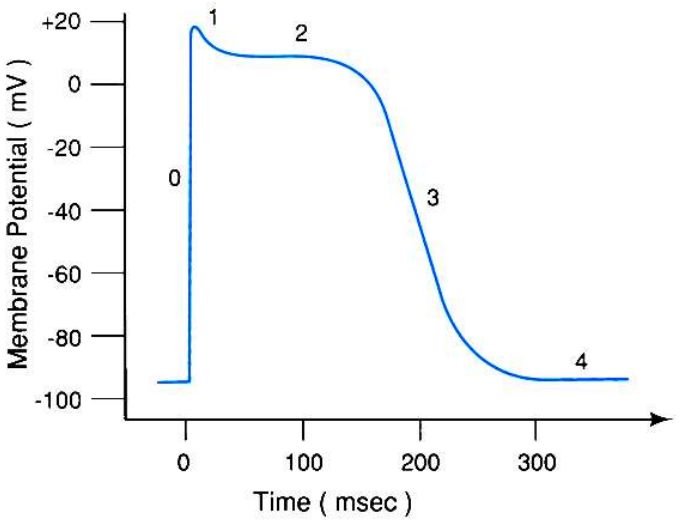


Figure 2.5. A typical action potential from a cardiac muscle cell (L. R. Johnson 2003).

TMP rapidly increases to a value of 10 mV in the *depolarization* stage of action potential and maintains this level for about 200 ms before it returns to its resting potential value in the *repolarization* stage (Fig. 2.5) (Andrew Pullan, Cheng, and Buist 2005),(Macfarlane et al. 2010).

An equivalent electrical circuit can be proposed for the ion movement across the cell membrane (Fig. 2.6). The cell membrane can be taken as a capacitance connected in parallel with resistances, each of which represents the passage of a specific ion through the ion channels. (Andrew Pullan, Cheng, and Buist 2005),(Barth, Keyes, and Roose 2007).

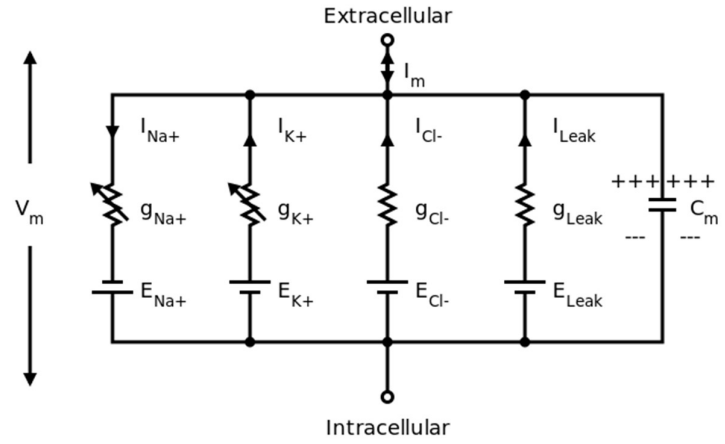


Figure 2.6. The electric circuit representing the cell membrane.

2.4. Electrocardiogram

ECG involves the recording of the electrical activity of the heart using electrodes placed on the body surface (Katz 2011).

Cardiac myocytes respond to an electrical stimulus and transmit action potentials but cannot initiate the action potential themselves. The profile of the action potential, while always possessing a depolarization and a repolarization phase, has some variability in different types of cells of the of heart conduction system (Fig. 2.7) (Katz 2011).

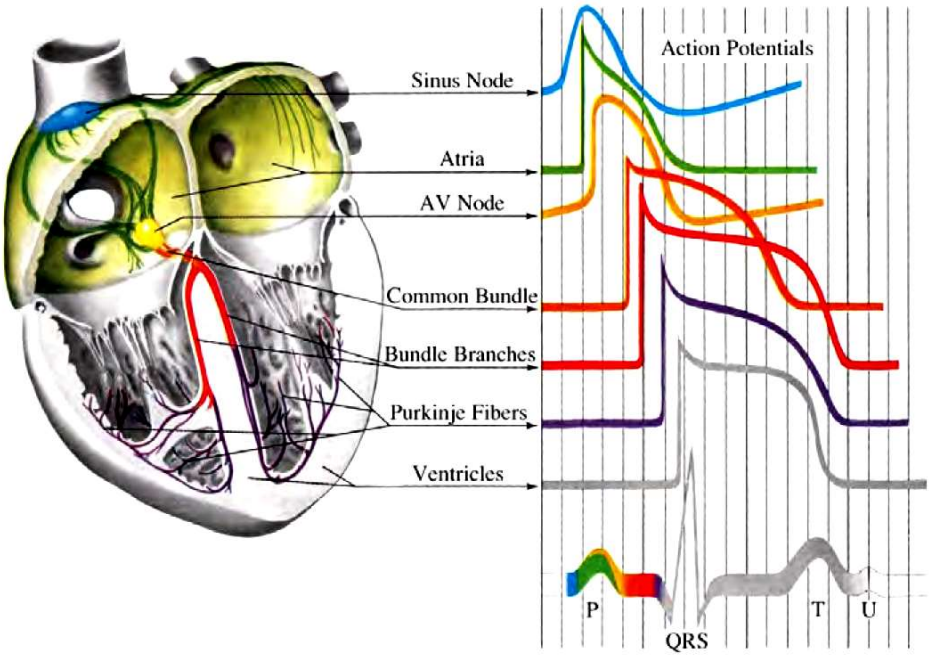


Figure 2.7. Action potential curves in different tissues of the heart. The segments of the ECG curve defined by each cardiac tissue are shown with corresponding colors (Farina 2008b).

Human body is a three-dimensional conductor (i.e. a *volume conductor*). In ECG, we monitor the combined electrical effect of all cells in this volume conductor. As the depolarization wave sweeps through the heart tissue, a distributed dipole forms across the boundary of the depolarized region with the rest of the heart, which is still in the resting phase. The distributed dipole can be represented with a single dipole vector, which is called the *heart vector*. What we measure in ECG is the projection of this vector, which is time-dependent in magnitude and direction, along different axes defined with respect to the human body (Barth, Keyes, and Roose 2007).

Historically, three electrodes are connected to the right arm (RA), the left arm (LA), and the left leg (LL) of the subject in ECG (Fig. 2.8). Consequently, three leads are defined where lead I is between LA and RA; lead II between LL and RA

and lead III between LL and LA. This lead configuration forms the well-known *Einthoven triangle*, in the frontal plane of the body. The projections of the heart vector on the three Einthoven leads are represented by the potentials recorded on these leads (Fig. 2.9). Mathematically, it is possible to reconstruct the heart vector from the three lead potentials (Barth, Keyes, and Roose 2007).

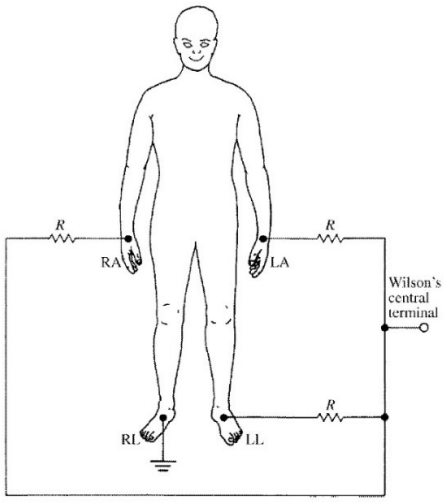


Figure 2.8. Connection of electrodes to the body.

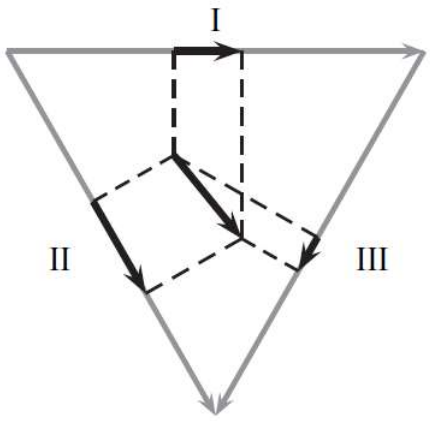


Figure 2.9. The Einthoven triangle, with leads I, II, and III and the projection of the heart vector on the leads (Barth, Keyes, and Roose 2007).

In clinical electrocardiography, some redundant electrodes are used in the frontal plane and some in the transverse plane to better monitor heart's activity. The additional frontal leads are based on a reference electrode. One such reference electrode is the *Wilson central terminal* (Fig. 2.8), whose potential is the average of the voltages at each main electrode. The potentials read with respect to the Wilson terminal result to the *augmented leads* which are called aVR, aVL, and aVF in ECG terminology (Fig. 2.10) (John G. 2010).

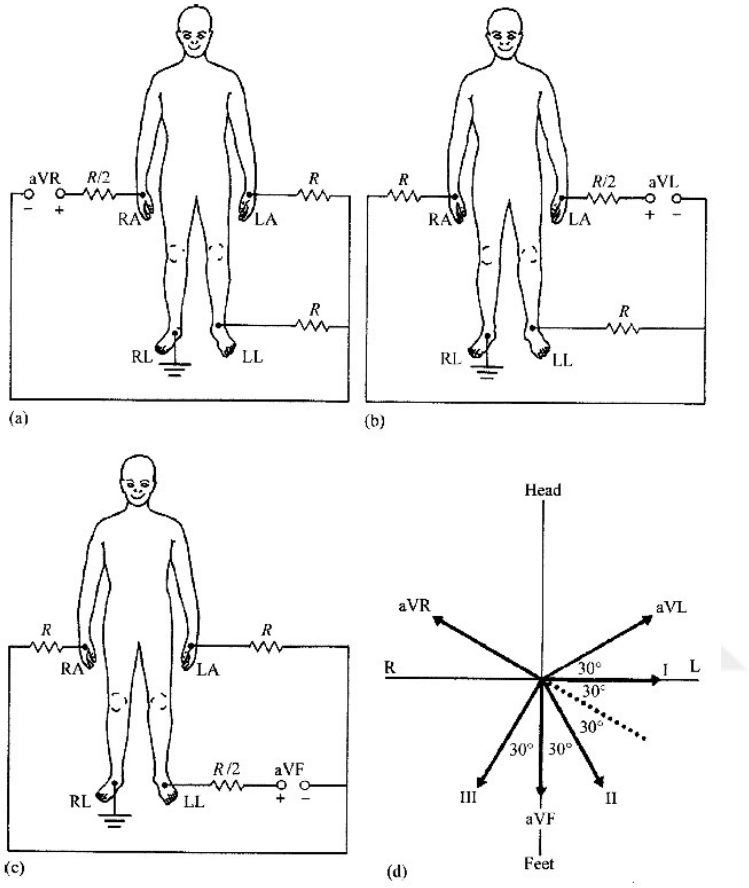


Figure 2.10. (a), (b), (c) Connections of electrodes for the three augmented limb leads. (d) Standard and augmented lead-vector directions in the frontal plane (Andrew Pullan, Cheng, and Buist 2005).

To capture the projection of heart vectors in the transverse plane, six electrodes are placed to the chest of the subject. The potentials between these electrodes and Wilson's central terminal result to the six *precordial* (chest) leads (Fig. 2.11).

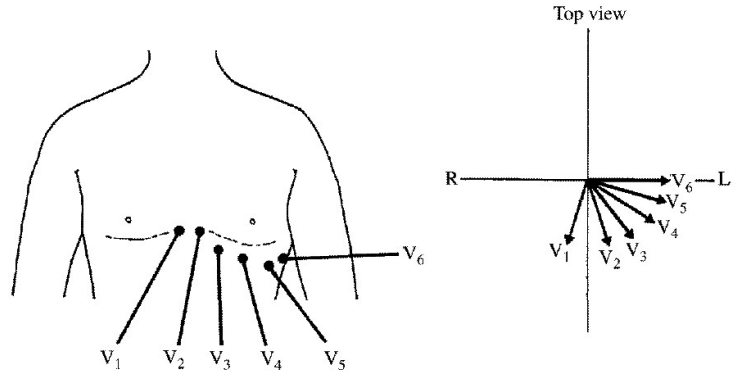


Figure 2.11. Pericardial leads and their direction of lead vectors in the transverse plane (Andrew Pullan, Cheng, and Buist 2005).

The frontal and pericardial leads constitute the 12-lead ECG, which is the standard system in use today. The ECG graph paper is usually output with a speed of 25 mm/s, so that each vertical division corresponds to a time of 0.04 s and each block to a time of 0.20 s. The voltage between two horizontal lines is equivalent to 0.1 mV such that a block corresponds to a voltage of 0.5 mV (Katz 2011). A sample graph paper with output from a 12-lead system is shown in (Fig. 2.12).

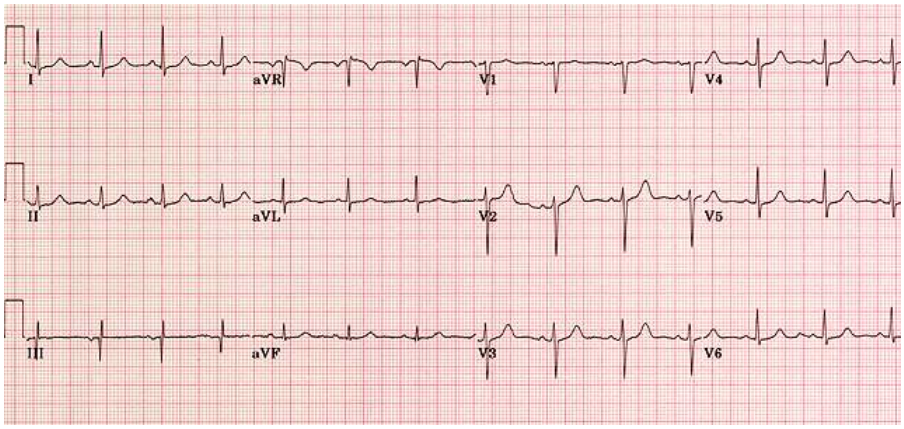


Figure 2.12. Normal 12-lead electrocardiogram.

One beat cycle of a healthy heart reflects itself on the ECG reading as a wave form of a specific shape (Fig. 2.13). The P wave results from the depolarization of the atria. Depolarization slows down as the action potential reaches the AV node, which causes the short zero voltage plateau (PR segment) after the P wave. The depolarization of the ventricles results to the QRS complex, which is a rapid rise and fall (0.06 to 0.1 s.) in the recorded voltage. During the ventricular depolarization, atrial repolarization also takes place but it is masked by the QRS complex since it is of much lower amplitude. The ST segment is related to the time between the end of the depolarization and start of the repolarization in the ventricles, which is followed by T wave associated with ventricular repolarization. As we shall see later, the ST segment plays a role in the diagnosis of ischemia and time-independent inverse simulation of ischemic heart is often done during the ST phase of the heart cycle (Andrew Pullan, Cheng, and Buist 2005),(Macfarlane et al. 2010).

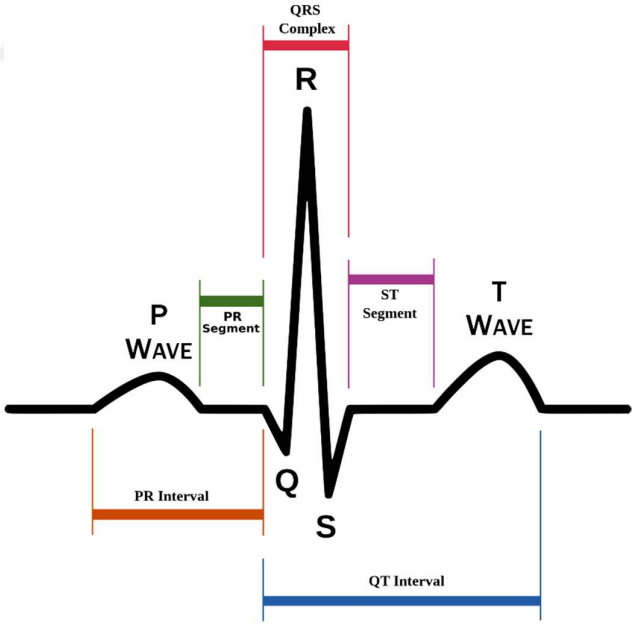


Figure 2.13. An idealized ECG signal from a modern ECG recording device.

2.5. The Ischemic Heart

The heart requires a continuous supply of oxygen due to its high energy need. The perfusion of the heart tissue is achieved with coronary arteries. Coronary artery occlusion causes an almost immediate loss of function and a relatively rapid death of affected myocytes. Ischemic myocardial cell death, called *myocardial infarction*, is a major public health problem in developed countries (Katz 2011). Most clinical infarctions involve the left ventricle; right ventricular infarction can occur, but is less frequent (Katz 2011).

ECG has become the most common choice for the immediate detection and monitoring of myocardial ischemia, because it is a rapid, noninvasive and cheap method. Depending on the location of the ischemic regions and of recording electrodes, myocardial infarction reflects itself usually as a depression relative to the normal in the patient's ECG. Still, ECG has a modest sensitivity and specificity (65-80%) in detecting and in localizing myocardial ischemia. Hence, ECG alone is not sufficient for localizing ischemic regions, and it is of clinical interest to recover the bioelectric field within the myocardium (Wang 2012),(Fletcher et al. 1998),(Stern 2002).

During the plateau phase of the action potential, a uniform TMP exists in the ventricles that lasts approximately 200 ms. This equipotential condition corresponds to the ST segment of ECG, where no significant voltage is read on the body surface (Fig. 2.13). In the cells of the ischemic tissue, however, TMP of the plateau-phase of the action potential has a decreased amplitude (Fig. 2.14). The difference in the TMP of the healthy and ischemic tissues forms a distributed dipole across their common boundary, which acts as a current source. The abnormal presence of the source in the ST-phase causes a shift in the ST-segment of the ECG (Stern 2002).

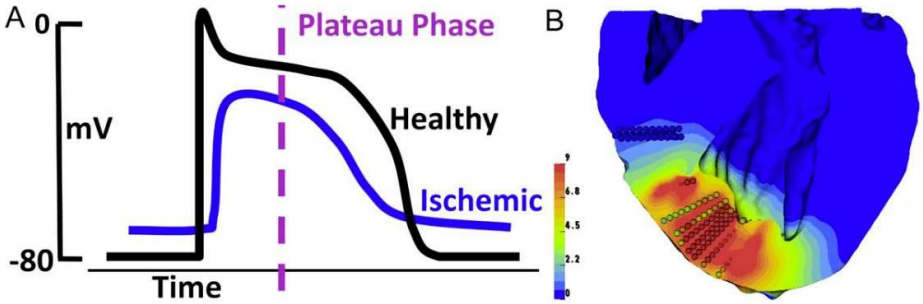


Figure 2.14. Electrophysiology of myocardial ischemia. (A): typical action potentials of an ischemic myocardial cell and a healthy one. (B): extracellular potentials measured from a live ischemic canine heart at the plateau phase, shown in a longitudinal cross section view (Wang 2012).

3. FINITE ELEMENT METHOD

3.1. Introduction

The *finite element method* (FEM) is well-known and widely used in different fields of science and engineering. In this chapter, we give a brief summary of this approach for unfamiliar reader in connection to the problem we have tried to solve in this work. For further details, the reader is referred to the numerous textbooks available in this topic.

The FEM, is a method that provides a numerical solution to a wide range of engineering problems governed by PDE's. In this method, a region defining a continuum is subdivided into simple geometric shapes, called *elements*, to form the FE mesh (Fig. 3.1). The FEM can be viewed as an element-wise application of the *weighted residual methods*. The residual of the governing equations is multiplied with a *weighting function* and the derivative order in the weighted-residual statement is reduced using mathematical identities in order to obtain the *weak form* of the problem. The weak form is satisfied on each element with polynomials of a specified order, yet the solution has to be continuous on the entire problem domain, i.e. across the element boundaries. The approximation polynomials used to interpolate the solution are called *interpolation* or *shape functions* (W. and White 2006),(Reddy 2014). Shape functions are defined using specific points associated with the elements, called *nodes*. Typically, a node is shared by several elements in the mesh. The shape function N_j of the jth node always equals unity on that node and zero on all other nodes. As a result, the approximate solution U to the problem can be constructed using nodal shape functions N_j as:

$$U = \sum_{j=1}^{M} c_j N_j \tag{3.1}$$

where M is the total the number of free (i.e. not constrained by a boundary condition) nodes in the mesh and c_j is the solution at the jth node which is yet to be determined.

The details of this procedure will be detailed in a two-dimesional problem in the coming sections.

3.2. The Finite Element Formulation

In its most general form, the method of weighted residual can be described using a differential operator *A(u)*. The operator *A(u)* operates on the problem variable u and, in the sense of FEM, it represents the weak form of the PDE:

$$A(u) = f \qquad \text{in } \Omega \tag{3.2}$$

where Ω represents the problem domain. Substitution of the approximate solution U, given in Eq.(3.1), into the left hand side of Eq. (3.2) will result to a residual R since it is not an exact solution to the problem:

$$R(x,y) = A(U) - f = A\left(\sum_{j=1}^{M} c_j N_j\right) - f \tag{3.3}$$

In the FEM, the parameters c_j are determined by requiring the weighted integral of the residual R over the problem domain Ω to vanish:

$$\int_{\Omega} w(x,y) R(x,y) d\Omega = 0 \tag{3.4}$$

where w is the weighting function (Reddy 2014). The residual can be evaluated separately over each element and summed up:

$$\sum_{k=1}^{L} \int_{\Omega} w_k(x,y) R_k(x,y) d\Omega = 0 \qquad (3.5)$$

where the index k refers to the quantities defined on the kth element. In a two-dimensional problem, an approximate solution is sought for the two-variable exact solution $u(x,y)$ of the PDE. The two-dimensional problem domain is discretized into elements with a triangular mesh (Fig. 3.1(a)). In case of an approximation with first order polynomials, three nodes are placed at the vertices of each triangular element. The nodes as well as the elements are numbered for appropriate processing in the computer environment (Grandin 1986b).

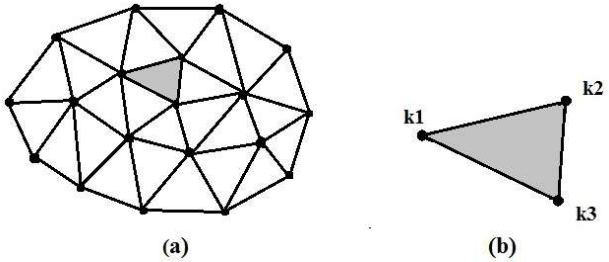


Figure 3.1. (a) A two-dimensional finite element mesh with vertex nodes and (b) an element with its node numbers indicated.

Let $N_j(x,y)$ be the shape function associated with node j. As mentioned before, $N_j(x,y)$ is equal to one at the jth node and is zero at every other node. If picked as a linear polynomial, the function resembles a two-dimensional hat function (Fig. 3.2).

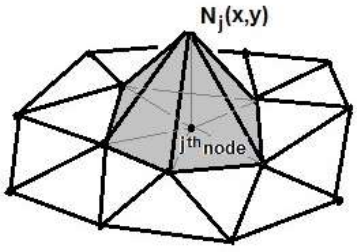


Figure 3.2. Linear shape function of the jth node in two-dimesion.

In a given element, only the shape functions of those nodes associated with that element is nonzero. Let (x_1,y_1), (x_2,y_2) and (x_3,y_3) be the coordinates of first, second and third vertex of the element. Then, the linear shape function $N_j\ (x, y)$ associated with vertex j satisfies

$$N_j(x_k, y_k) = \delta_{jk} \quad , \quad j, k = 1, 2, 3 \tag{3.6}$$

where δ_{jk} is the Kronecker delta. Since N_j is linear, it can be written in the form:

$$N_j(x, y) = a + bx + cy \tag{3.7}$$

and the values of a, b and c can be found by solving the 3x3 system given in Eq.(3.6)

Assume that the three nodes of the kth element in a given mesh have the node numbers $k1$, $k2$ and $k3$ (Fig. 3.1 (b)). In that case, the approximate solution u_k in this element can be written using the shape functions of these nodes, namely $N_{k1}(x, y)$, $N_{k2}(x, y)$ and $N_{k3}(x, y)$, as:

$$u_k(x, y) = c_{k1}N_{k1}(x, y) + c_{k2}N_{k2}(x, y) + c_{k3}N_{k3}(x, y) \tag{3.8}$$

where c_{k1}, c_{k2} and c_{k3} are the value of the solution on these nodes. In the Galerkin approach, the weighting function is selected from the same function space as the shape function. Hence:

$$w_k(x, y) = d_{k1}N_{k1}(x, y) + d_{k2}N_{k2}(x, y) + d_{k3}N_{k3}(x, y) \tag{3.9}$$

Since we want to find the best approximate solution for the chosen function space, the parameters d are arbitrary.

Note that Eqs 3.7 and 3.8 can be written in matrix form as:

$$u_k(x,y) = \begin{bmatrix} c_{k1} & c_{k2} & c_{k3} \end{bmatrix} \begin{bmatrix} N_{k1} \\ N_{k2} \\ N_{k3} \end{bmatrix} \tag{3.10}$$

$$w_k(x,y) = \begin{bmatrix} d_{k1} & d_{k2} & d_{k3} \end{bmatrix} \begin{bmatrix} N_{k1} \\ N_{k2} \\ N_{k3} \end{bmatrix} \tag{3.11}$$

When inserted into the Eq. 3.6, the above expressions result to matrix equation as:

$$\mathbf{d}^T(\mathbf{Kc} - \mathbf{f}) = \mathbf{0} \tag{3.12}$$

where the column vectors **c** and **d** contain all *c* and *d* values of each node. **K** is called the global stiffness matrix and **f** is called the global force vector. Since **d** contain arbitrary values, the equation holds when:

$$\mathbf{Kc} = \mathbf{f} \tag{3.13}$$

Solving the above linear system gives us the solution c_j at each node. Using the nodal shape functions, the solution at any point can be calculated by substituting the (*x,y*) coordinates of this nodes into Eq. 3.7.

It is possible to have higher order shape functions by introducing additional nodes to the element (Fig. 3.2).

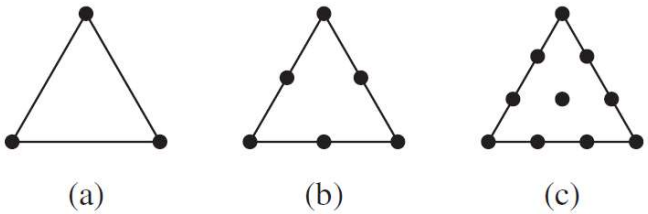


Figure 3.3. Triangular elements: (a) 3-node linear, (b) 6-node quadratic, (c) 10-node cubic (Grandin 1986b).

The integrals used to calculate the stiffness terms are usually evaluated numerically using the so-called *quadrature rules*. With quadrature rules, the integrals can be exactly calculated through a weighted average of integrand values evaluated at specific points in the elements.

4. FORWARD PROBLEM OF ELECTROCARDIOGRAPHY

4.1. Introduction

Forward problem of ECG can be formulated in two different ways. In the simpler case, heart is removed from the problem domain leaving a pericardial inner surface. The effect of the heart is introduced to the problem by imposing realistic pericardial potentials to this surface as a boundary condition. This amounts to a Laplace PDE to be solved in the torso domain.

The second case includes the heart geometry in the problem domain. In this approach, heart can be taken either as a regular volume conductor or a bidomain continuum. If heart is assumed to be a regular volume conductor, it is necessary to place a dipole or a distributed dipole at a physiologically relevant spot in the heart geometry. The equation to be solved in this case is a Poisson PDE.

If the heart is taken to be a bidomain continuum, then the complexity of the problem depends very much on the additional assumptions that one may take when tackling this problem.

The above mentioned issues are discussed in detail in this chapter.

4.2. Electrostatic Modelling of a Conductive Medium

Maxwell's equations gives the following relationship between electric field **E** and magnetic field **M** (Barth, Keyes, and Roose 2007):

$$\nabla \times \mathbf{E} + \frac{\partial \mathbf{B}}{\partial t} = 0 \tag{4.1}$$

Human body is a volume conductor, where capacitive and inductive effects are relatively weak. Considering the frequencies at which the heart operates, time-dependence may be ignored. In other words, at each time instant, the electrical activity of the heart can be regarded as static, a case often named as *quasi-static*

(Andrew Pullan, Cheng, and Buist 2005),(Barth, Keyes, and Roose 2007),(Lines et al. 2003).

In case of quasi-static fields, Eq. (4.1) becomes

$$\nabla \times \mathbf{E} = 0 \tag{4.2}$$

Equation (4.2) implies that **E** can be expressed as the gradient of a scalar potential Φ:

$$\mathbf{E} = -\nabla \Phi \tag{4.3}$$

The current density vector **J** is related to **E** through

$$\mathbf{J} = \sigma \mathbf{E} \tag{4.4}$$

with σ indicating the conductivity of the medium. Using Eq. (4.3), Eq. (4.4) can be written as:

$$\mathbf{J} = -\sigma \nabla \Phi \tag{4.5}$$

If current sources are present somewhere in the medium and no charge is accumulated, then the net flux across the boundary of the medium is:

$$\int_S \mathbf{J} \cdot \mathbf{n} \, dS = I \tag{4.6}$$

where I represents the net current across the boundary.

$$\int_S \mathbf{J} \cdot \mathbf{n} \, dS = 0 \tag{4.7}$$

where **n** is the outward surface normal of the surface *S*. Applying the divergence theorem to Eq. (4.7) gives:

$$\int_V \nabla \cdot \mathbf{J}\, dV = 0 \tag{4.8}$$

where *V* is the volume bounded by the surface *S*. Since this relation must hold for an arbitrary volume, the integrand itself must vanish:

$$\nabla \cdot \mathbf{J} = f \tag{4.9}$$

If no current source or sink exists and no charge is accumulated in the medium, Eq. (4.9) becomes:

$$\nabla \cdot \mathbf{J} = 0 \tag{4.10}$$

Substituting Eq.(4.5) into this equation, we obtain:

$$\nabla \cdot (\sigma \nabla \Phi) = 0 \tag{4.11}$$

which describes the electric potential of a volume conductor in the absence of current sources (Sundnes et al. 2006).

4.3. Electrostatic Modelling of the Torso

In the active heart, we have current sources in the form of distributed dipoles. With the presence of dipoles as sources, Eq. (4.9) takes the inhomogeneous form given by $\nabla \cdot (\sigma \nabla \Phi) = f$. Since the body is surrounded by non-conducting air, the normal component of the current must be zero at the body surface, meaning:

$$\mathbf{J} \cdot \mathbf{n} = 0 \tag{4.12}$$

where **n** is the outward unit normal of the body surface. Using Eq. (4.5), the boundary condition in Eq. (4.10) can be written as:

$$\sigma \nabla \Phi \cdot \mathbf{n} = 0 \tag{4.13}$$

The electrostatic problem can now be stated as:

$$\nabla \cdot (\sigma \nabla \Phi) = f \ , \quad x \in \Omega \tag{4.14}$$

$$\sigma \nabla \Phi \cdot \mathbf{n} = 0 \ , \ x \in \partial\Omega \tag{4.15}$$

where Ω represent the problem domain, which is the entire body including the heart in our case, and $\partial\Omega$ is the boundary of the problem domain, i.e. the body surface. f is the source term indicating charge creation. Since no net charge is created in the body:

$$\int_{\Omega} f dx = 0 \tag{4.16}$$

It should be noted that the conductivity σ is generally inhomogeneous throughout the body, since different types of tissues have different chemical composition and conductivities (Andrew Pullan, Cheng, and Buist 2005),(Barth, Keyes, and Roose 2007).

The torso, denoted as T in Fig. 4.1, is a passive conductor since it does not contain any current sources, meaning:

$$\nabla \cdot (\sigma_T \nabla \Phi) = 0 \qquad x \in T \tag{4.17}$$

where σ_T and Φ refer now to torso conductivity and potential, respectively. The torso is surrounded by nonconducting air such that the normal component of the current density vector on its outer boundary, denoted as ∂T, is zero:

$$\sigma_T \nabla \Phi \cdot \mathbf{n} = 0 \qquad x \in \partial T \tag{4.18}$$

This type of boundary condition involving the gradient of the main variable is called a *Neuman boundary condition*.

The inner boundary of the torso, denoted as ∂H in Fig. 4.1, interfaces the heart. Due to the continuity of the potential across boundaries of different media, we assume that the potential distribution on the inner torso boundary matches with the pericardial potentials (M. L. Buist and Pullan 2003) which gives:

$$\Phi = \Phi_H \qquad x \in \partial H \tag{4.19}$$

where Φ_H is the pericardial potential distribution on the outer heart surface (Andrew Pullan, Cheng, and Buist 2005),(Barth, Keyes, and Roose 2007),(M. Buist and Pullan 2002),(Bradley, Pullan, and Hunter 2000). The boundary condition in Eq. (4.19), where the value (and not value of its gradient) of the main variable is set, is called a *Dirichlet boundary condition*.

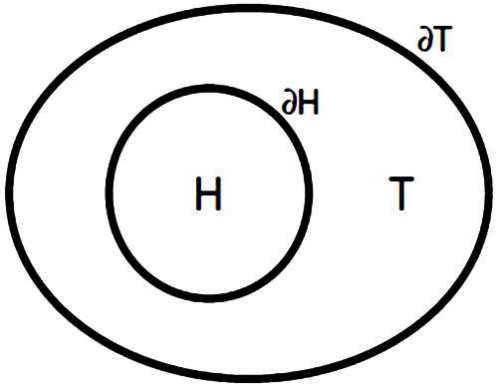


Figure 4.1. Schematic depiction of the heart domain H, surrounded by the torso domain T. ∂T and ∂H denote the outer boundary of the torso and the heart-torso interface, respectively (Barth, Keyes, and Roose 2007).

4.4. Finite Element Formulation of the Torso Problem

In the case of the epicardial forward problem, FEM is used to solve the Laplace PDE given in Eq. (4.17) subject to the boundary conditions given in Eqs. (4.18-4.19).

The weighted residual form for this equation is obtained by multiplying Eq. (4.15) with a weighting function *w*, integrating the resulting term over the problem domain Ω and equating the integral to zero (Gulrajani 1998a):

$$\int_{\Omega} \nabla \cdot (\sigma \nabla \Phi) w \, d\Omega = 0 \tag{4.20}$$

Using the identity

$$\int_{\Omega} \nabla \cdot (\sigma \nabla \Phi) w d\Omega = \int_{\Omega} \nabla \cdot (w \sigma \nabla \Phi) d\Omega - \int_{\Omega} (\sigma \nabla \Phi) \cdot \nabla w d\Omega \tag{4.21}$$

and applying Green-Gauss theorem, given by:

$$\int_{\Omega} \nabla \cdot (w\sigma \nabla \Phi) d\Omega = \int_{\Gamma} (w\sigma \nabla \Phi) \cdot \mathbf{n} d\Gamma \tag{4.22}$$

to Eq. (4.18) yields

$$\int_{\Omega} \nabla \cdot (\sigma \nabla \Phi) w d\Omega = \int_{\Gamma} (w\sigma \nabla \Phi) \cdot \mathbf{n} d\Gamma - \int_{\Omega} (\sigma \nabla \Phi) \cdot \nabla w d\Omega = 0$$

where Γ represents the boundary of the problem domain. Since a current density J injected to the domain at the boundary fulfills $(\sigma \nabla \Phi) \cdot \mathbf{n} = -J$ the weak form becomes:

$$\int_{\Omega} (\sigma \nabla \Phi) \cdot \nabla w d\Omega = -\int_{\Gamma} \mathbf{J} \cdot \mathbf{n} w d\Gamma \tag{4.23}$$

To satisfy the Eq. (4.23) in an approximate sense, the domain is first subdivided into L triangular finite elements

$$\Omega = \sum_{k=1}^{L} \Omega_k \tag{4.24}$$

Then, Eq.(4.21) can be written as:

$$\sum_{k=1}^{L} \int_{\Omega_k} (\sigma \nabla \Phi_k) \cdot \nabla w \, d\Omega_k = -\sum_{k=1}^{L} \int_{\Gamma_k} \mathbf{J} \cdot \mathbf{n} w_k d\Gamma_k$$

where Φ_k and w_k are the solution and the weigting function within the kth element. It should be noted that the right-hand side of Eq. (4.23) is one-dimensional integral. It is evaluated only on the boundary edges of the boundary elements.

Considering that

$$\nabla\Phi = \frac{\partial\Phi}{\partial x}\mathbf{i} + \frac{\partial\Phi}{\partial y}\mathbf{j} \tag{4.25}$$

$$\nabla w = \frac{\partial w}{\partial x}\mathbf{i} + \frac{\partial w}{\partial y}\mathbf{j} \tag{4.26}$$

the contribution to the left hand side of Eq. (4.21) by the *k*th element can be written as:

$$\int_{\Omega_k} (\sigma_k \nabla\Phi_k)\cdot\nabla w_k \, d\Omega_k = \int_{\Omega_k} \sigma_k \left[\frac{\partial\Phi_k}{\partial x}.\frac{\partial w_k}{\partial x} + \frac{\partial\Phi_k}{\partial y}.\frac{\partial w_k}{\partial y} \right] d\Omega_k \tag{4.27}$$

Using Eqs. (3.9-3.10), the above expression can be written in matrix form as:

$$\int_{\Omega_k} \sigma_k \begin{bmatrix} d_{k1} & d_{k2} & d_{k3} \end{bmatrix} \left(\begin{bmatrix} \frac{\partial N_{k1}}{\partial x} \\ \frac{\partial N_{k2}}{\partial x} \\ \frac{\partial N_{k3}}{\partial x} \end{bmatrix} . \begin{bmatrix} \frac{\partial N_{k1}}{\partial x} & \frac{\partial N_{k2}}{\partial x} & \frac{\partial N_{k3}}{\partial x} \end{bmatrix} + \begin{bmatrix} \frac{\partial N_{k1}}{\partial y} \\ \frac{\partial N_{k2}}{\partial y} \\ \frac{\partial N_{k3}}{\partial y} \end{bmatrix} . \begin{bmatrix} \frac{\partial N_{k1}}{\partial y} & \frac{\partial N_{k2}}{\partial y} & \frac{\partial N_{k3}}{\partial y} \end{bmatrix} \right) . \begin{bmatrix} c_{k1} \\ c_{k2} \\ c_{k3} \end{bmatrix} d\Omega_k \tag{4.28}$$

$$\int_{\Omega_k} \sigma_k \begin{bmatrix} d_{k1} & d_{k2} & d_{k3} \end{bmatrix} . \left(\begin{bmatrix} \frac{\partial N_{k1}}{\partial x}\frac{\partial N_{k1}}{\partial x} & \frac{\partial N_{k1}}{\partial x}\frac{\partial N_{k2}}{\partial x} & \frac{\partial N_{k1}}{\partial x}\frac{\partial N_{k3}}{\partial x} \\ \frac{\partial N_{k2}}{\partial x}\frac{\partial N_{k1}}{\partial x} & \frac{\partial N_{k2}}{\partial x}\frac{\partial N_{k2}}{\partial x} & \frac{\partial N_{k2}}{\partial x}\frac{\partial N_{k3}}{\partial x} \\ \frac{\partial N_{k3}}{\partial x}\frac{\partial N_{k1}}{\partial x} & \frac{\partial N_{k3}}{\partial x}\frac{\partial N_{k2}}{\partial x} & \frac{\partial N_{k3}}{\partial x}\frac{\partial N_{k3}}{\partial x} \end{bmatrix} + \begin{bmatrix} \frac{\partial N_{k1}}{\partial y}\frac{\partial N_{k1}}{\partial y} & \frac{\partial N_{k1}}{\partial y}\frac{\partial N_{k2}}{\partial y} & \frac{\partial N_{k1}}{\partial y}\frac{\partial N_{k3}}{\partial y} \\ \frac{\partial N_{k2}}{\partial y}\frac{\partial N_{k1}}{\partial y} & \frac{\partial N_{k2}}{\partial y}\frac{\partial N_{k2}}{\partial y} & \frac{\partial N_{k2}}{\partial y}\frac{\partial N_{k3}}{\partial y} \\ \frac{\partial N_{k3}}{\partial y}\frac{\partial N_{k1}}{\partial y} & \frac{\partial N_{k3}}{\partial y}\frac{\partial N_{k2}}{\partial y} & \frac{\partial N_{k3}}{\partial y}\frac{\partial N_{k3}}{\partial y} \end{bmatrix} \right) \begin{bmatrix} c_{k1} \\ c_{k2} \\ c_{k3} \end{bmatrix} d\Omega_k \tag{4.29}$$

Since *c*'s and *d*'s are constants, they can be taken out of the integral in Eq.(4.31). Evaluating the integral will result to an expression in the form $\mathbf{d}^T\mathbf{K}_k\mathbf{c}$, where $\mathbf{K}_k$ is called the *element stiffness matrix*. All element stiffness matrices are

assembled into the *global stiffness matrix* **K**. In **K**, the *j*th row and column is associated with c_j. The stiffness matrix of every element that contains the *j*th node will contribute to the entries of the *j*th row and column in the assembly procedure.

The *k*th element contributes to the boundary integral on the right hand side of Eq. (4.21) only if it possesses a boundary edge where a nonzero current boundary condition is prescribed. If this is the case, the current density term $J=\mathbf{J}\cdot\mathbf{n}$ is interpolated using the shape functions of the boundary nodes of this element (Fig. 4.2):

$$J(x,y) = J_{k1}.N_{k1}(x,y) + J_{k3}N_{k3}(x,y) \tag{4.30}$$

The resulting line integral in Eq. (4.21) is written in matrix form as:

$$\int_{(x_1,y_1)}^{(x_3,y_3)} \begin{bmatrix} d_{k1} & d_{k3} \end{bmatrix}.\begin{bmatrix} N_{k1} \\ N_{k3} \end{bmatrix}.\begin{bmatrix} N_{k1} & N_{k3} \end{bmatrix}.\begin{bmatrix} J_{k1} \\ J_{k3} \end{bmatrix}.d\Gamma_k \tag{4.31}$$

which, when evaluated, will be in the form $\mathbf{d}^T\mathbf{f}_k$. Here, $\mathbf{f}_k$ is the *element force vector*. After assembly, the element force vectors will form the *global force vector*.

Calculation and assembly of element matrices and vectors will results to Eq. (3.12):

$$\mathbf{Kc} = \mathbf{f}$$

The above system does not have a unique solution unless the potential at least at one node is set to a reference value per Eq. (4.19). Thus, the Dirichlet boundary condition is called an *essential boundary condition* in the FE jargon. The Neumann boundary condition given in Eq. (4.18) is naturally satisfied through the weak form (Eq. (4.21)) of the problem and thus called a *natural boundary condition* of the FE formulation.

Note that in the epicardial forward problem, the natural boundary condition is identically zero (meaning **f**=**0**) since J=0 (Eq. (4.18)). The essential boundary conditions represent the epicardial potentials imposed on the epicardial surface.

Epicardial forward FE simulation has been widely used to study the effect of inhomogeneities, anisotropies and other physiological factors (C. R. Johnson, MacLeod, and Ershler 1992), (Shahidi, Savard, and Nadeau 1994), (Klepfer, Johnson, and Macleod 1997), (Zemzemi et al. 2015). It has been also a benchmark problem with which different variations of FEM has been tested for computational efficiency (Klepfer, Johnson, and Macleod 1997)

FE simulation of the torso involving a heart with a dipole source has been done (Gulrajani, 1983) but is no longer very popular in the literature. As we will see, a simplified bidomain model is almost as straightforward and thus preferred by researchers.

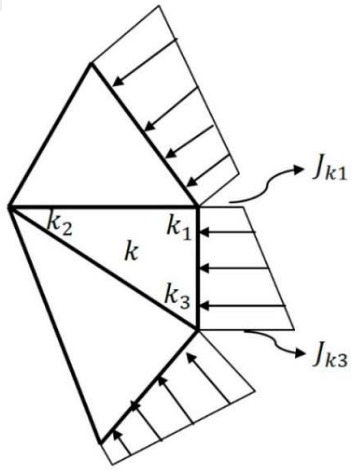


Figure 4.2. Boundary condition for kth element of a mesh.

4.5. Bidomain Model of the Heart

As mentioned earlier, for the frequencies and conductance values that are relevant for the heart, electric and magnetic fields within the heart can be taken as

quasi-static, where temporal variations have minimal inductive and capacitive effect (Plonsey and Heppner 1967),(Denisov et al. 2012). In such a passive conductive environment, the electric potential $\Phi=\Phi(x,y,z)$ is modeled by Poisson PDE:

$$\nabla \cdot (\sigma \nabla \Phi) = I_h \tag{4.32}$$

where I_h is the transmembrane current density per unit volume. If there is no current source, the PDE is reduced to a Laplace equation:

$$\nabla \cdot (\sigma \nabla \Phi) = 0 \tag{4.33}$$

The Dirichlet boundary condition associated with this PDE is:

$$\Phi = \Phi_0 \tag{4.34}$$

which matches the extracellular potentials to the boundary extramyocardial potentials on ∂H part of the boundary, and the Neumann boundary condition

$$\sigma \nabla \Phi \cdot \mathbf{n} = I_0 \tag{4.35}$$

where the current at ∂T, in the direction of the outward unit normal $\boldsymbol{n}$ is assigned to a value of I_0 (Y. Wang and Rudy 2006).

The heart tissue can be taken as two separate overlapping continua to account for the separate dynamics of the intracellular and the extracellular medium and their interaction across the cell membrane. Consequently, every point in the heart muscle is assumed to be a part of both the intracellular and the extracellular media simultaneously and assigned both an intracellular and an extracellular potential. This model is called the *bidomain model* of the heart (Fig. 4.3).

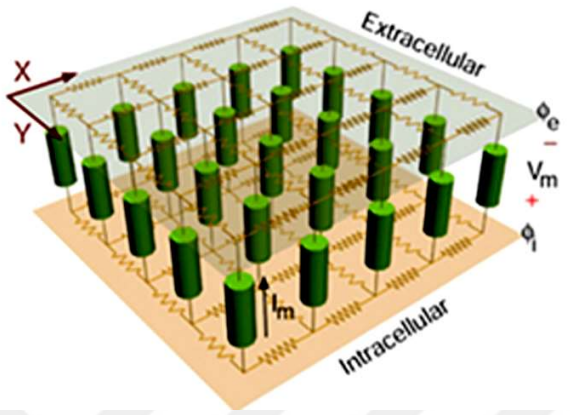


Figure 4.3. Schematic representation of bidomain model with circuit elements.

Let Φ_i and Φ_e denote the intracellular and extracellular potentials, respectively. Then, the potential difference across the cell membrane, i.e. the TMP, is expressed as:

$$V_m = \Phi_i - \Phi_e \tag{4.36}$$

Since the heart is a strongly anisotropic conductor, it is proper to replace scalar conductivities with conductivity matrices at this point. Both potentials above satisfy the Poisson equation as

$$\nabla \cdot (\boldsymbol{\sigma}_i \nabla \Phi_i) = A_m I_m \tag{4.37}$$

$$\nabla \cdot (\boldsymbol{\sigma}_e \nabla \Phi_e) = -A_m I_m \tag{4.38}$$

with $\boldsymbol{\sigma}_i$ and $\boldsymbol{\sigma}_e$ symbolizing the conductivities of the two domains. A_m is the surface to volume ratio of the cell membrane and I_m indicates the transmembrane current density per unit area (Wei et al. 2003),(Henriquez 2014).

The three equations are combined into one as:

$$\nabla \cdot ((\boldsymbol{\sigma}_i + \boldsymbol{\sigma}_e)\nabla \Phi_e) = -\nabla \cdot (\boldsymbol{\sigma}_i \nabla V_m) \tag{4.39}$$

This is the first equation describing the bidomain model.

The current flow across the membrane, I_m, has time-dependent capacitive and ionic components and is written as:

$$I_m = C_m \frac{\partial V_m}{\partial t} + I_{ion} \tag{4.40}$$

where C_m is the cell membrane capacitance and I_{ion} is the sum of the ionic currents. I_{ion} depends on V_m and is governed by an ordinary differential equation. Substituting Eq. (4.48) into Eqs. (4.45) and (4.46) gives

$$\nabla \cdot (\boldsymbol{\sigma}_i \nabla V_m) + \nabla \cdot (\boldsymbol{\sigma}_i \nabla \Phi_e) = A(C_m \frac{\partial V_m}{\partial t} + I_{ion}) \tag{4.41}$$

Equation (4.41) is the second equation of the bidomain model. If it is assumed that $\boldsymbol{\sigma}_e = k\boldsymbol{\sigma}_i$ for some scalar k, the model reduces to a simpler one-variable *monodomain* model (Bradley, Pullan, and Hunter 2000),(Clayton and Panfilov 2008).

At the resting potential (such as during the ST phase), the time derivative and the net ion flux I_{ion} in Eq.(4.41) vanish, the bidomain model reduces to Eq. (4.39), which is a quasi-static monodomain equation. In this work, we have solved Eq. (4.39), using the FEM.

The torso is typically surrounded with air, so that the normal component of the current density vanishes on the outer torso boundary:

$$(\sigma_T \nabla \Phi) \cdot \mathbf{n} = 0 \quad \text{at } \partial T \tag{4.42}$$

where σ_T indicates torso conductivity and Φ indicates the torso potential. Across the boundary of the torso and epicardium, torso potential must match with the extracellular potential of the heart. This condition is expressed as:

$$\Phi_e = \Phi \qquad \text{at } \partial H \tag{4.43}$$

It is assumed that the intracellular space has a connection only to the extracellular space and is isolated from the rest of the torso. Hence, no current flows between the intracellular and extramyocardial (epicardial) domain, which can be expressed with the following condition at the heart boundary:

$$(\boldsymbol{\sigma}_i \nabla \Phi_i) \cdot \mathbf{n}_H = 0 \qquad \text{at } \partial \mathrm{H} \tag{4.44}$$

where $\mathbf{n}_H$ is the outward unit normal of the heart surface.

The intracellular potential Φ_i is often eliminated from the governing equations of the bidomain model. Using Eq. (4.36), the boundary condition given in Eq. (4.44) can be written as:

$$(\boldsymbol{\sigma}_i \nabla V_m) \cdot \mathbf{n}_H = -(\boldsymbol{\sigma}_i \nabla \Phi_e) \cdot \mathbf{n}_H \qquad \text{at } \partial \mathrm{H} \tag{4.45}$$

Current can flow across the heart domain only through extracellular space. Hence, continuity of the current across the heart surface requires:

$$(\boldsymbol{\sigma}_e \nabla \Phi_e) \cdot \mathbf{n}_H = -(\sigma_T \nabla \Phi) \cdot \mathbf{n}_H \qquad \text{at } \partial H \tag{4.46}$$

4.6. Finite Element Formulation of the Bidomain Heart

Physiologically, the potential formed at every point of the heart is time-dependent. Especially in approaches where the membrane potential V_m is also modeled through an ordinary differential equation, the solution of the bidomain

model problem requires excessive computational resources (Lines et al. 2003). In this work, we investigate the heart potentials during the ST period of the heart cycle. In this period, the transmembrane potential has a constant value in the entire myocardium in a healthy heart. Since, capacitive and inductive terms are negligible, the heart is in a quasi-static state in the duration of the ST segment. In the quasi-static state, the bidomain model reduces to Eq. (4.39). Hence, the FE formulation is started by writing the weighted residual of Eq. (4.39) over the problem domain as:

$$\int_{\Omega}\left[\nabla\cdot((\boldsymbol{\sigma}_i+\boldsymbol{\sigma}_e)\nabla\Phi_e)+\nabla\cdot(\boldsymbol{\sigma}_i\nabla V_m)\right]w d\Omega=0 \tag{4.47}$$

Using tensorial identities and Green-Gauss theorem on both terms of Eq. (4.49) yields:

$$\int_{\Omega}(\boldsymbol{\sigma}_i+\boldsymbol{\sigma}_e)\nabla\Phi_e\cdot\nabla w\, d\Omega=-\int_{\Omega}\boldsymbol{\sigma}_i\nabla V_m\cdot\nabla w\, d\Omega \tag{4.48}$$

The integrals in Eq. (4.49) are the sum of individual integrals evaluated over the L elements of the problem domain:

$$\sum_{k=1}^{L}\int_{\Omega_k}(\boldsymbol{\sigma}_i+\boldsymbol{\sigma}_e)\nabla\Phi_e\nabla w d\Omega_k=-\sum_{k=1}^{L}\int_{\Omega_k}\boldsymbol{\sigma}_i\nabla V_m\cdot\nabla w d\Omega_k \tag{4.49}$$

This integral can be evaluated to form a linear system of equations with stiffness matrix **K** and a load vector **f**.

$$\mathbf{Kc}=\mathbf{f} \tag{4.50}$$

At least one nodal potential must be set to a reference value so that the above system has a unique solution. These essential (i.e. Dirichlet) boundary conditions

Φ_{ei}, i = 1, 2, …, N, are imposed to the system before solving it (Katz 2011),(Reddy 2014),(Grandin 1986b).

Note that V_m takes a constant value throughout myocardium during the ST period in a healthy heart. As a consequence, the source term ∇V_m is zero, meaning that the heart is not physiologically active in this period. In fact, the ST segment of ECG follows the baseline as a reflection of this inactivity. In the FE formulation, after applying the essential boundary condition by setting a reference node potential to zero, the solution of Eq. (4.49) will yield a zero potential for the entire problem domain simulating the clinical baseline potential. If, on the other hand, an ischemic region is present in the heart, ∇V_m will be nonzero around the boundary of the healthy tissue and ischemic tissue, since ischemic tissue has a lower V_m than the healthy one. This acts as a source term and will shift the ST potential from its baseline value, which is considered a clinical sign of ischemia (MacLachlan et al. 2006),(Hopenfeld, Stinstra, and MacLeod 2004).

4.7. Material Properties of Heart Tissue

Both intracellular and extracellular conductivities are anistropic in the myocardium. The anisotropy originates from the fibrious structure of the heart muscle. In the muscle fiber, the conductivity is higher in the fiber direction than in the cross-fiber direction (Pullan 1996),(Barth, Keyes, and Roose 2007),(Zemzemi et al. 2015). Furthermore, the muscle fibers are organized in sheets such that cross-fiber conductivity is different in the directions parallel and perpendicular to the sheet. Accordingly, in three-dimension, these three directions (parallel to the fiber, perpendicular to the fiber and parallel to the sheet, perpendicular to both the fiber and the sheet) form the principal directions of tissue conductivity tensor. The fiber directions, and hence the conductivity tensor, will vary throughout the heart muscle. At every muscle fiber, a local orthogonal coordinate system is defined with unit vectors $\mathbf{a}_l$, $\mathbf{a}_t$, and $\mathbf{a}_n$ indicating the principal directions (Young and Panfilov

2010),(Hooks and Trew 2008). In this local coordinate system, the extracellular or intracellular conductivity tensor is a diagonal matrix and given as:

$$\boldsymbol{\sigma}^* = \begin{bmatrix} \sigma_l & 0 & 0 \\ 0 & \sigma_t & 0 \\ 0 & 0 & \sigma_n \end{bmatrix} \tag{4.51}$$

In two-dimension, we have:

$$\boldsymbol{\sigma}^* = \begin{bmatrix} \sigma_l & 0 \\ 0 & \sigma_t \end{bmatrix} \tag{4.52}$$

In FE formulation, the conductivity matrix given in the local coordinates need to be transformed to the global Cartesian coordinates (Gulrajani 1998b),(Johnston R 2011),(Johnston R. 2011). In two-dimension, if the local coordinates system has a positive (clockwise) rotation of θ with respect to the Cartesian coordinates, the conductivity tensor is transformed to the Cartesian coordinates as:

$$\boldsymbol{\sigma} = \mathbf{A}\boldsymbol{\sigma}^*\mathbf{A}^T \tag{4.53}$$

where $\boldsymbol{\sigma}$ is the conductivity tensor in the global coordinates, and the matrix $\mathbf{A}$ is an orthogonal rotation matrix given by (Johnston R. 2011),(Sebastian et al. 2008):

$$\mathbf{A} = \begin{bmatrix} \cos\theta & \sin\theta \\ -\sin\theta & \cos\theta \end{bmatrix} \tag{4.54}$$

Equation (4.53) can be written as:

$$\boldsymbol{\sigma} = \begin{bmatrix} \sigma_l \cos^2\theta + \sigma_t \sin^2\theta & -\sigma_l \sin\theta\cos\theta + \sigma_t \sin\theta\cos\theta \\ -\sigma_l \sin\theta\cos\theta + \sigma_t \sin\theta\cos\theta & \sigma_l \cos^2\theta + \sigma_t \sin^2\theta \end{bmatrix} \tag{4.55}$$

Using the generalized helicoid model (GHM) the fiber orientation can be expressed with an orientation function θ (x, y) in two-dimension that is given in the literature (Ben-Shahar and Zucker 2003),(Le Floch et al. 2011),(Savadjiev, Zucker, and Siddiqi 2007)

$$\theta(x,y) = \tan^{-1}\left(\frac{K_T x + K_N y}{1 + K_N x - K_T y}\right) \tag{4.56}$$

where $K_T = 0.3$ and $K_N = 0.2$ are the GHM constants (Le Floch et al. 2011). In this formula, the (x,y) coordinates are defined with respect to the geometric center of the heart.

It is well-known that, during action potential, the transmembrane potential jumps from -90 mV to close to 0 mV for a healthy tissue, but may reach only -30 mV in case of ischemia (J. G. Stinstra et al. 2005). It is also known that both intracellular and extracellular conductivity values decrease in case of ischemia or more advanced lesions (Bjørn Fredrik Nielsen, Lysaker, and Tveito 2007),(Rodriguez, Trayanova, and Noble 2006),(J. G. Stinstra et al. 2005). In this work, ischemic and healthy tissue conductivity characteristics taken from the literature (Ruud et al. 2009) have been used in the FE simulation (Tables 4.1 and 4.2).

Table 4.1. Healthy intracellular and extracellular conductivities (Ruud et al. 2009).

Conductivity	Value (mS/cm)
Healthy intracellular longitudinal (σ_{il})	3.0
Healthy intracellular transverse (σ_{it})	0.31525
Healthy extracellular longitudinal (σ_{el})	2.0
Healthy extracellular transverse (σ_{et})	1.3514

Table 4.2. Ischemic intracellular and extracellular conductivities (Ruud et al. 2009).

Conductivity	Value (mS/cm)
Ischemic intracellular longitudinal (σ_{il})	0.3
Ischemic intracellular transverse (σ_{it})	0.006305
Ischemic extracellular longitudinal (σ_{el})	1.0
Ischemic extracellular transverse (σ_{et})	1.01

4.8. Geometric Model

The two-dimensional geometric model used in this study consists of a single two-dimensional MRI slice image obtained from Utah University (Pullan 1996),(Geneser et al. 2006),(Geneser, Kirby, and MacLeod 2008). The slice image is taken 50 mm superior to the apex of the heart and processed for the segmentation of lungs, skeletal muscle, fat, and torso cavity (Fig. 4.4). Different conductivity values are assigned to these regions (Table 4.3) (Geneser, Kirby, and MacLeod 2008),(Klepfer, Johnson, and Macleod 1997).

Table 4.3. Conductivity values corresponding to organs in the model.

Organ Category	Conductivity Value (mS/cm)
Lungs	0.96
Skeletal muscle	2.0
Fat	0.45
Torso cavity	2.39
Blood	2.39

Rather than a three-dimensional analysis, we have preferred a two-dimensional computational study to ease the computational burden and to visualize the results more effectively. Important conclusions can be still drawn from two-dimensional simulations and this approach is still popular in the literature (Sovilj et

al. 2014) (Geneser, Kirby, and MacLeod 2008),(Klepfer, Johnson, and Macleod 1997).

The goal of the current study is to investigate the relation between the conductivity changes associated with ischemic heart disease and the resulting shift in the ST segment of the ECG. As mentioned earlier, ST segment shift observed in ECG is a clinical indicator for ischemic heart disease (Barth, Keyes, and Roose 2007).

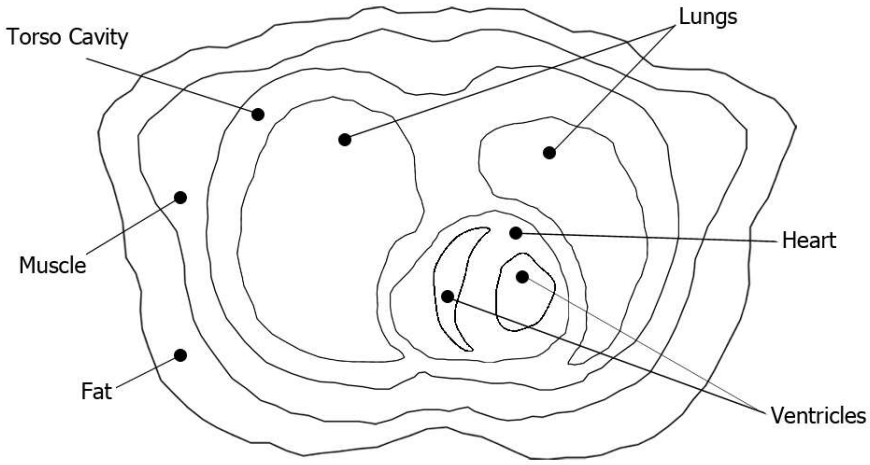


Figure 4.4. Two-dimensional geometric model of the torso (Geneser et al. 2006).

4.9. Modelling of ischemic region

In this study, to simulate ischemia myocardium, we set the TMP during the ST interval to 0 mV for the healthy tissue and to -30 mV for the ischemic tissue (Wang 2012).:

$$V_m(x) = \begin{cases} 0\ \text{mV}, & x \text{ in healthy tissue} \\ -30\ \text{mV}, & x \text{ in ischemic tissue} \end{cases} \tag{4.57}$$

Furthermore, we have taken the conductivity change in the ischemic tissue into account, something that is not properly done before.

The transition from a healthy tissue to a diseased tissue occurs not abruptly but through a transition zone. Clearly, the size of the transition zone and the profile of V_m across this zone will affect ∇V_m (i.e. the source magnitude) and the problem outcome. We have defined a strip of thickness H of the ischemic region next to the healthy region as our transition zone and proposed the following functional variation within this zone:

$$V_m = 30.\cos(\frac{\pi d}{H}) - 30 \tag{4.58}$$

where H is the thickness of transition zone, which varies between 0.4 – 1 mm (MacLachlan, Sundnes, and Lines 2005). d is the perpendicular distance of the considered point to ischemic region border. Accordingly, Eq. (4.58) can be written more accurately as:

$$V_m(d) = \begin{cases} 0, & d \text{ in } \Omega_{Healthy} \\ 30.\cos(\frac{\pi d}{H}) - 30, & \Omega_{Ischemic\,Region} < d < \Omega_{Healthy} \\ -30, & d \text{ in } \Omega_{Ischemic} \end{cases} \tag{4.59}$$

where Ω_{Healthy} is the healthy tissue of the heart and Ω_{Ischemic} is the ischemic tissue of the heart.

The transition zone has been described by different functional forms in other studies (Nielsen 2007 “On the use of…”, Johnston 2010, Burton 2018, Johnston 2018 I ve II). However, the profile of the transition zone in those studies looks similar to ours.

4.10. Programming of the Forward Problem of Electrocardiography

To solve the forward problem of ECG, we have programmed a FE code from scratch in Python language using Spyder environment. The code is designed in such a way that it can solve both the Poisson and Laplace PDE’s where appropriate in the

problem domain simultaneously. Also, different conductivity tensors can be assigned to different elements according to Eqs. 4.55-4.56. These features are not typically available in commercial FE packages.

The code has been tested for correctness by comparing its results with those obtained from COMSOL Multiphysics package in some test problems.

The pseudo code for the developed code runs as given below:

- Read element connectivity, nodal coordinates, boundary conditions information, node number, element number, and etc. from the input file.
- Do the following in a loop over all elements:
    - Calculate the conductivity tensor
    - Calculate the element stiffness matrix.
    - Assemble the element stiffness matrix to a global system.
- Apply the natural boundary conditions (if any) to form the force vector.
- Apply the essential boundary conditions to the final system.
- Solve the linear system.
- Output the results.

5. INVERSE PROBLEM OF ELECTROCARDIOGRAPHY

5.1. Introduction

The forward problem of ECG, as most forward problems are, is *well-posed* or *well-conditioned* in the sense of Hadamard (Barth, Keyes, and Roose 2007) meaning:

I. A solution exists for the problem.
II. The solution is unique.
III. The solution depends continuously on the input data, i.e. a change in the problem input (source magnitude, material properties etc.) causes a *proportional* change in the problem output.

By contrast, the inverse problems of engineering are often *ill-posed* or *ill-conditioned*. While item I in the above list is often valid for inverse problems, items II and III usually do not hold. In other words, the solution may not be unique, and a slight change in the problem input will cause disproportionately large changes in the problem output. Consequently, inverse problems are generally much harder to solve than their forward counterparts. (Barth, Keyes, and Roose 2007),(Lopez-Perez, Sebastian, and Ferrero 2015).

To obtain a unique solution and to eliminate the fluctuating nature of the solution, some constraints have to be applied to the solution of the inverse problem. These constraints can cast the solution into a certain functional form, effectively removes certain types of possible solutions and push discussion shows that ill-posed problems, in their original form, are not suitable for performing computer simulations. Application of such constraints that would turn an otherwise irregular solution into a more regular one is called *regularization*.

Here, we have created pseudo-experimental data by running the forward problem with ischemic and healthy conductivities. These data are used as input in

the inverse problem and the outcome originating from a healthy and ischemic conductivities are compared.

We have applied two of these techniques, namely *Truncated Singular Value Decomposition* (TSVD) regularization and *Tikhonov* regularization (Barth, Keyes, and Roose 2007) which we briefly discussed here. There are different variants of Tikhonov regularization that we have employed in the solution of inverse problem, namely 0^{th} order, 1^{st} order and mean value regularization. Mean value regularization, although based on a simple idea, has not been used in inverse ECG problem before.

This dissertation considers two types of inverse ECG problems, hereafter referred to as the *epicardium-based inverse ECG problem* (reconstruction of epicardial potentials from torso potentials) and *the bidomain-based inverse ECG problem* (reconstruction of TMP from torso potentials), according to how the cardiac bioelectric source is modeled (Wang 2012).

5.2. Reconstruction of Epicardial Potential

In many studies, the heart is removed from problem domain; instead, potential boundary conditions applied to the outer surface of the heart surface (epicardial potentials) that would impose the effect of the heart to the problem. (The epicardial potentials can be measured during open chest surgery on a patient or in experiments with animal hearts places in electrolytic tanks (Skipa 2004)). Calculation of the torso potentials from the prescribed epicardial potentials is a well-posed forward problem and involves solving Laplace's equation in the source-free volume between the torso and heart surface. Computation of epicardial potentials from torso potentials is the corresponding inverse problem. In actual ECG, torso potentials are measured at a limited number of points. Consequently, the inverse problem is usually formulated in such a way that the epicardial potentials in its entirety are predicted from torso potentials measured at a limited number of points. (Shahidi, Savard, and Nadeau 1994) (Y. Wang and Rudy 2006),(Yamashita 1981),(Tuboly, Kozmann, and Maros 2015),(D. Wang, Kirby, and Johnson 2009).

To tackle the inverse problem, we first subdivide the nodes of the FE mesh into three groups: a) All nodes on the epicardium, b) torso nodes where surface potentials are measured, c) the rest of the nodes. The value of the corresponding nodal potentials are collected in vectors $\mathbf{\Phi}_H$, $\mathbf{\Phi}_T$, and $\mathbf{\Phi}_R$, respectively. Then, the stiffness matrix $\mathbf{K}$ in Eq. (4.52) can be reordered and divide into submatrices. It can be rewritten as follows:

$$\begin{bmatrix} \mathbf{S}_{TT} & \mathbf{S}_{TR} & \mathbf{0} \\ \mathbf{S}_{RT} & \mathbf{S}_{RR} & \mathbf{S}_{RH} \\ \mathbf{0} & \mathbf{S}_{HR} & \mathbf{S}_{HH} \end{bmatrix} \begin{bmatrix} \mathbf{\Phi}_T \\ \mathbf{\Phi}_R \\ \mathbf{\Phi}_H \end{bmatrix} = \begin{bmatrix} \mathbf{0} \\ \mathbf{0} \\ \mathbf{0} \end{bmatrix} \tag{5.1}$$

Note that there is no source in the epicardial formulation and thus the global force vector $\mathbf{f}$ vanishes. There is no direct connections between the epicardial nodes and torso nodes, and therefore the submatrices $\boldsymbol{S}_{TH}$ and $\mathbf{S}_{HT}$ are zero in the above expression (Farina 2008b),(Shahidi, Savard, and Nadeau 1994),(Wang 2012). At this point, it is possible to presuppose that the available torso potentials $\mathbf{\Phi}_T$ can be imposed as essential boundary conditions in Eq. (5.2) and the system can be solved to obtain $\mathbf{u}_H$ and $\mathbf{u}_R$. However, due to the ill-conditioned nature of the problem, this would result to unrealistic, fluctuating potentials in $\mathbf{\Phi}_H$.

Instead, Eq. (5.2) is manipulated to directly relate the input to the output, i.e. $\mathbf{u}_T$ to $\mathbf{u}_H$, to give:

$$(\mathbf{S}_{TT} - \mathbf{S}_{TR}\mathbf{S}_{RR}^{-1}\mathbf{S}_{RT})^{-1}\mathbf{S}_{TR}\mathbf{S}_{RR}^{-1}\mathbf{S}_{RH}\mathbf{\Phi}_H = \mathbf{\Phi}_T \tag{5.2}$$

The coefficient matrix on the left hand side is called the *transfer matrix* $\mathbf{K}_T$:

$$\mathbf{K}_T = (\mathbf{S}_{TT} - \mathbf{S}_{TR}\mathbf{S}_{RR}^{-1}\mathbf{S}_{RT})^{-1}\mathbf{S}_{TR}\mathbf{S}_{RR}^{-1}\mathbf{S}_{RH} \tag{5.3}$$

Equation 5.2 can be now written as:

$$\mathbf{K}\boldsymbol{\Phi}_H = \boldsymbol{\Phi}_T \tag{5.4}$$

The linear system above is not a square system in general. If torso potentials are available at m nodes and the epicardial potentials are sought for at n nodes, then $\mathbf{K}_T$ is an $m \times n$ matrix, i.e. $\mathbf{K}_T \in \mathbb{R}^{m \times n}$. Since $n \neq m$ in practice, the system described by Eq. (5.4) is either an *underdetermined system* or an *overdetermined system* with differing number of unknowns and equations (Farina 2008b),(Farina 2008a),(Wang 2012). Furthermore, $\mathbf{K}_T$ is an ill-conditioned matrix. It is not possible to find a viable solution to Eq. (5.4) without applying some constraints, i.e. without regularization. Regularization methods will be discussed in Section 5.4.

5.3. Reconstruction of Transmembrane Potential

Traditional ECG diagnosis of myocardial ischemia, relying on human interpretation of the body-surface signals, has limited ability to localize ischemic regions. As myocardial ischemia can be characterized by the TMP's, reconstructing a whole-heart TMP map will promote the determination of the location and extent of ischemia (Wang 2012),(Cimponeriu, Starmer, and Bezerianos 2001),(Shaw 2002).

This inverse problem is typically formulated based on the bidomain heart model described in Section 4.3, in which the cardiac source is represented either by the myocardial TMP or the current density derived from it (Bjorn Fredrik Nielsen, Lysaker, and Grottum 2013),(Shaw 2002). Since torso potentials depend only on the TMP distribution at the same time instant, the inverse problem is formulated with the quasi-static form of the bidomain equation.

Since we are interested in modeling only the ST-segment shift, we take advantage of the fact that during the ST interval V_m is homogeneous throughout the heart and its value is different in ischemic and healthy tissue (MacLachlan et al. 2006),(Carmeliet 2017),(MacLeod et al. 2005),(Johnston 2005).

To produce realistic synthetic data for acute ischemia myocardium, we set the TMP during the ST interval to 0 mV in the healthy tissue and -30 mV in the ischemic tissue.(Wang 2012),(Li et al. 1998),(Jeroen G Stinstra, Hopenfeld, and Macleod 2004)

$$V_m(x) = \begin{cases} 0 \text{ mV}, & x \text{ in healthy tissue} \\ 30 \text{ mV}, & x \text{ in ischemic tissue} \end{cases} \tag{5.5}$$

Our complete mathematical model can be summarized as follows:

$$-\nabla \cdot (\sigma(x)\nabla\Phi(x)) = f(x), \qquad x \in \Omega \tag{5.6}$$

where

$$f(x) = \begin{cases} 0, & x \in T \\ \nabla.\sigma_i \nabla V_m(x), & x \in H \end{cases} \tag{5.7}$$

$$\Phi(x) = \begin{cases} \Phi & x \in T \\ \Phi_e & x \in H \end{cases} \tag{5.8}$$

$$\sigma(x) = \begin{cases} \sigma_T, & x \in T \\ \sigma_i + \sigma_e, & x \in H \end{cases} \tag{5.9}$$

$$(\sigma_T \nabla\Phi) \cdot \mathbf{n}_T = 0, \qquad on\ \partial T \tag{5.10}$$

$$\Phi_e = \Phi, \qquad on\ \partial H \tag{5.11}$$

$$(\sigma_e \nabla\Phi_e) \cdot \mathbf{n}_H = -(\sigma_T \nabla\Phi) \cdot \mathbf{n}_T, \qquad on\ \partial H \tag{5.12}$$

$$(\sigma_i \nabla \Phi_i) \cdot \mathbf{n}_H = (\sigma_i \nabla (V_m + \Phi_e)) \cdot \mathbf{n}_H = 0, \quad on\ \partial H \tag{5.13}$$

The integral form of Eq. (5.6) after applying the Galerkin method, Green's theorem, and the natural boundary conditions is given by:

$$\int_{\Omega} (\sigma(x) \nabla \Phi(x)).\nabla w(x) dx = -\int_{H} (\sigma_i \nabla V_m(x)).\nabla w(x) dx \tag{5.14}$$

where T represents the torso domain bounded between the heart surface and the body surface, H represents the heart domain, $\Omega = T \cup H$ is the entire domain, ∂T and ∂H are the boundaries of torso and heart surfaces, respectively (Wang 2012),(MacLachlan et al. 2007),(MacLachlan, Sundnes, and Lines 2005),(Ruud et al. 2009)(MacLachlan et al. 2006),(Bjørn Fredrik Nielsen, Lysaker, and Tveito 2007).

We can rewrite Eq. (5.14) in matrix form as follows:

$$\begin{bmatrix} \mathbf{S}_{TT} & \mathbf{S}_{TR} & \mathbf{0} \\ \mathbf{S}_{RT} & \mathbf{S}_{RR} & \mathbf{S}_{RH} \\ \mathbf{0} & \mathbf{S}_{HR} & \mathbf{S}_{HH} \end{bmatrix} \begin{bmatrix} \mathbf{\Phi}_T \\ \mathbf{\Phi}_R \\ \mathbf{\Phi}_H \end{bmatrix} = \begin{bmatrix} \mathbf{0} \\ \mathbf{0} \\ \mathbf{M}\mathbf{\Phi}_H \end{bmatrix} \tag{5.15}$$

Note that a source can exist only in the heart domain. Hence, the FE representation of the source term (the right hand side of Eq. (5.14)) can be expressed using heart potentials as $\mathbf{M}\mathbf{\Phi}_H$.

$$\Phi_T = (\mathbf{S}_{HR}\mathbf{S}_{RR}^{-1}\mathbf{S}_{RT})^{-1}(\mathbf{S}_{HH} - \mathbf{S}_{HR}\mathbf{S}_{RR}^{-1}\mathbf{S}_{RH} - \mathbf{M})\mathbf{\Phi}_H \tag{5.16}$$

5.4. Regularization Methods

In the inverse problem of ECG, we solve the ill-posed system:

$$\mathbf{K}_T\mathbf{\Phi}_H = \mathbf{\Phi}_T$$

that represents either Eq. (5.2) or Eq.(5.16).

Regularization towards an efficient and meaningful solution of the above equation has been one of the main research areas of computational cardiac research. Tikhonov(Shahidi, Savard, and Nadeau 1994), (Rudy and Oster 1997), Kalman filter (Berrier, Sorensen, and Khoury 2004) , generalized eigensystem, Truncated total least squares (Throne, Olson, and Hrabik 1999), (Shou et al. 2008) TSVD, and Total Variation regularization (Wang 2012) are some of the commonly used methods in the inverse problem of ECG.

Ill-conditioned systems, that are highly sensitive to changes in their input, appear in many problems of physical sciences. For the sake of notational simplicity, let us write the above linear system in a more familiar way as:

$$\mathbf{Ax} = \mathbf{b} \tag{5.17}$$

where $\mathbf{x} \in \mathbb{R}^n$ and $\mathbf{b} \in \mathbb{R}^m$ represent the nodal value vectors of epicardial potentials Φ_H and the torso potentials Φ_T , respectively, and $\mathbf{A} \in \mathbb{R}^{m\times n}$ is the ill-conditioned transfer matrix. In our problem, $m \geq n$ and the resulting system is overdetermined. The solution of this overdetermined system is sought by solving the linear least-squares minimization problem associated with the linear system

$$\min\|\mathbf{Ax} - \mathbf{b}\| \tag{5.18}$$

where the symbol $\| \ \|$ indicates the L^2 norm of the equation residuals. As mentioned before, small numerical changes in the entries of **A** and/or **b** causes disproportionately large changes in **x**. In order to be able to obtain a physically meaningful solution to the linear system from Eq. (5.18), a constraint has to be

enforced to the entries of **x** (i.e. to the solution) such that they do not behave chaotically. This is what is referred to as regularization in the literature.

5.4.1. Pseudo-Inverse Matrix

Matrix inverse is defined for square matrices. Given an $m \times n$ non-square matrix **A**, a *generalized inverse* (or a *Moore-Penrose inverse* or a *pseudoinverse*) of matrix **A** is a unique $n \times m$ matrix $\mathbf{A}^{\dagger}$ which can be expresses through the following derivation (Grandin 1986a),(Mueller and Siltanen 2012).

$$\begin{aligned} &\mathbf{A}\mathbf{x} = \mathbf{b} \\ &\mathbf{A}^T(\mathbf{A}\mathbf{x}) = \mathbf{A}^T\mathbf{b} \\ &\mathbf{x} = (\mathbf{A}^T\mathbf{A})^{-1}\mathbf{A}^T\mathbf{b} \\ &\mathbf{A}^{\dagger} = (\mathbf{A}^T\mathbf{A})^{-1}\mathbf{A}^T \end{aligned} \tag{5.19}$$

If the columns of **A** is linearly independent such that $m \geq n$, then $\mathbf{A}^T\mathbf{A}$ is invertible. Therefore we can decompose **A** and $\mathbf{A}^{\dagger}$ with the so-called *singular value decomposition* (SVD) to use them in regularization process.

5.4.2. The Singular Value Decomposition

Let $\mathbf{A} \in \mathbb{R}^{m \times n}$ be a rectangular matrix with $m \geq n$ Then, SVD of **A** is a decomposition of the form

$$\mathbf{A} = \mathbf{U}\mathbf{D}\mathbf{V}^T = \sum_{i=1}^{P} \mathbf{u}_i \sigma_i \mathbf{v}_i^T,\ P = rank(\mathbf{A}) = \min(m, n) \tag{5.20}$$

where $\mathbf{U} = (\mathbf{u}_1, \mathbf{u}_2, \dots, \mathbf{u}_m) \in \mathbb{R}^{m \times m}$ and $\mathbf{V} = (\mathbf{v}_1, \mathbf{v}_2, \dots, \mathbf{v}_n) \in \mathbb{R}^{n \times n}$ are matrices with orthonormal columns, $\mathbf{U}^T\mathbf{U} = \mathbf{V}^T\mathbf{V} = \mathbf{I}_n$ and where

$\mathbf{D} = diag(\sigma_1, \sigma_2, ..., \sigma_n) \in \mathbb{R}^{m \times n}$ has non-negative diagonal elements appearing in non-increasing order such that

$$\sigma_1 \geq \sigma_2 \geq ... \geq \sigma_n \geq 0 \tag{5.21}$$

The numbers symbolized by σ_i are the singular values of **A** while the vectors $\mathbf{u}_i$ and $\mathbf{v}_i$ are the left and right singular vectors of **A**, respectively. The condition number of **A** is equal to the ratio $\frac{\sigma_1}{\sigma_n}$ (Johnson and MacLeod 2012),(Wu et al. 2013),(Engl, Hanke, and Neubauer 1996),(Groetsch and Groetsch 1993).

The *rank* of a matrix is defined as the maximum number of linearly independent rows (or equivalently columns) in the matrix. For an $m \times n$ matrix, the maximum possible value for *rank(***A***)* is min(m,n).

If $m > n$ then

$$\mathbf{D} = \begin{bmatrix} \sigma_1 & 0 & \cdots & 0 \\ 0 & \sigma_2 & \cdots & 0 \\ \vdots & & \ddots & \\ 0 & \cdots & \cdots & \sigma_n \\ 0 & \cdots & \cdots & 0 \\ \vdots & & & \\ 0 & \cdots & \cdots & 0 \end{bmatrix} \tag{5.22}$$

And in the case $n > m$ the matrix D takes the form

$$\mathbf{D}=\begin{bmatrix}\sigma_1 & 0 & \cdots & 0 & 0 & \cdots & 0\\ 0 & \sigma_2 & & \vdots & \vdots & & \vdots\\ \vdots & & \ddots & \vdots & \vdots & & \vdots\\ 0 & \cdots & \cdots & \sigma_m & 0 & \cdots & 0\end{bmatrix} \tag{5.23}$$

According to the definition of pseudo-inverse matrix

$$\mathbf{A}^{\dagger}=\mathbf{V}\mathbf{D}^{\dagger}\mathbf{U}^{T}=\sum_{i=1}^{Rank(A)}\frac{\mathbf{v}_i\mathbf{u}_i^{T}}{\sigma_i} \tag{5.24}$$

$$\mathbf{D}^{\dagger}=diag(\frac{1}{\sigma_1},\frac{1}{\sigma_2},...,\frac{1}{\sigma_n}) \tag{5.25}$$

$$\mathbf{D}=\begin{bmatrix}\frac{1}{\sigma_1} & 0 & \cdots & 0\\ 0 & \frac{1}{\sigma_2} & \cdots & 0\\ \vdots & & \ddots & \\ 0 & \cdots & \cdots & \frac{1}{\sigma_n}\\ 0 & \cdots & \cdots & 0\\ \vdots & & & \\ 0 & \cdots & \cdots & 0\end{bmatrix} \tag{5.26}$$

So,

$$\mathbf{x} = \mathbf{A}^{\dagger}\mathbf{b} = \sum_{i=1}^{Rank(A)} (\frac{\mathbf{v}_i \mathbf{u}_i^T}{\sigma_i})\mathbf{b} \tag{5.27}$$

5.4.3. Truncated Singular Value Decomposition

TSVD approximation of **A** will effectively ignore the smallest singular values. Consider the best rank *k* approximation of **A** with respect to the Euclidean norm. It is given by the sum of the first *k* rank-one matrices in the SVD, i.e.

$$\mathbf{A}_k = \mathbf{U}\mathbf{D}_k\mathbf{V}^T = \sum_{i=1}^{k} \mathbf{u}_i \sigma_i \mathbf{v}_i^T \tag{5.28}$$

For $k < rank(\mathbf{A})$, The TSVD method gives the approximate solutions of Eq.(5.27) in the form

$$\mathbf{x}_k = \mathbf{A}_k^{\dagger}\mathbf{b} = (\mathbf{V}\mathbf{D}_k^{\dagger}\mathbf{U}^T) = \sum_{i=1}^{k} (\frac{\mathbf{v}_i \mathbf{u}_i^T}{\sigma_i})\mathbf{b} \tag{5.29}$$

Where $\mathbf{x}_k$ is the vector that satisfies Eq.(5.18). In other words:

$$\mathbf{x}_k = \left(\mathbf{x} \,\middle|\, \min \|\mathbf{A}\mathbf{x} - \mathbf{b}\|\right) \tag{5.30}$$

5.4.4. Tikhonov Regularization

This regularization method replaces the minimization problem given in Eq. (5.18) by the penalized least squares problem (Hou and Jin 1997),(Chamorro-Servent, Dubois, and Coudière 2018),(Johnston Peter R. 2018)

$$\min\left\{\|\mathbf{A}\mathbf{x} - \mathbf{b}\|^2 + \alpha^2 \|\mathbf{L}\mathbf{x}\|^2\right\} \tag{5.31}$$

Matrix **L** is termed the regularization matrix and used to incorporate *a priori* information into the solution. The *regularization pa*rameter α is a weight term that

adjusts the contribution of the regularization term $\|\mathbf{Lx}\|^2$ to the minimized functional (Oster and Rudy 1992),(Rudy and Oster 1997),(Wu et al. 2013),(Cheng, Bodley, and Pullan 2003),(Tuboly, Kozmann, and Maros 2015).

Two choices of **L** used in this work are:

i. the unit matrix **I**;

$$\mathbf{L} = \mathbf{I} = \begin{bmatrix} 1 & 0 & \cdots & 0 \\ 0 & 1 & \cdots & 0 \\ \vdots & \vdots & \ddots & \vdots \\ 0 & 0 & \cdots & 1 \end{bmatrix}$$

ii. the discrete first order derivative operator;

$$\mathbf{L} = \begin{bmatrix} -1 & 1 & 0 & \cdots & 0 \\ 0 & -1 & 1 & \cdots & 0 \\ \vdots & \vdots & \ddots & & \vdots \\ & & \ddots & \ddots & \\ 0 & \cdots & & -1 & 1 \end{bmatrix}$$

The corresponding regularization methods are called 0^{th} and 1^{st} order Tikhonov regularization, respectively.

The pseudo-inverse of **A** in this method is given by

$$\mathbf{A}_\alpha^\dagger = (\mathbf{A}^T\mathbf{A} + \alpha^2\mathbf{L}^T\mathbf{L})^{-1}\mathbf{A}^T \tag{5.32}$$

So,

$$\mathbf{x}_\alpha = \mathbf{A}^\dagger\mathbf{b} \tag{5.33}$$

When the SVD of **A** is available, we see that the solution vector $\mathbf{x}_\alpha$ can be expressed as

$$\mathbf{x}_\alpha = \mathbf{V}(\mathbf{D}^2 + \alpha^2\mathbf{L}^T\mathbf{L})^{-1}\mathbf{D}\mathbf{U}^T\mathbf{b} \tag{5.34}$$

If we insert the singular values and vectors, we get

$$\mathbf{x}_\alpha = \sum_{i=1}^{n}(\mathbf{v}_i(\frac{\sigma_i}{\sigma_i^2 + \alpha_i^2})\mathbf{u}^T)\mathbf{b} \tag{5.35}$$

5.4.5. Mean Value Regularization

While epicardial potentials change across the epicardium of the heart, no major fluctuations are expected in their values. Hence, another possible constraint could be forcing the values in **x** as close to their mean value as possible. To enforce this constraint **L** should be defined in such a way that:

$$\|\mathbf{L}\mathbf{x}\| = (x_1 - x_{ave})^2 + (x_2 - x_{ave})^2 + \cdots + (x_n - x_{ave})^2 \tag{5.36}$$

which can be achieved if **L** is chosen as:

$$\mathbf{L} = \begin{bmatrix} 1-\frac{1}{n} & -\frac{1}{n} & \cdots & -\frac{1}{n} \\ -\frac{1}{n} & 1-\frac{1}{n} & \cdots & -\frac{1}{n} \\ \vdots & \vdots & \ddots & \vdots \\ -\frac{1}{n} & -\frac{1}{n} & \cdots & 1-\frac{1}{n} \end{bmatrix}$$

5.4.6. Choice of Regularization Parameter

For the majority of methods discussed above, the regularization parameter sets the balance between the residual term and the regularization term (Skipa 2004). It determines how close the regularized inverse $\mathbf{A}^{\dagger}$ approximates the pseudoinverse of **A**.

In TSVD solution, there would be an optimum number of σ's chosen for a given α that will minimize the difference between estimated $\mathbf{x}_k$ and experimental (exact) **x,** i.e. $\left\|\mathbf{x}_{exact} - \mathbf{x}_k\right\|$ (Fig. 5.1). Similarly, for a given number of σ's, regularization parameter α has also an optimal value (Fig. 5.2).

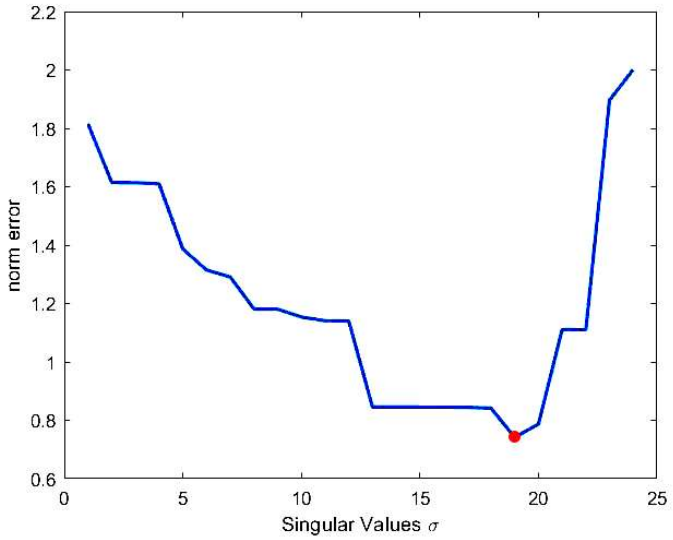


Figure 5.1. Number of singular values σ versus error norm for a given α. The optimal σ value is indicated with a dot.

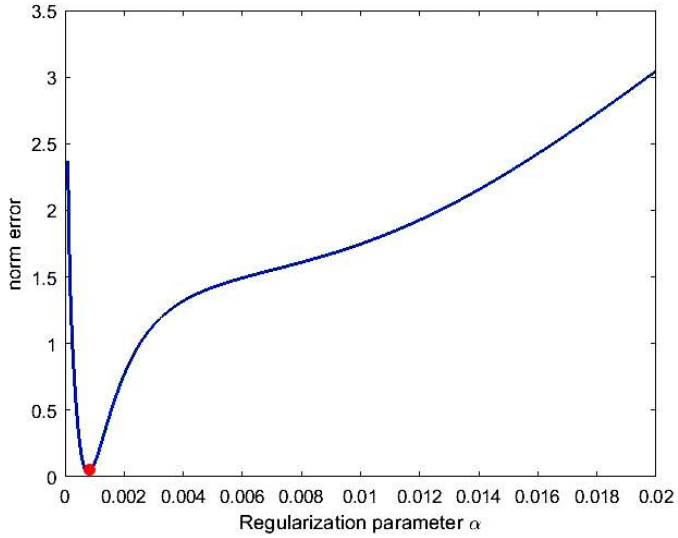


Figure 5.2. α versus error norm for a given number of singular values σ. The optimal value is indicated with a dot.

6. AN ITERATIVE OPTIMIZATION METHOD FOR THE INVERSE PROBLEM

6.1. Introduction

In many engineering optimization problems, the quantity that is to be optimized can be assumed to have a functional form. That way, a *parameterization* is enforced to the quantity of interest, since the functional form will have certain undetermined coefficients that will act as *parameters*. The simplest example of this approach is statistical regression, where a simple functional relation is assumed between dependent and independent variables. Then, the coefficients of the functions are optimized by minimizing the error between the assumed function and the experimental observations.

In FE method, the relation between the FE input (geometry, material properties, boundary conditions etc.) and the FE output (nodal solutions) is typically very complex. *Finite element optimizition* can be used to determine the input that will produce a specific output. This method is frequently applied in the material property estimation or topology optimization in mechanical structures.

6.2. Finite Element Optimization Based on Sensitivity Analysis

To apply FE optimization to the inverse problem of ECG (i.e. to the localization of the ischemic region), TMP distribution should be parameterized and optimization should be applied with respect to these parameters.

We have assumed a continuous TMP that can be expressed as

$$\begin{aligned} V_m = A\,&[-\arctan(B(x-a)) + \arctan(B(x-b))] \\ &\cdot[-\arctan(B(y-c)) + \arctan(B(y-d))] \end{aligned} \tag{6.1}$$

The defined function takes a value of 0 mV everywhere except a rectangular region where it smoothly decreases to -30 mV (Fig. 6.1). This region signifies the ischemic region in the heart, and its size and location depends continuously on the parameter a, b, c and d of the function. The factor A is adjusted such that the minimum value of the function is equal to -30. (The value of A changes with the values of a, b, c and d.) The multiplier B is chosen such that the transition from 0 to -30 occurs within the transition distance H. For H=1 mm, B is approximately equal to 35. Assuming a functional form prevents V_m from fluctuating. In other words, enforcing V_m to take a certain functional form regularizes this quantity.

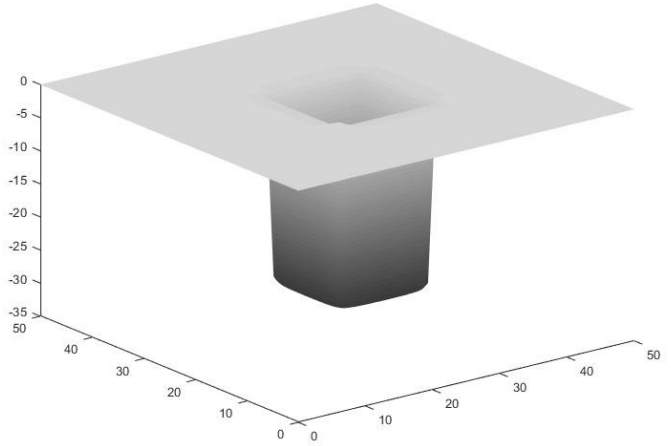


Figure 6.1. Transmembrane potential function.

Let **e** denote the vector of given torso potentials in the inverse analysis and **y** indicate the torso potentials estimated by the FE simulation. The outcome of the FE simulation will depend on the values parameters a, b, c and d. used in the FE run.

$$\mathbf{y} = \mathbf{y}(a,b,c,d) \tag{6.2}$$

The *objective function* is a measure of the difference between the experimental and estimated torso potentials can be written as

$$J = J(\mathbf{e}, \mathbf{y}(a,b,c,d)) \tag{6.3}$$

In general, the relation between **y** and *a, b, c* and *d* is nonlinear, independent from the linearity of the problem. Hence, to find the minimum value of the objective function an iterative scheme is required.

6.2.1. Objective Function Minimization

Let **p** be the vector that contains the optimized parameters *a, b, c* and *d*. The simplest objective function simply sums the square of the error for each torso potential and can be expressed as:

$$J = (\mathbf{e} - \mathbf{y}(\mathbf{p}))^T (\mathbf{e} - \mathbf{y}(\mathbf{p})) \tag{6.4}$$

Since the objective function depends continuously to parameters in **p**, a gradient method can be devised for the minimization of the objective function. We have taken the variation of the objective function with respect to an infinitesimal change in the material property vector **p** and set it to zero, an obvious way to find a the extremum of a function.

The variation of Eq. (6.4) with respect to a variation in **y** can be expressed as:

$$\delta J = (\delta \mathbf{y}(\mathbf{p}))^T (\mathbf{e} - \mathbf{y}) + (\mathbf{e} - \mathbf{y})^T (\delta \mathbf{y}(\mathbf{p})) = 0 \tag{6.5}$$

Using the variation in the parameters **p**, the vector δ**y** can be written as:

$$\delta \mathbf{y}(\mathbf{p}) = \frac{\partial y(\mathbf{p})}{\partial \mathbf{p}} \partial \mathbf{p} = \mathbf{S} \delta \mathbf{p} \tag{6.6}$$

S is called the *sensitivity matrix* and describes the change in the FE simulation output **y** with respect to a change in **p**. Substituting Eq. (6.6) into Eq. (6.5) gives:

$$\delta J = (\mathbf{S}\delta\mathbf{p})^T(\mathbf{e}-\mathbf{y}(\mathbf{p})) + (\mathbf{e}-\mathbf{y}(\mathbf{p}))^T(\mathbf{S}\delta\mathbf{p}) = 0 \tag{6.7}$$

Since J is a scalar, both terms of the above matrix expression are equal to each other, which allows Eq.(6.7) to be written as:

$$\delta J = \delta\mathbf{p}^T\mathbf{S}^T(\mathbf{e}-\mathbf{y}(\mathbf{p})) = 0 \tag{6.8}$$

Since $\delta\mathbf{p}$ is arbitrary, the above equation holds only if

$$\mathbf{r}(\mathbf{p}) = \mathbf{S}^T(\mathbf{e}-\mathbf{y}(\mathbf{p})) = \mathbf{0} \tag{6.9}$$

Here $\mathbf{r}(\mathbf{p})$ is the residual which approaches $\mathbf{0}$ as predicted potentials **y** approaches the actual potentials **e**. Equation (6.9) represents a nonlinear system of equations in **p**, whose solution minimizes the objective function J. The system is solved through Newton-Raphson iteration. If $\mathbf{p}_k$ is the estimate of **p** obtained at the kth iteration, the system is linearized at $\mathbf{p}=\mathbf{p}_k$ as:

$$\left.\frac{\partial\mathbf{r}}{\partial\mathbf{p}}\right|_{\mathbf{p}=\mathbf{p}_k} \delta\mathbf{p}_{k+1} = -\mathbf{r}(\mathbf{p}_k) \tag{6.10}$$

The above system is setup using $\mathbf{p}_k$ and its solution gives the correction term $\delta\mathbf{p}_{k+1}$ which is used to update $\mathbf{p}_k$ to obtain $\mathbf{p}_{k+1}$. If the scheme is convergent, the norm of the residual $\mathbf{r}(\mathbf{p}_k)$ should eventually vanish.

Differentiating Eq. (6.9) with respect to **p** gives

$$\frac{\partial \mathbf{r}(\mathbf{p})}{\partial \mathbf{p}} = (\boldsymbol{S}_k)^T (-\frac{\partial \boldsymbol{y}}{\partial \mathbf{p}})_k + \left(\frac{\partial (\boldsymbol{S}^T)}{\partial \mathbf{p}} \right)_k (\mathbf{e} - \mathbf{y}(\mathbf{p}_k)) \tag{6.11}$$

Recalling that $\mathbf{S} = \frac{\partial \mathbf{y}}{\partial \mathbf{p}}$ by definition, Eq.(6.11) can be written as:

$$\frac{\partial \mathbf{r}(\mathbf{p})}{\partial \mathbf{p}} = (\mathbf{S}_k)^T \mathbf{S}_k + \left(\frac{\partial (\mathbf{S}^T)}{\partial \mathbf{p}} \right)_k (\mathbf{e} - \mathbf{y}(\mathbf{p})_k) = \mathbf{0} \tag{6.12}$$

The change of sensitivity matrix with respect to **p**, i.e. $\frac{\partial \boldsymbol{S}}{\partial \mathbf{p}}$, is a second order term and usually ignored to decrease computational complexity of the iterative scheme. Since the scheme described by Eq.(6.9) is iterative, it will still converge to the correct value with this simplification as long as residual **r**(**p**) is exactly evaluated. With this consideration, the linearized system of Eq.(6.10) can be written as

$$[(\boldsymbol{S}_k)^T \boldsymbol{S}_k](\delta \mathbf{p}_{k+1}) = (\boldsymbol{S}_k)^T (\mathbf{e} - \mathbf{y}(\mathbf{p})_k) \tag{6.13}$$

Once the system is solved, the current estimate for the ischemic region parameters $\mathbf{p}_k$ is updated as

$$\mathbf{p}_{k+1} = \mathbf{p}_k + \delta \mathbf{p}_{k+1} \tag{6.14}$$

and the procedure is repeated again.

If torso potentials are estimated at *n* points, then the sensitivity matrix $\mathbf{S} = \frac{\partial \boldsymbol{y}(\mathbf{p})}{\partial \mathbf{p}}$ for our problem will be:

$$\mathbf{S} = \begin{bmatrix} \frac{\partial y_1}{\partial a} & \frac{\partial y_2}{\partial a} & \cdots & \frac{\partial y_{n-1}}{\partial a} & \frac{\partial y_n}{\partial a} \\ \frac{\partial y_1}{\partial b} & \frac{\partial y_2}{\partial b} & \cdots & \frac{\partial y_{n-1}}{\partial b} & \frac{\partial y_n}{\partial b} \\ \frac{\partial y_1}{\partial c} & \frac{\partial y_2}{\partial c} & \cdots & \frac{\partial y_{n-1}}{\partial c} & \frac{\partial y_n}{\partial c} \\ \frac{\partial y_1}{\partial d} & \frac{\partial y_2}{\partial d} & \cdots & \frac{\partial y_{n-1}}{\partial d} & \frac{\partial y_n}{\partial d} \end{bmatrix}$$

where y_l indicate the FE outcome for torso potentials at the n nodes. The derivative terms in the above matrix are evaluated numerically by changing each time one of the parameters (a, b, c or d) slightly, running the FE simulation with this set of parameters, observing the change in y_l values and calculating $\frac{\Delta y_l}{\Delta p_m}$ for the parameter p_m. Each FE run will produce one row of the above matrix.

6.3. Programming of the Inverse Problem of Electrocardiography

As we discussed in Section 4.8, a general FE code was written to solve the forward problem in Python language. The FE optimization procedure is an iterative procedure which runs the related FE code which was written in the forward problem, calculates the sensitivity after every FE run and updates the material properties for the next FE run. This iteration is repeated until the objective function takes a minimum value. The optimization scheme is schematically described in (Fig. 6.1).

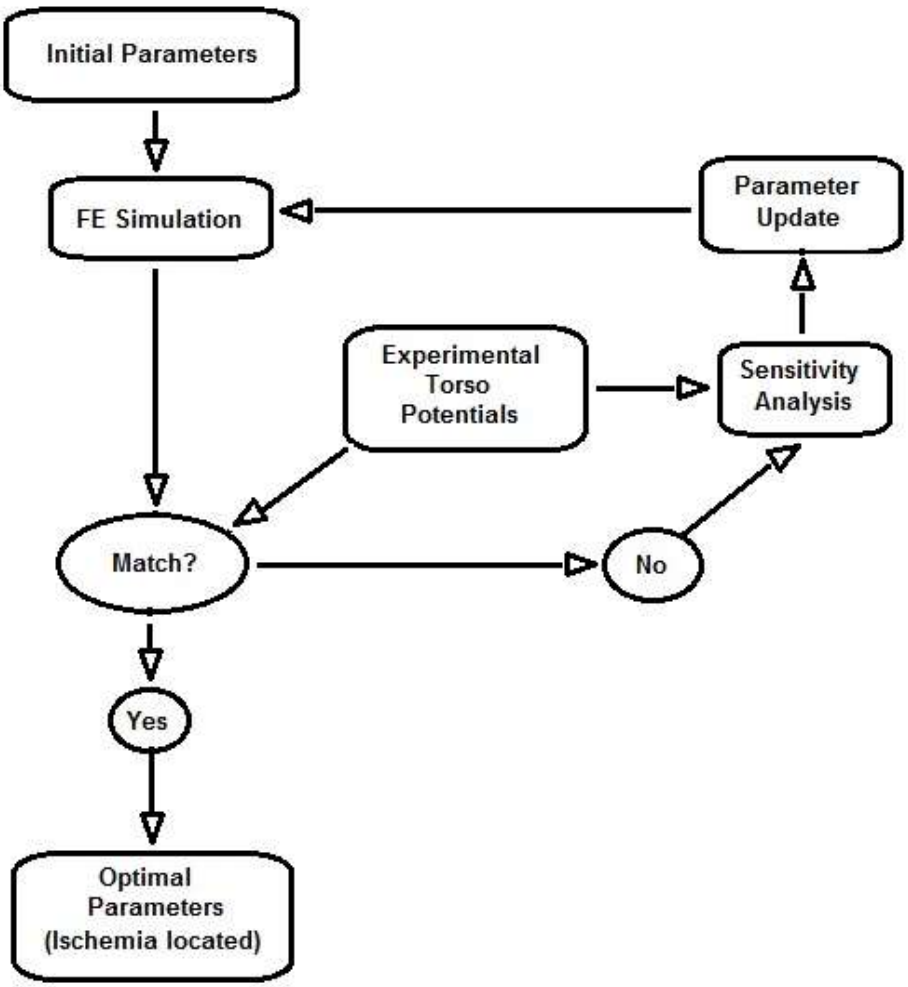


Figure 6.2. Optimization Algorithm Scheme.

6. AN ITERATIVE OPTIMIZATION METHOD FOR THE INVERSE PROBLEM

Hamed KAGHAZCHI

7. RESULTS

7.1. Introduction

The two-dimensional model is manipulated to create epicardial and full models both with homogeneous and inhomogeneous versions. The models are separately meshed using the mesh generator tool of COMSOL package. The resulting mesh data are transferred to our Python code. In all meshes, the torso potentials are measured/enforced at 29 nodes that correspond to the locations of pericardial leads in standard ECG. In epicardial simulations, the epicardial potentials are measured/enforced at 24 nodes (Fig. 7.1).

7.2. Forward Problem Examples

We have solved the forward problem in two different configuration.

The first one involves estimating the torso potentials from known epicardial potentials. The problem is solved first by assuming a homogeneous torso model with an average conductivity assigned to the entire torso without distinguishing different tissues. Then, the same problem is solved with an inhomogeneous torso model where different tissue are distinguished by assigning them the appropriate conductivities Table (4.3). The imposed epicardial potentials are taken from the literature (Wang 2012). The objective of these examples are to test the coded FE program and to create pseudo-experimental data to be used in the inverse analyses. The testing of the code has been accomplished by comparing its results with those obtained from COMSOL package.

In the second configuration, the torso model includes the heart and its blood-filled chambers, and inhomogeneity is taken into account by distinguishing different types of tissues table (4.3). To fulfill one of the main objectives of this dissertation work, examples are run with ischemic (unhealthy) and healthy conductivity values to assess the effect of ischemic conductivity on the torso potentials. Furthermore, the effect of anisotropic conductivity per Eq. (4.55) has been also evaluated by

comparing the results of anisotropic conductivity with those obtained with isotropic conductivity.

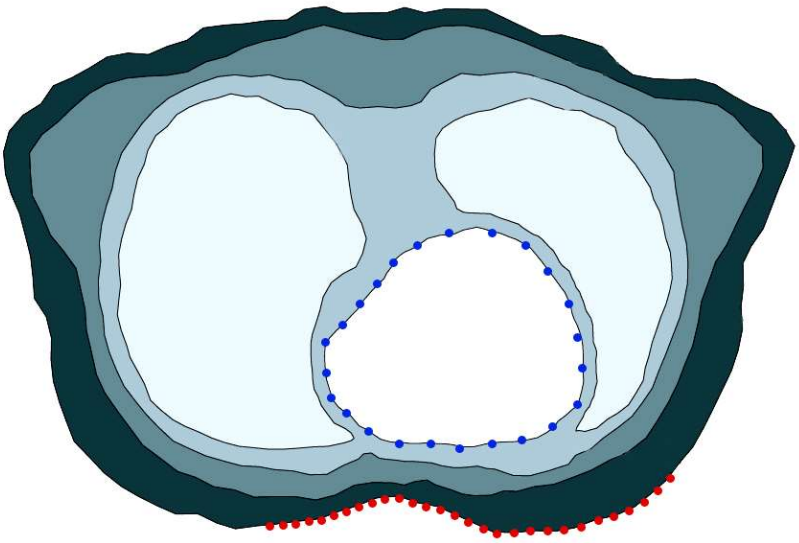


Figure 7.1. Inhomogeneous torso model with epicardial potential nodes shown with blue nodes and torso potential nodes shown with red nodes.

7.2.1. Results of the Homogeneous Torso Model

This problem is used to test the correctness of the developed code. The same simulation has been run both on the developed code and the COMSOL package using

the same mesh and enforcing the same epicardial potential boundary conditions (Fig. 7.2).

The results of our code on the entire mesh (Fig. 7.3), specifically on the torso nodes (Fig. 7.4) match perfectly with the COMSOL results.

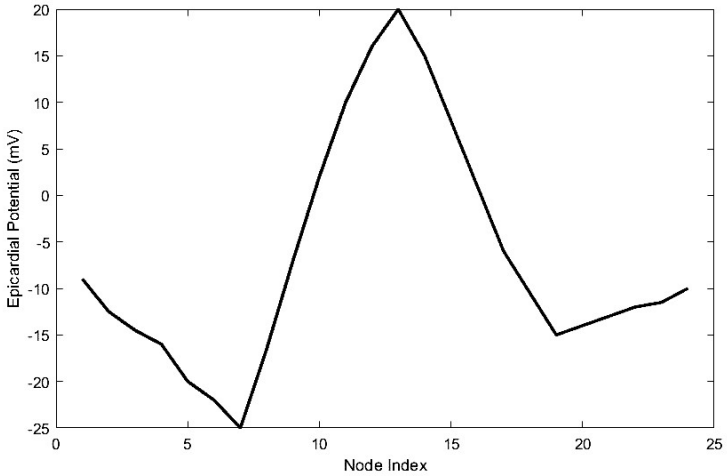


Figure 7.2. Potentials enforced at 24 epicardial nodes in the forward problem simulations (Taken from(Wang 2012)).

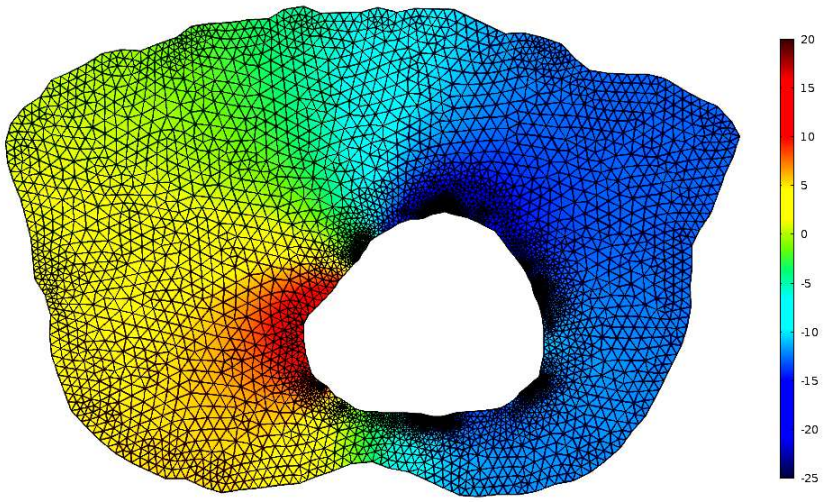


Figure 7.3. Potentials (mV) in homogeneous torso model. The mesh has 4299 nodes and 8154 elements.

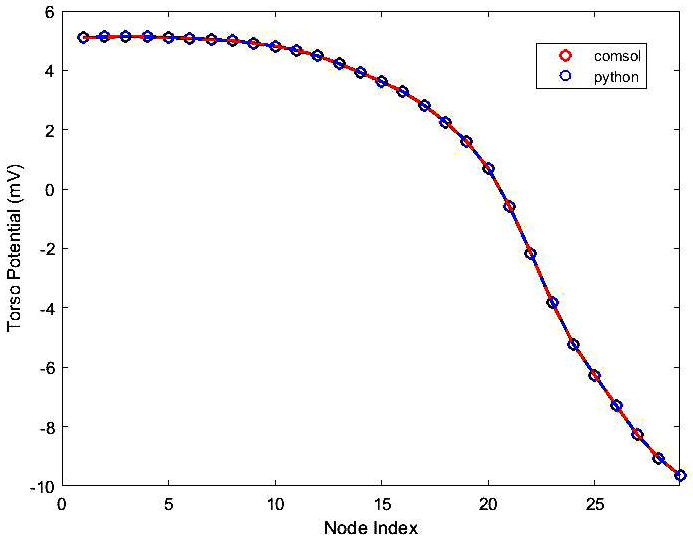


Figure 7.4. Torso surface potentials that is obtained from homogeneous torso model.

7.2.2. Results of the Inhomogeneous Torso Model

The same comparison is made using the same epicardial potentials as boundary conditions (Fig. 7.2) with an inhomogeneous model (Fig. 4.4) where proper conductivity values are assigned to different tissues.

It is observed that the results obtained from our code and COMSOL package, again, match perfectly on the entire mesh Fig. (7.5) including the torso nodes (Fig. 7.6).

These simulations has demonstrated that the developed FE code runs correctly.

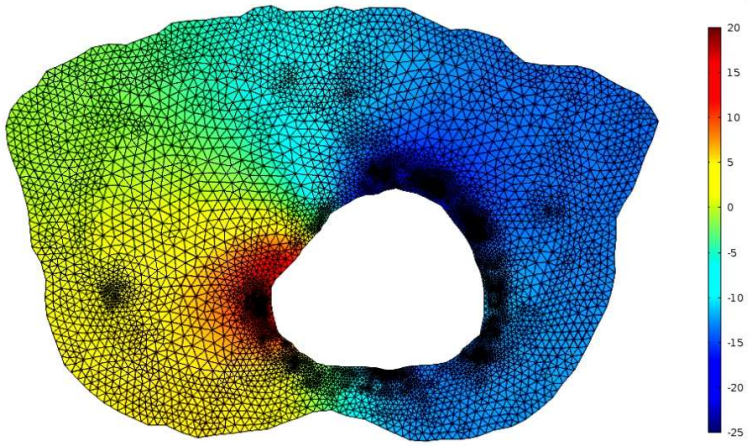


Figure 7.5. Potentials (mV) in inhomogeneous torso model. The mesh has 6128 nodes and 11871 elements.

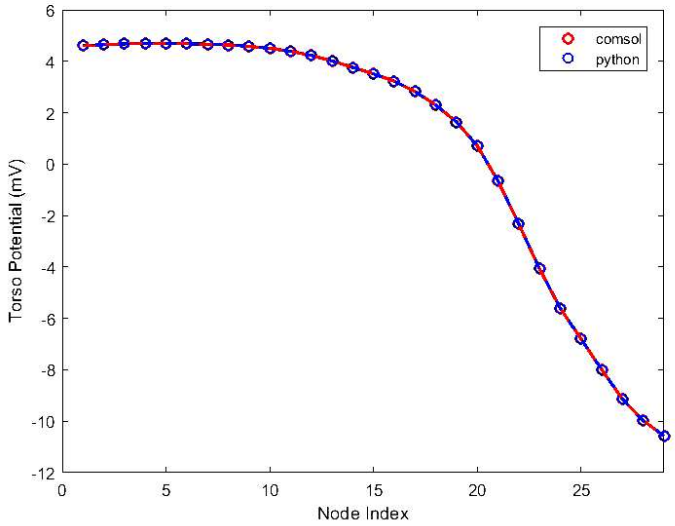


Figure 7.6. Torso surface potentials that is obtained from inhomogeneous torso model.

7.2.3. Results of Inhomogeneous Torso, Isotropic, and Anisotropic Heart

An ischemic region is created in three different spots in the heart and a membrane potential of -30 mV is applied to this region. The region acts as a source and creates nonzero torso potentials (Fig. 7.7). We will refer to these cases as "Ischemia 1", "Ischemia 2" and "Ischemia 3".

The heart and the ischemic regions are assumed to have different but isotropic conductivities. For both healthy and ischemic tissues, the isotropic conductivities are taken to be equal to the longitudinal conductivity values given on Tables 4.1 and 4.2. The resulting potentials are compared with those obtained with healthy conductivities imposed to the whole heart including the ischemic region. The example is repeated then with anisotropic conductivities both in the heart and the ischemic region. (Recall that, in the existing literature, ischemia has been imposed

only through ischemic membrane potential and conductivity change with ischemia has never been taken into consideration.)

In the first example (Ischemia 1), the results have shown that taking ischemic conductivity into account increases the magnitude of the measured torso potentials both in isotropic case (Fig. 7.8) and anisotropic case (Fig. 7.9). the difference seems significant in the anisotropic case.

In the next example (Ischemia 2), an ischemic region is created again in the right ventricle but closer to the posterior side of the chest (Fig. 7.10). A similar comparison is made as in the first example. Since the ischemic region in this example is closer to the nodes where torso potentials are measured, the measured potentials are larger in magnitude. Taking the ischemic conductivity into account seems to make a difference in this example as well. While the difference in measured potentials is relatively small in the isotropic case (Fig. 7.11), it is significantly higher in the anisotropic case (Fig. 7.12).

The third example (Ischemia 3) involves an ischemic region on the left ventricle (Fig. 7.13). the observations we have made for this example is the same as the previous two examples (Figs. 7.14-7.15).

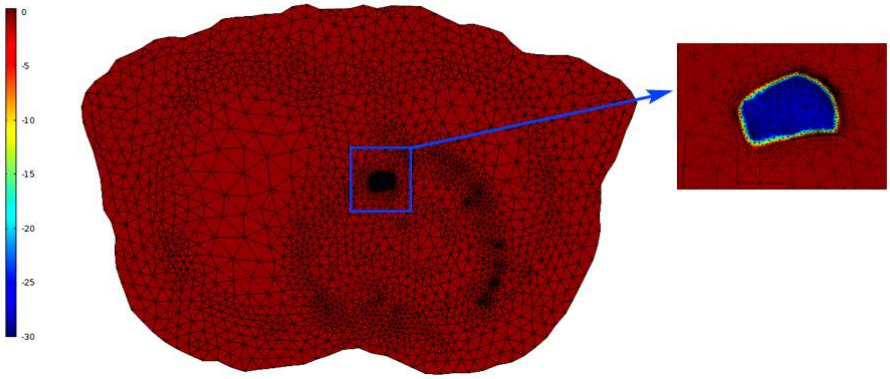


Figure 7.7. Inhomogeneous torso model, isotropic heart conductivity and ischemic region on the top of left ventricle (Ischemia 1). The mesh has 3181 nodes and 6252 elements.

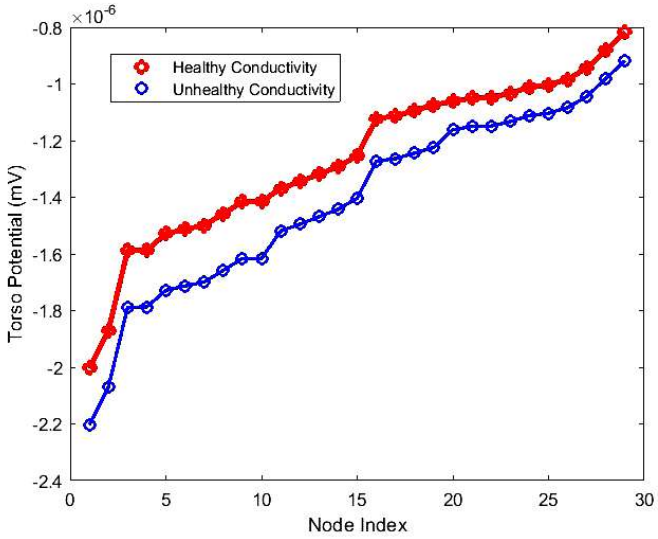


Figure 7.8. Change of torso potentials with isotropic heart tissue, healthy, and unhealthy conductivities. (Ischemia 1)

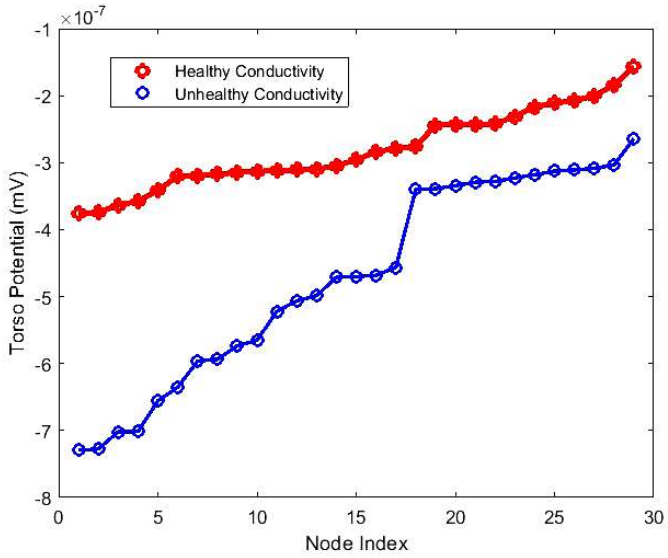


Figure 7.9. Change of torso potentials with anisotropic heart tissue, healthy, and unhealthy conductivities (Ischemia 1).

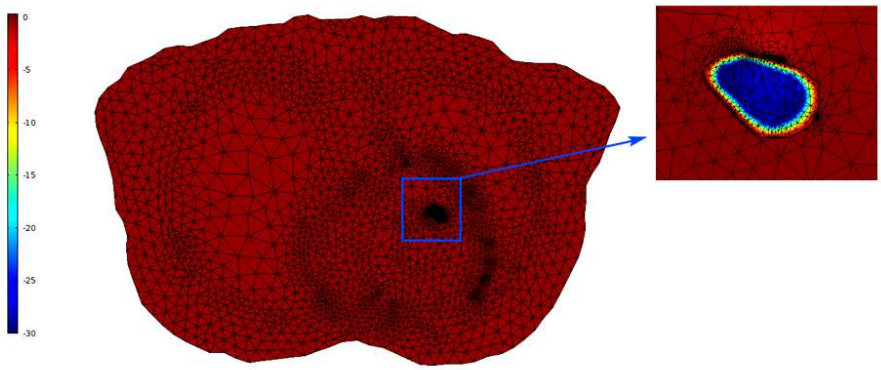


Figure 7.10. Inhomogeneous torso model, isotropic heart conductivity and ischemic region on the right hand side of left ventricle (Ischemia 2). The mesh has 4641 nodes and 9172 elements.

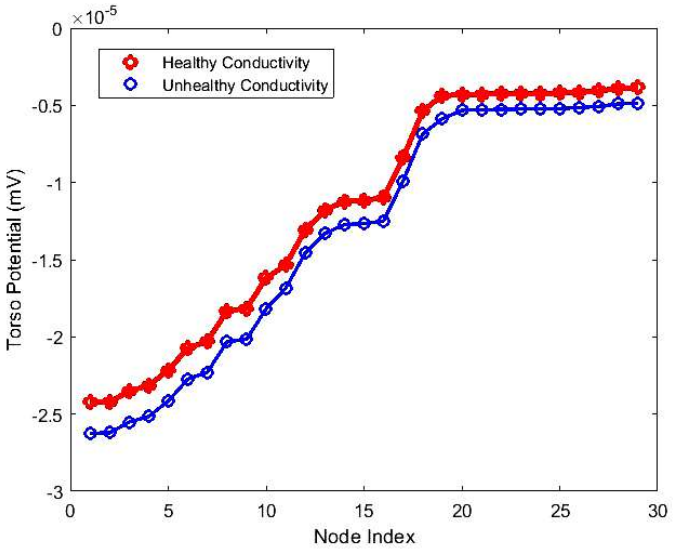


Figure 7.11. Change of torso with isotropic heart tissue, healthy, and unhealthy conductivities (Ischemia 2).

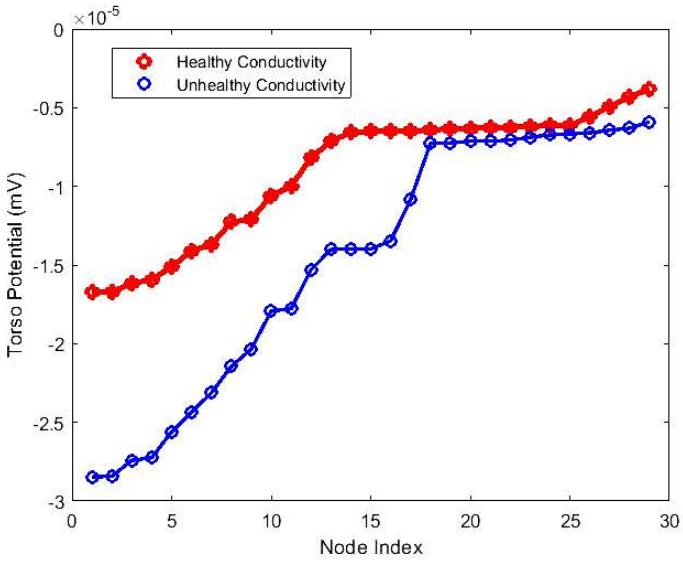


Figure 7.12. Change of torso potentials with anisotropic heart tissue, healthy, and unhealthy conductivities (Ischemia 2).

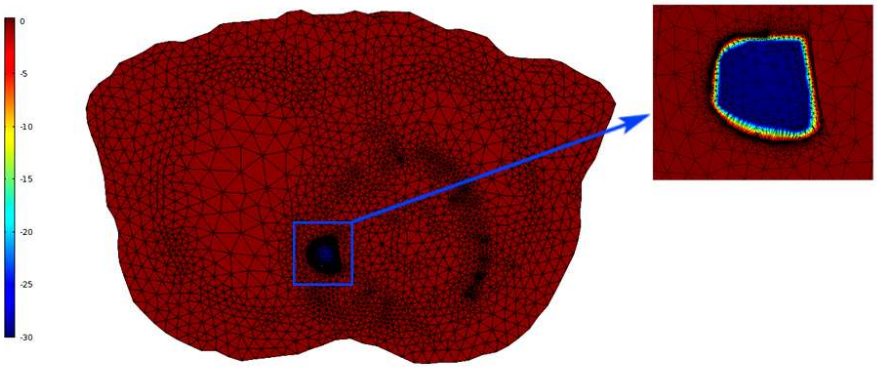


Figure 7.13. Inhomogeneous torso model, isotropic heart conductivity and ischemic region on the left hand side of right ventricle (Ischemia 3). The mesh has 2863 nodes and 5616 elements.

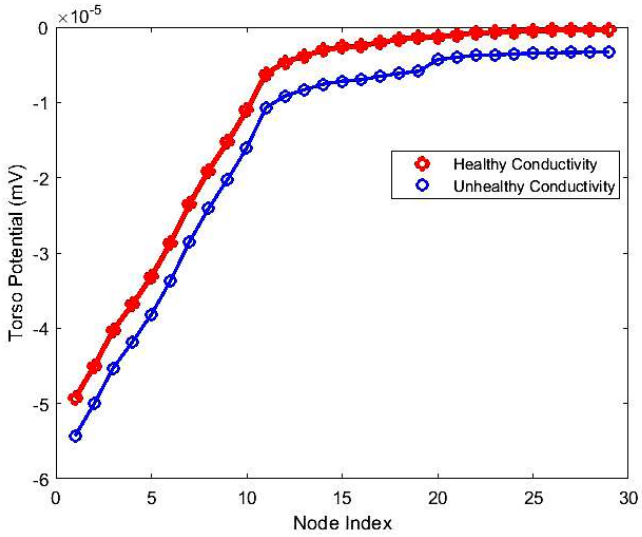


Figure 7.14. Change of torso potentials with isotropic heart tissue, healthy, and unhealthy conductivities (Ischemia 3).

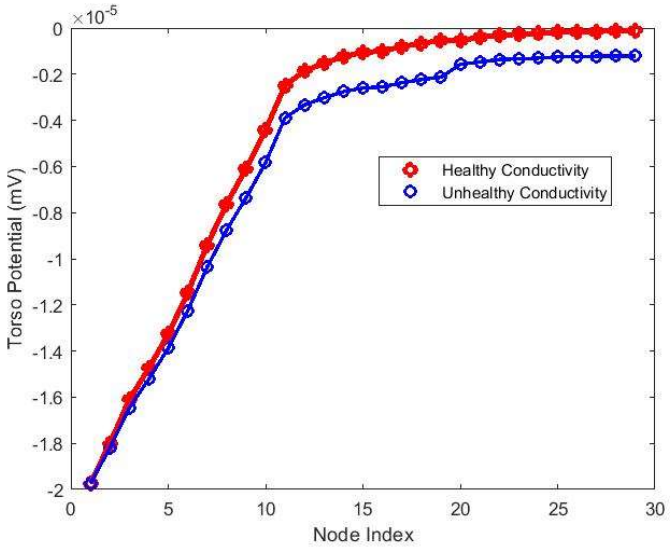


Figure 7.15. Change of torso potentials with anisotropic heart tissue, healthy, and unhealthy conductivities (Ischemia 3).

7.3. Inverse Problem Examples

As mentioned earlier, the inverse problem of ECG can involve either the reconstruction of epicardial potentials or reconstruction of TMP from a given set of torso potentials, both of which lead to ill-posed systems and handled with regularization methods.

As commonly done in the testing of solution methods for inverse problems, we have created pseudo-experimental data by running the forward analysis. Forward analysis gives us torso potentials from epicardial potential data (or TMP data) that are consistent with each other. In the inverse analysis, input and output of the forward analysis change roles. The torso potentials calculated in the forward analysis constitutes the input of the inverse problem and the objective is to reconstruct the underlying epicardial potentials (or TMP distribution) as output. All examples of inverse problem involves the inhomogeneous torso model shown in (Fig. 4.4).

The ischemic conductivity does not play a role in the epicardial potential reconstruction. We have run this problem in order to test the correctness of the inverse scheme.

The reconstruction of TMP allows us to locate the ischemic region due to its altered TMP. The ischemic conductivity is indirectly involved in this analysis, when torso potentials used in the inverse analysis is created by taking the ischemic conductivity into account in the forward analysis.

7.3.1. Reconstruction of Epicardial Potential

In the forward analysis examples, the epicardial potential distribution shown in (Fig. 7.2) has produced a torso potential distribution displayed on (Fig. 7.6) for inhomogeneous torso model. For the inverse analysis, now the torso potential given in (Fig. 7.6) is taken as input to estimate the epicardial potential given in (Fig. 7.2.).

Reconstruction of the epicardial potentials have been accomplished successfully with TSVD (Fig. 7.16), and zero order (Fig. 7.17), first order (Fig. 7.18) and mean value (Fig. 7.19) Tikhonov regularizations. A comparison of these four

approaches (Fig. 7.20) indicate that there is no appreciable difference between their performances.

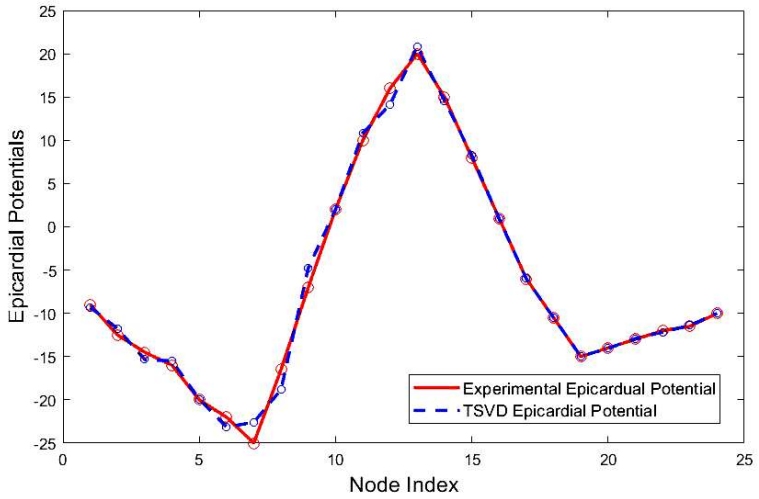


Figure 7.16. Reconstructed epicardial potentials obtained by TSVD regularization method.

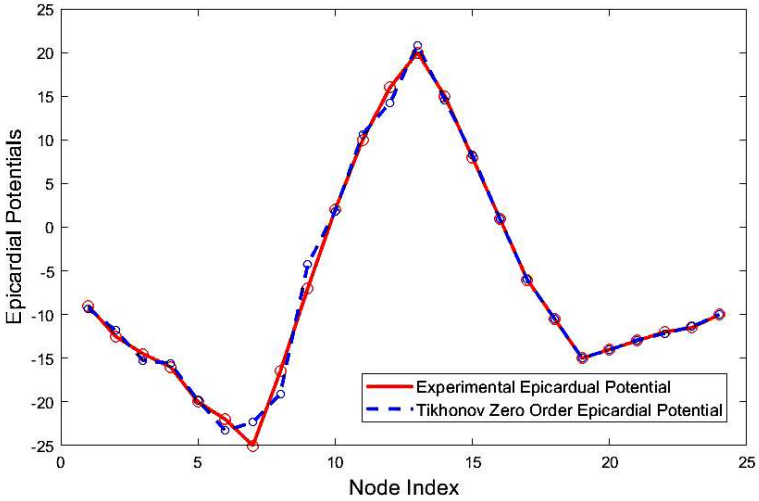


Figure 7.17. Reconstructed epicardial potentials obtained by Tikhonov zero order regularization method.

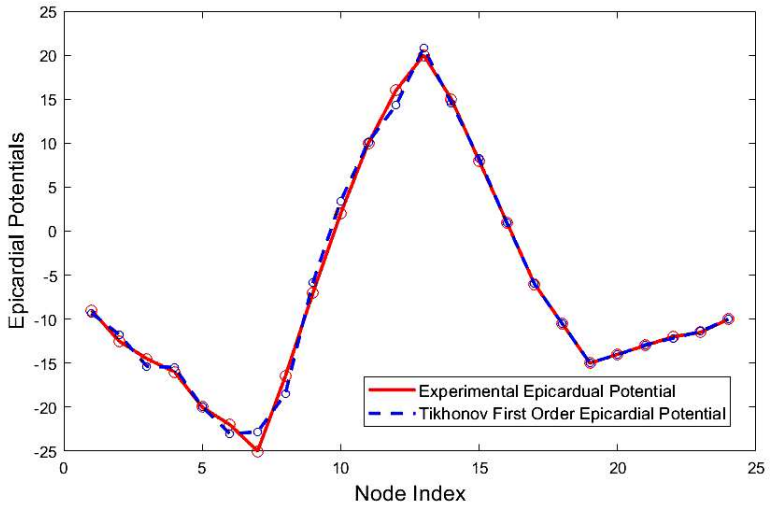


Figure 7.18. Reconstructed epicardial potentials obtained by Tikhonov first order regularization method.

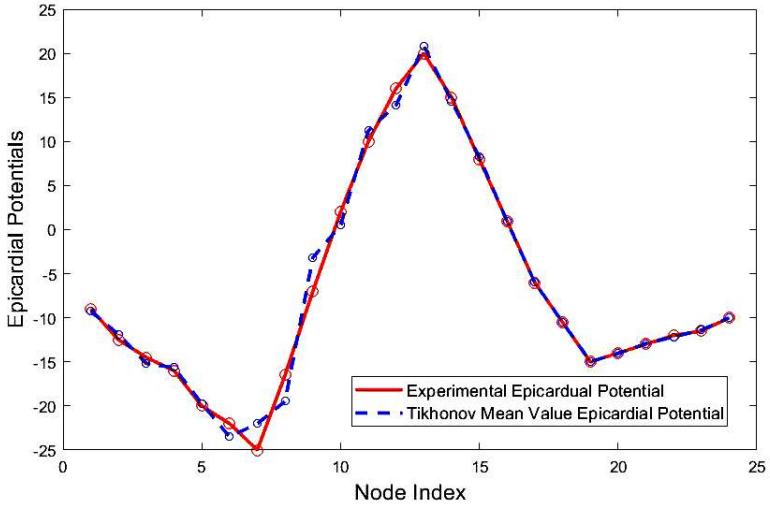


Figure 7.19. Reconstructed epicardial potentials obtained by Tikhonov mean value regularization method.

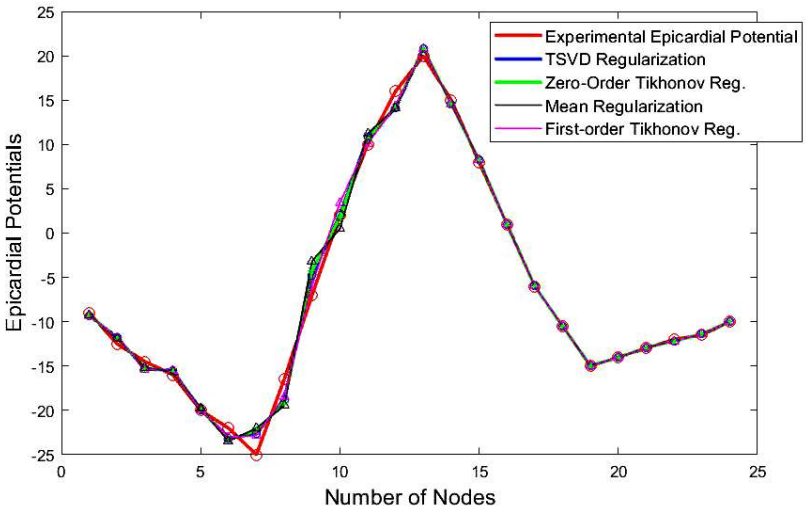


Figure 7.20. Comparison of different approaches in the reconstruction of the epicardial potentials.

7.3.2. Reconstruction of Transmembrane Potentials

The pseudo-experimental data for TMP reconstruction is obtained from the forward simulation of the inhomogeneous torso model per Ischemia 1, 2 and 3 cases. The input is again the torso potentials calculated in the forward analysis. The objective is to determine the TMP in the heart tissue. Clearly, the nodes where the reconstructed TMP significantly deviates from its healthy value of 0 mV towards the unhealthy value of -30 mV should belong to the ischemic region. In this work, a node whose TMP turns out to be lower than -0.001 mV is considered to be located in the ischemic region.

7.3.2.1. Isotropic Heart

Assuming isotropic conductivity in the heart, the TVSD and all three regularization techniques has performed very well for Ischemia 1 case with or

without ischemic conductivity taken into account (Figs. 7.21-7.24). The experimental ischemic region has been located almost exactly with all methods.

For Ischemia 2 case, the location of the ischemic region has been found by all four methods, although not as accurately as in Ischemia 1 case. With the ischemic conductivity taken into account, the scheme seems to capture the boundaries of the experimental ischemic region slightly better (Figs. 7.25-7.28).

Taking the ischemic conductivity into account does not seem to make a difference in Ischemia 3 case. All regularization techniques utilized showed almost the same exact performance in locating the ischemic region with healthy or unhealthy conductivities imposed (Figs. 7.29-7.32). The boundary of the estimated ischemic region has deviated around its outer edge from the experimental boundaries in all results.

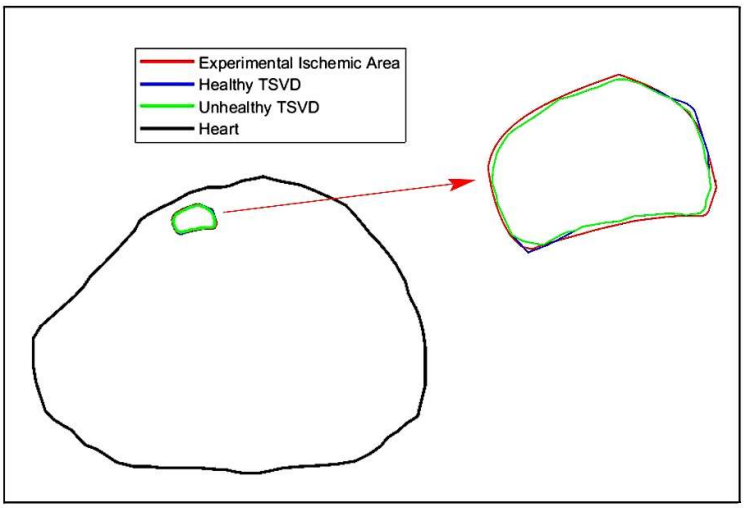


Figure7.21. Localizing the ischemic region with healthy and unhealthy conductivities using TSVD regularization (Ischemia 1).

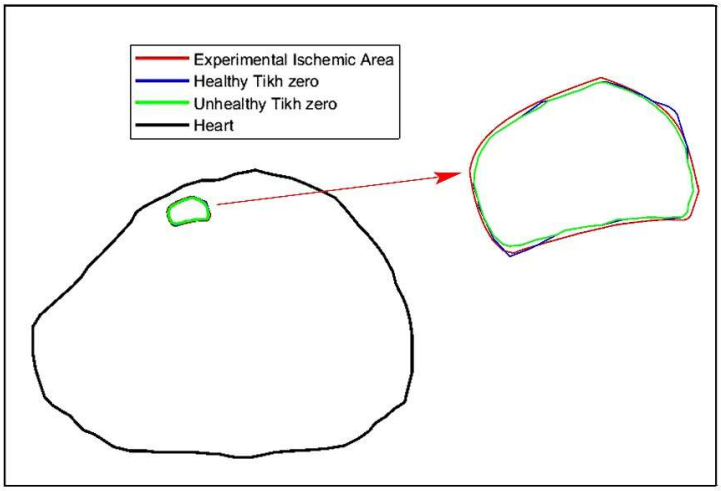


Figure7.22. Localizing the ischemic region with healthy and unhealthy conductivities using zero order Tikhonov regularization (Ischemia 1).

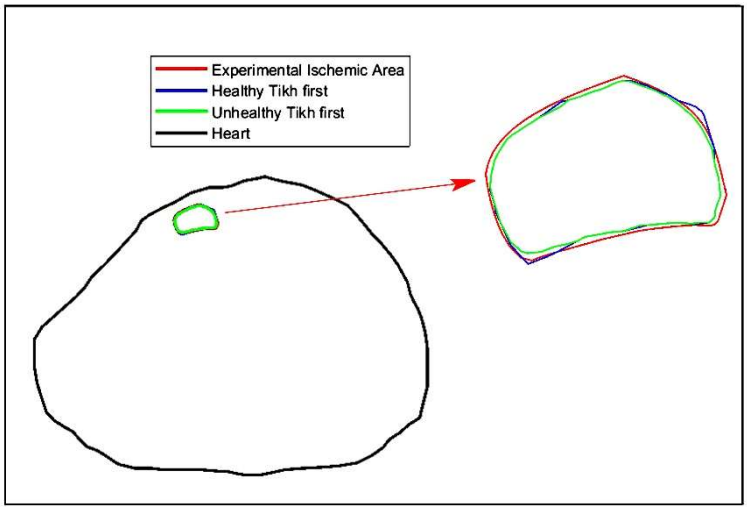


Figure7.23. Localizing the ischemic region with healthy and unhealthy conductivities using first order Tikhonov regularization (Ischemia 1).

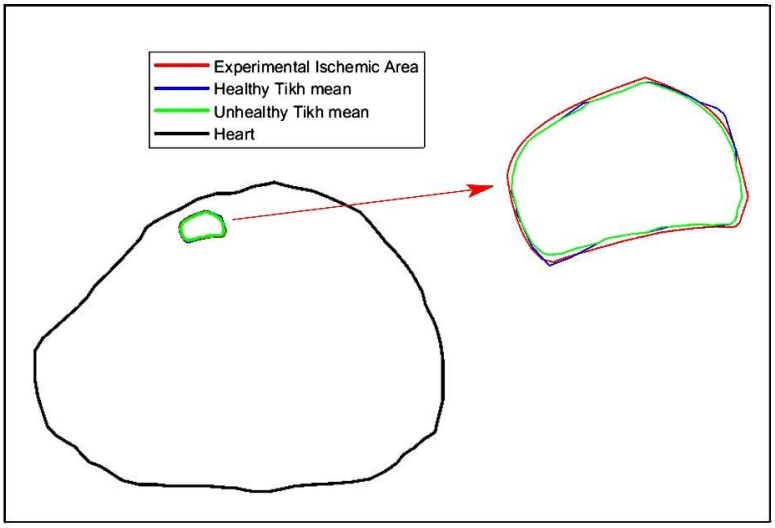


Figure7.24. Localizing the ischemic region with healthy and unhealthy conductivities using Mean value regularization (Ischemia 1).

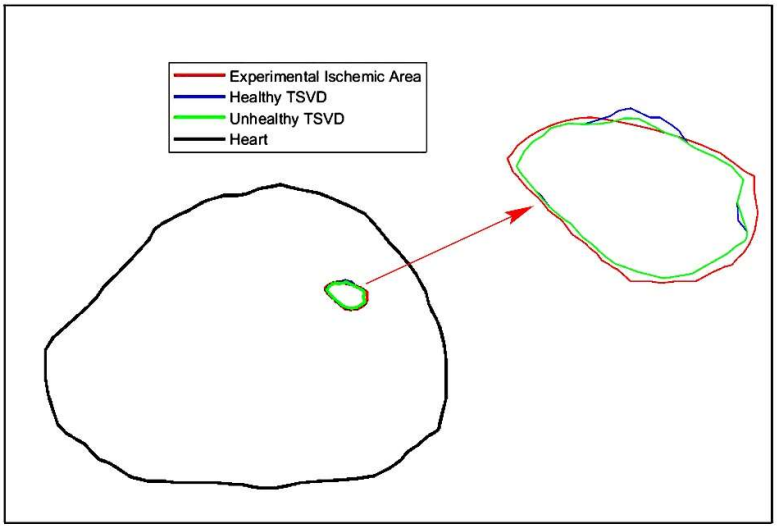


Figure7.25. Localizing the ischemic region with healthy and unhealthy conductivities using TSVD regularization (Ischemia 2).



Figure7.26. Localizing the ischemic region with healthy and unhealthy conductivities using Zero order Tikhonov regularization (Ischemia 2).

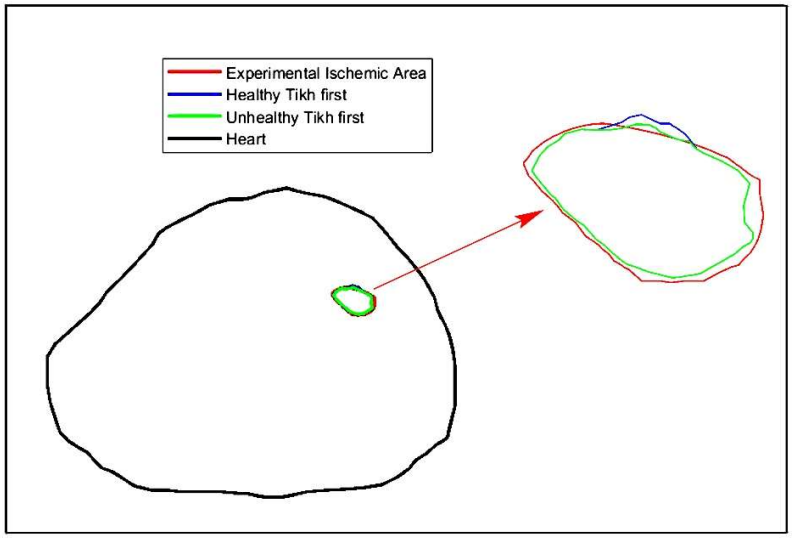


Figure7.27. Localizing the ischemic region with healthy and unhealthy conductivities using First order Tikhonov regularization (Ischemia 2).

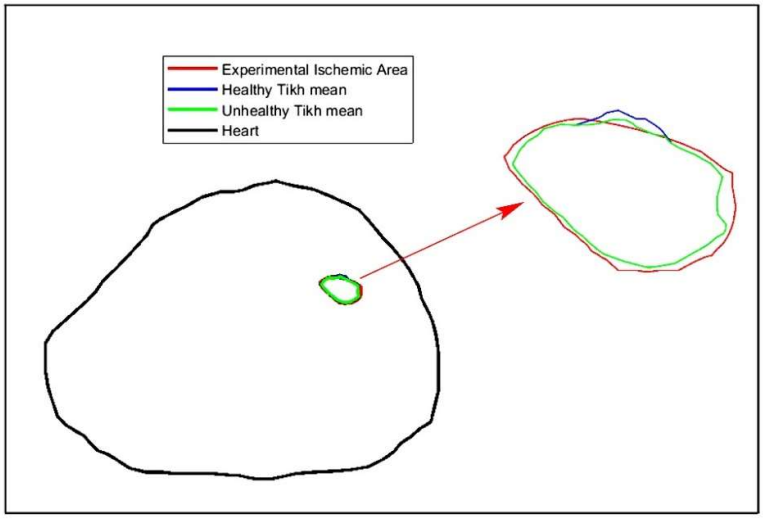


Figure7.28. Localizing the ischemic region with healthy and unhealthy conductivities using Mean value regularization (Ischemia 2).

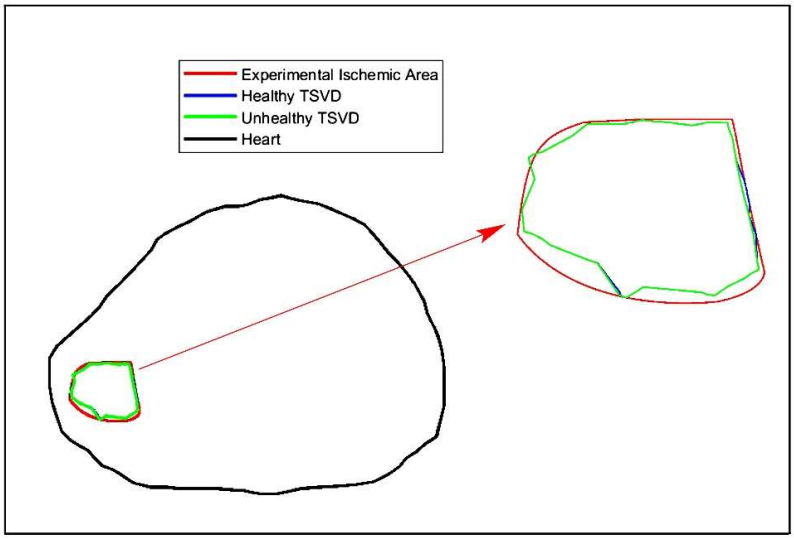


Figure7.29. Localizing the ischemic region with healthy and unhealthy conductivities using TSVD regularization (Ischemia 3).

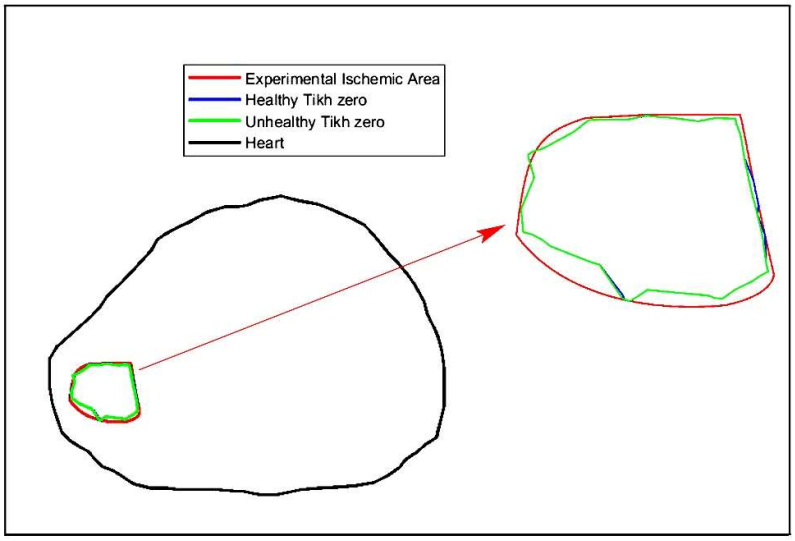


Figure7.30. Localizing the ischemic region with healthy and unhealthy conductivities using Zero order Tikhonov regularization (Ischemia 3).

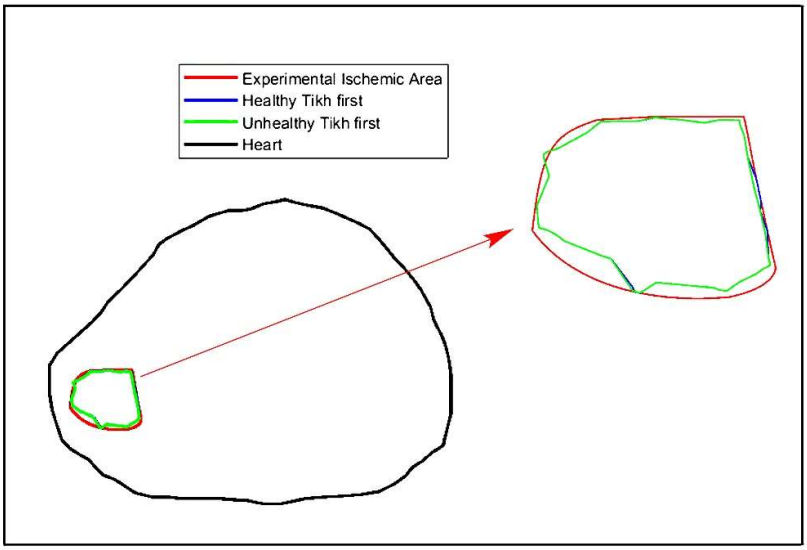


Figure7.31. Localizing the ischemic region with healthy and unhealthy conductivities using First order Tikhonov regularization (Ischemia 3).

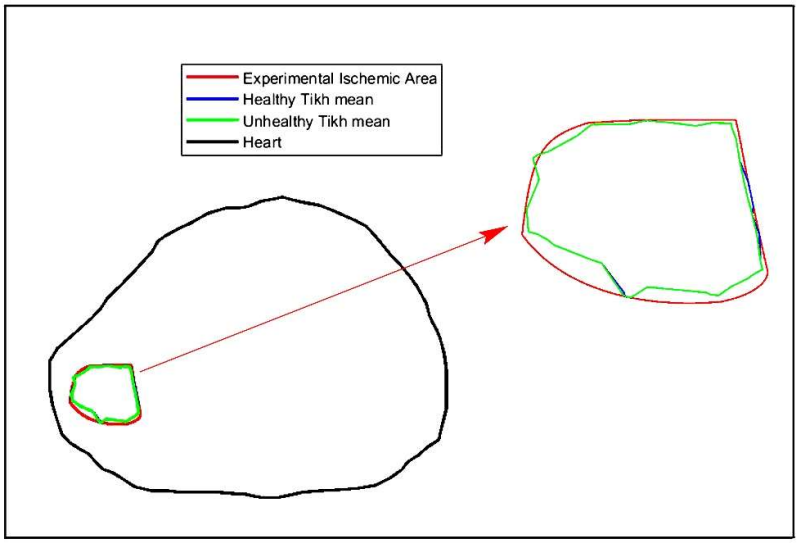


Figure7.32. Localizing the ischemic region with healthy and unhealthy conductivities using Mean value regularization (Ischemia 3).

7.3.2.2. Anisotropic Heart

For the three ischemia cases we have studies, incorporating the anisotropic conductivity does not seem to make much difference in locating the ischemic region over the isotropic case. Case by case, the performance of the utilized inverse schemes have been identical with assumed isotropic or anisotropic conductivities.

TVSD and all three regularization techniques has located the ischemic region almost perfectly for Ischemia 1 case with or without ischemic conductivity taken into account (Figs. 7.33-7.36).

For Ischemia 2 case, we have observed again that the utilized regularization methods capture the ischemic boundaries slightly better when the ischemic conductivity is taken into account. (Figs. 7.37-7.40). All four regularization techniques have performed at the same level for this case.

Assuming anisotropic conductivity, ischemic or not, has produced similar results in Ischemia 3 case as with assumed isotropic conductivity. The boundary of

the estimated ischemic region has deviated around its outer edge from the experimental boundaries with all regularization techniques (Figs. 7.41-7.44).

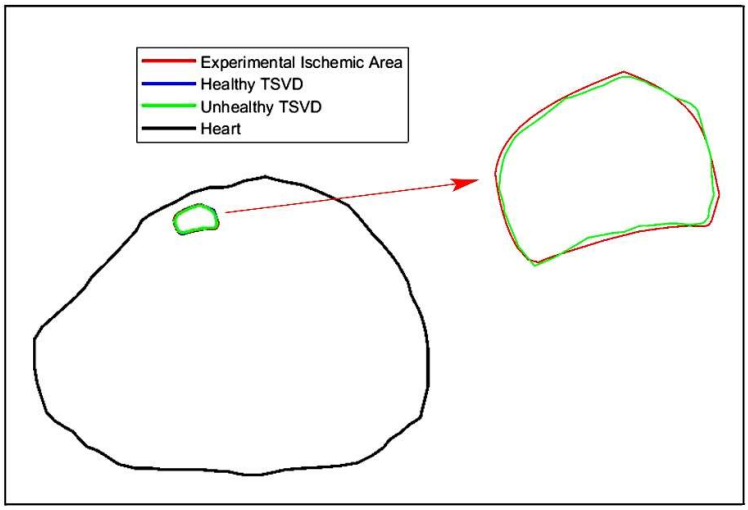


Figure7.33. Localizing the ischemic region with healthy and unhealthy conductivities using TSVD regularization (Ischemia 1).

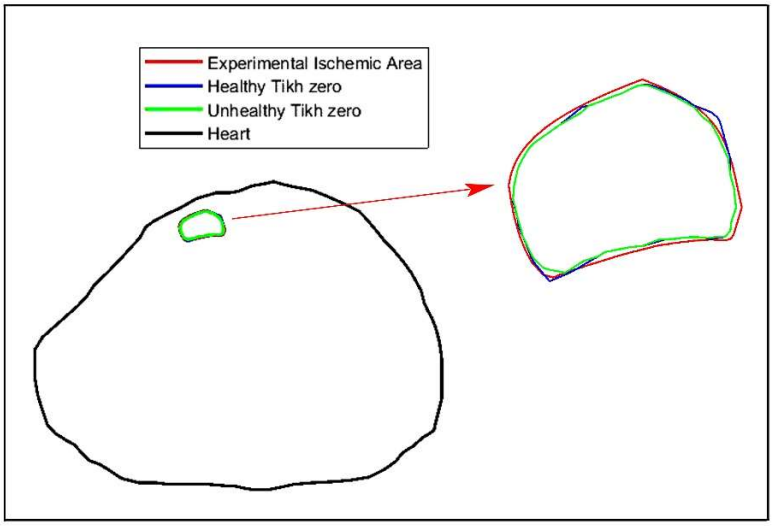


Figure7.34. Localizing the ischemic region with healthy and unhealthy conductivities using Zero order Tikhonov regularization (Ischemia 1).

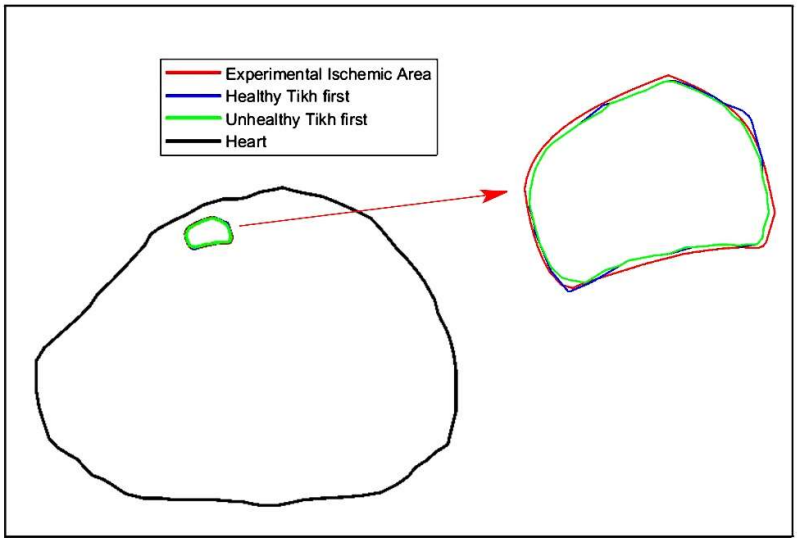


Figure7.35. Localizing the ischemic region with healthy and unhealthy conductivities using First order Tikhonov regularization (Ischemia 1).

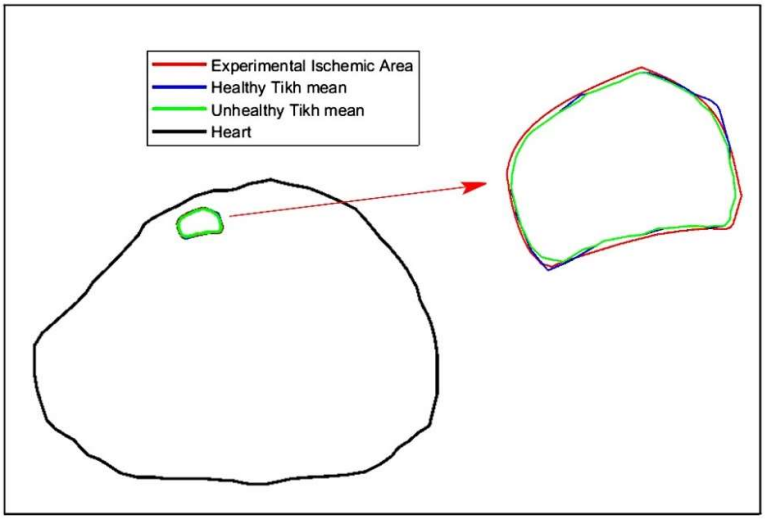


Figure7.36. Localizing the ischemic region with healthy and unhealthy conductivities using Mean value regularization (Ischemia 1).



Figure7.37. Localizing the ischemic region with healthy and unhealthy conductivities using TSVD regularization (Ischemia 2).



Figure7.38. Localizing the ischemic region with healthy and unhealthy conductivities using Zero order Tikhonov regularization (Ischemia 2).

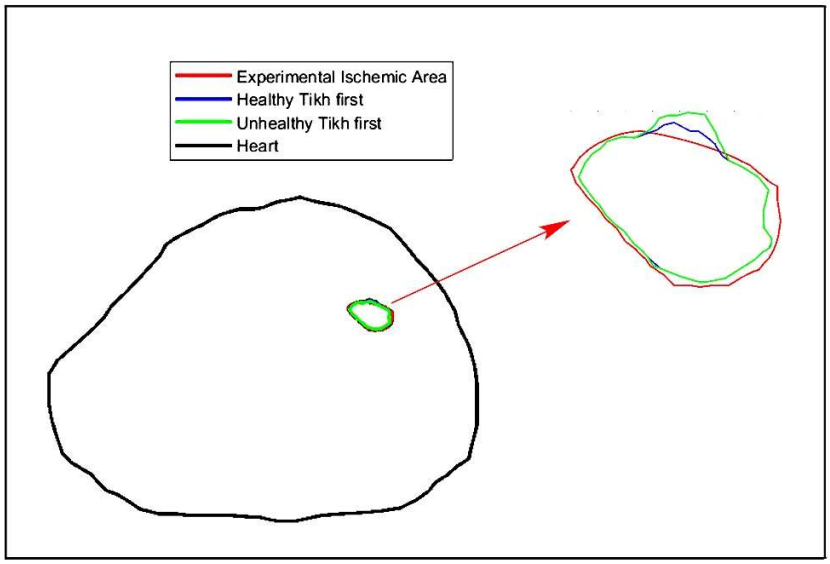


Figure7.39. Localizing the ischemic region with healthy and unhealthy conductivities using First order Tikhonov regularization (Ischemia 2).

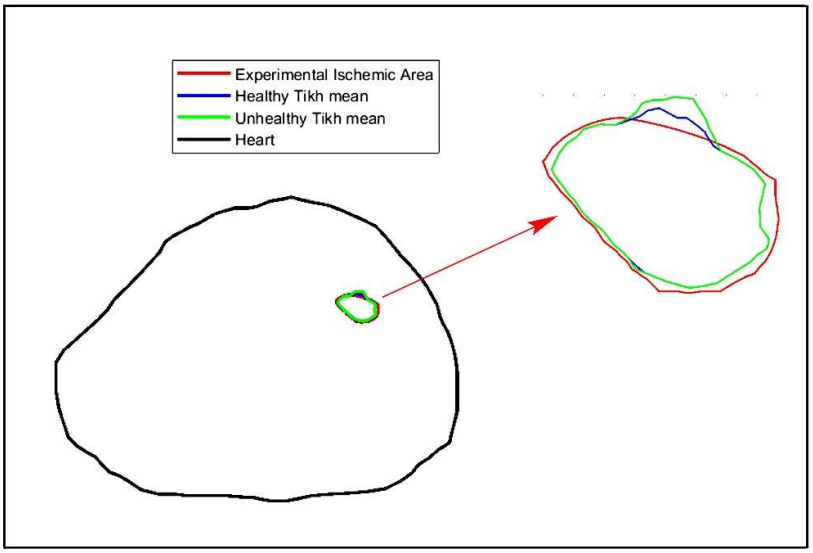


Figure7.40. Localizing the ischemic region with healthy and unhealthy conductivities using Mean value regularization (Ischemia 2).

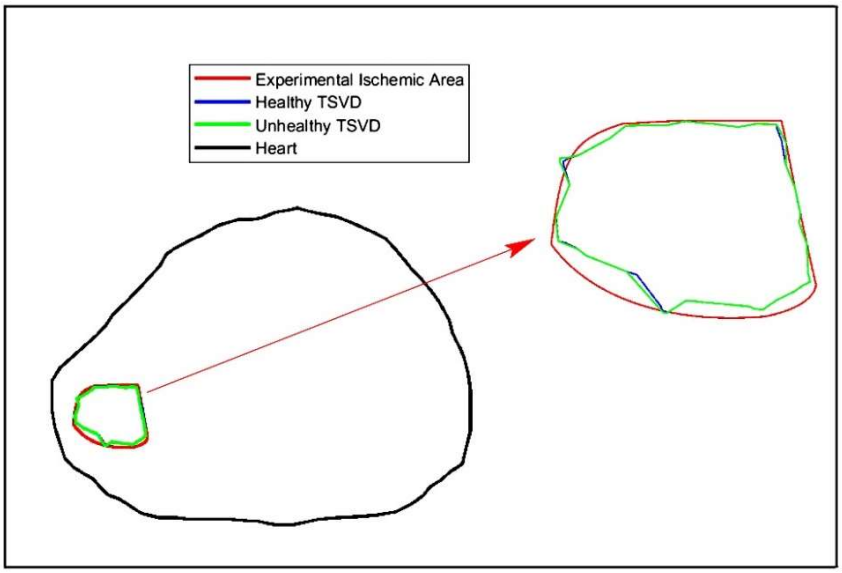


Figure 7.41. Localizing the ischemic region with healthy and unhealthy conductivities using TSVD regularization (Ischemia 3).



Figure7.42. Localizing the ischemic region with healthy and unhealthy conductivities using Zero order Tikhonov regularization (Ischemia 3).

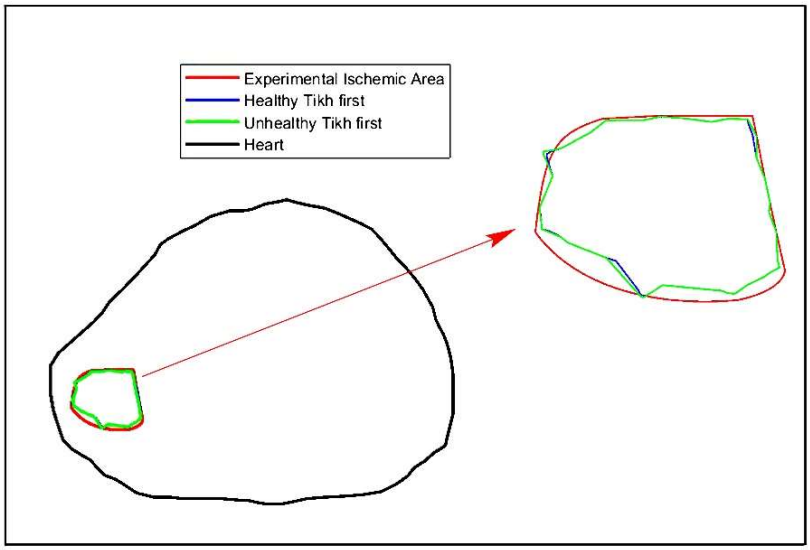


Figure7.43. Localizing the ischemic region with healthy and unhealthy conductivities using First order Tikhonov regularization (Ischemia 3).

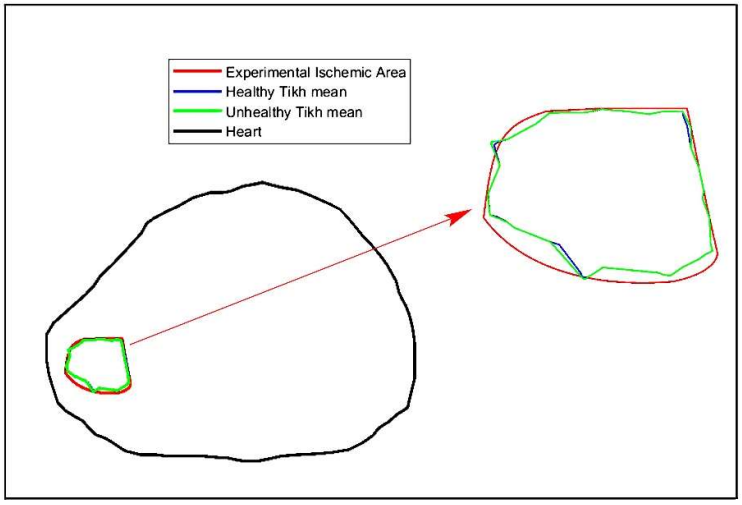


Figure7.44. Localizing the ischemic region with healthy and unhealthy conductivities using Mean value regularization (Ischemia 3).

7.3.3. Results of Finite Element Optimization

Sensitivity based FE optimization scheme is started with an initial estimate of ischemic region that is far from its actual location. In a convergent, scheme, as the parameters, (a, b, c and d) evolve iteratively, the ischemic region will approach its actual location.

Capturing the exact geometry of the ischemic region is not a concern in this method since we assume a priori its shape to be rectangular. If part of the rectangular region falls beyond the limits of the heart boundary during optimization iteration, the algorithm disregard that part. Hence, it is possible that the converged ischemic region may be a truncated rectangle. Furthermore, the patch of identified ischemic elements in the irregular FE mesh will look like a polygon rather than a rectangle.

It should be noted that the presented optimization method does not take the change in conductivity due to ischemia into account. In that sense, it bears some resemblance to existing regularization based inverse schemes.

7.3.3.1. Isotropic Heart

Assuming isotropic conductivity throughout the heart, the iterative optimization scheme has located the ischemic region in 20-40 iterations for Ischemia 1 (Fig. 7.41), Ischemia 2 (Fig. 7.42) and Ischemia 3 (Fig. 7.43) cases.

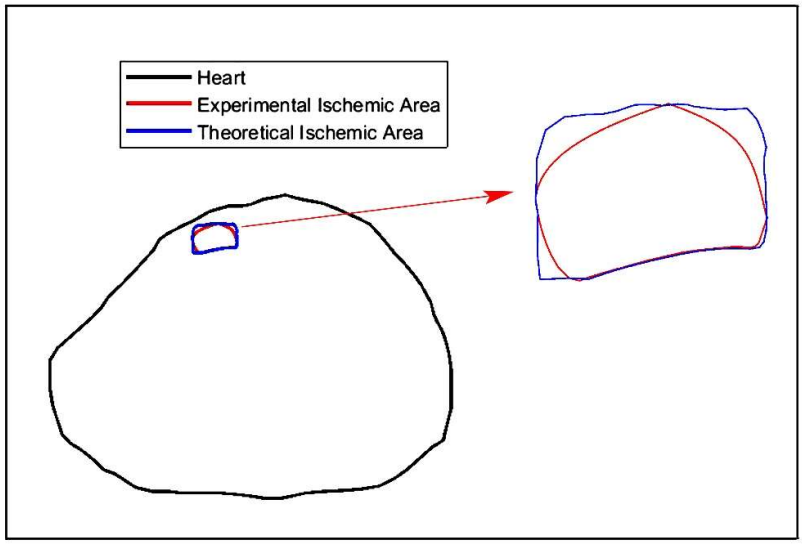


Figure7.45. Localizing the isotropic ischemic region using FE optimization (Ischemia 1).

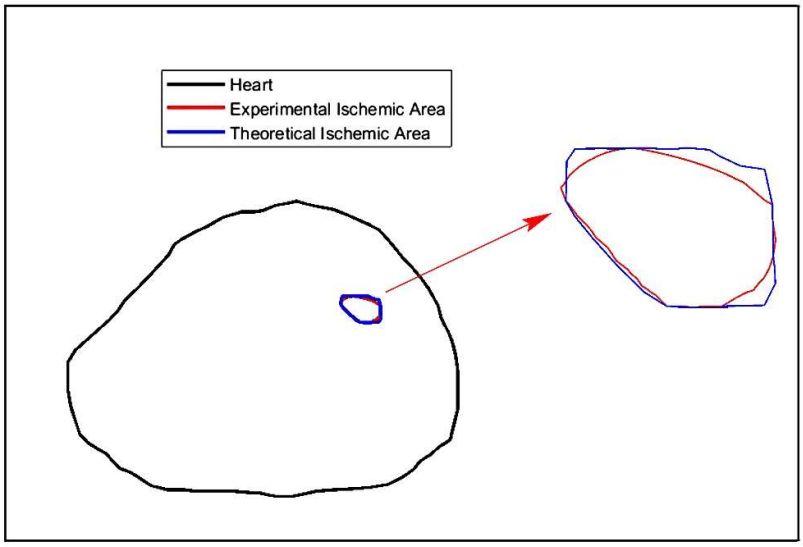


Figure7.46. Localizing the isotropic ischemic region using FE optimization (Ischemia 2).

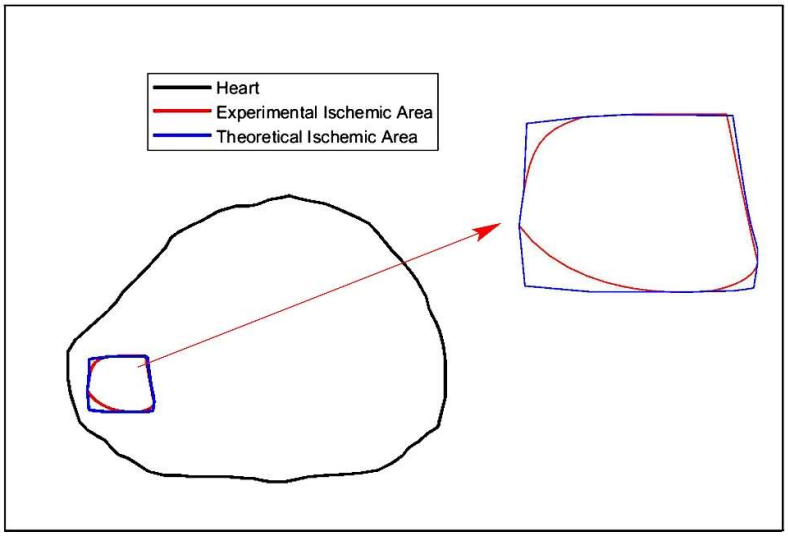


Figure7.47. Localizing the isotropic ischemic region using FE optimization (Ischemia 3).

7.3.3.2. Anisotropic Heart

Assuming anisotropic conductivity in the heart tissue does not seem to improve the performance of the iterative optimization scheme over the isotropic conductivity. Identical ischemic regions have been identified in the anisotropic heart for Ischemia 1 (Fig. 7.44), Ischemia 2 (Fig. 7.45) and Ischemia 3 (Fig. 7.46) cases. In anisotropic case, the number of iterations required for convergence has slightly increased compared to anisotropic case.

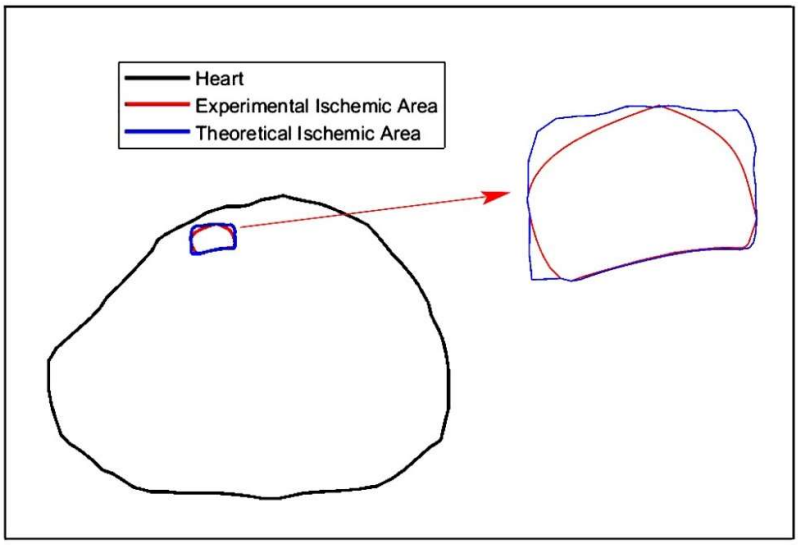


Figure7.48. Localizing the anisotropic ischemic region using FE optimization (Ischemia 1).

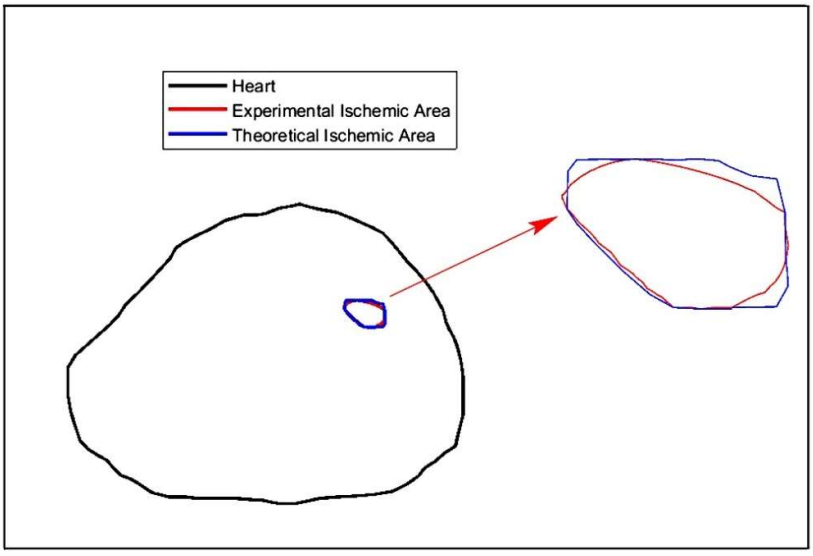


Figure7.49. Localizing the anisotropic ischemic region using FE optimization (Ischemia 2).

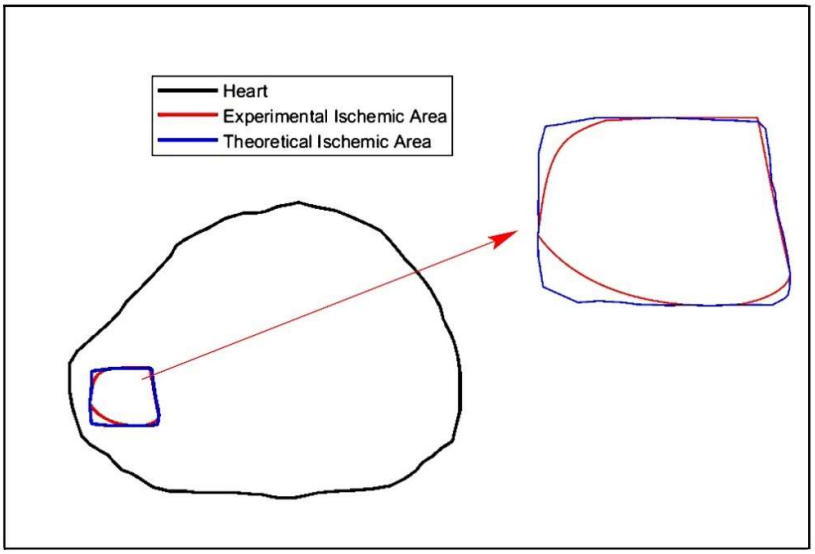


Figure7.50. Localizing the anisotropic ischemic region using FE optimization (Ischemia 3).

8. DISCUSSION AND CONCLUSION

8.1. Discussion and Conclusion

In this work, we have investigated the effect of ischemic conductivity on the outcome of forward and inverse problems of ECG.

Computational modelling of electrical activity of heart has been an active research area for more than three decades. During this period, the related literature has grown vast and the proposed models have increasingly become more detailed and sophisticated, evolving from two-dimensional to three-dimensional, from homogeneous to inhomogeneous, from isotropic to anisotropic.

Ischemia has been an important research topic in this vast research area due to its clinical significance. Forward problems are important in order to predict the effect of various factors associated with ischemic region (location, size, severity etc.). Inverse simulations has been realized to locate the ischemic region of the heart from torso or epicardial potential readings. In this study, we have demonstrated that ischemic conductivity is an important factor and should be taken into account, particularly in forward simulations. Since forward simulations are often used to produce pseudo-experimental data for inverse simulations, forward data produced with ischemic conductivity will be closer to reality. Clearly, inverse analysis run with more realistic data can be better evaluated (Bear et al. 2015).

We have written a custom-designed FE code to solve the quasi-static bidomain problem which is used in the solution of both forward and inverse problems of ECG. The main conclusions that can be drawn from the forward analysis of this study can be summarized as follows:

1- Torso potentials are affected differently depending on the size and location of the ischemic region. Larger ischemic regions that are closer to the precardial (chest) leads causes a larger depression in the torso potentials.

The size and shape of ischemic region has been shown to effect epicardial potentials before. Our results seem to confirm the observation of this work (Barnes and Johnston 2012).

2- Taking the ischemic conductivity into account can cause significant changes in the calculated torso potentials. The magnitude of this change depends on the size and location of the ischemic region. We have observed that the change is more pronounced if the ischemic region is larger and closer to the posterior of the heart (such as case Ischemia 1 described in Chapter 7). In other words, the larger the "heart material" between the ischemic region and the leads is, the stronger is the effect of ischemic conductivity. Epicardial potentials are shown to change significantly due to reduced conductivity caused by ischemia on a simple rectangular heart model (Barnes and Johnston 2012). Although we have observed the changes in torso potentials, our results seem to be in agreement with the observation of this study.

3- The anisotropy of the conductivity has a strong influence on the torso potentials. Ischemic conductivity has a stronger effect on torso potentials if the anisotropy of myocardium is taken into account. Depending on the size and the location of the ischemic region, anisotropic ischemic conductivity leads to torso potentials that are twice as large as the ones produced by anisotropic healthy ischemic conductivity. The importance of anisotropy in cardiac modelling has already been established in other studies (P. R. Johnston, Kilpatrick, and Yong Li 2001), (Ramon et al. 2002), (Potse et al. 2007). Consequently, it can be argued that a significant improvement in the heart modelling can be achieved if ischemic conductivity and the associated anisotropy are simultaneously taken into account in the model.

As mentioned before, ischemic conductivity is used in creating the pseudo-experimental input data of the inverse analysis and, in that sense, indirectly involved in the inverse scheme. The inverse scheme is solely based on locating the ischemic region by identifying the regions of depressed TMP. The following conclusions can be drawn from the inverse study accomplished in this work:

1- Input data produced with ischemic or healthy conductivities locate the ischemic region with equal effectiveness in the inverse analysis. While the distribution of TMP changes when healthy or ischemic conductivities are used, the boundary between the healthy and ischemic regions (where TMP drops below -0.001 mV) is not affected much by this factor.
2- All Tikhonov regularization methods and TSVD are equally effective in locating the ischemic region in the heart.
3- Mean value regularization, which has not been used before in similar inverse studies, seems to be a simple alternative to other common regularization techniques. The computational efficiency of this method should be compared with the existing methods to make a better comparison.

Sensitivity based optimization is a novel and promising technique to tackle the inverse problem of ECG that has been proposed in that work. The only study that bears partial resemblance to this method due to its iterative characteristics seems significantly more complicated than the one we have proposed (Bjørn Fredrik Nielsen, Lysaker, and Tveito 2007). With certain improvements, the sensitivity based iterative method has the potential to be an alternative to existing regularization techniques.

In the mathematical modelling of ischemia, the pathology is usually modeled by imposing an altered TMP to the diseased tissue. The conductivity change that

comes with this pathology has been only recently incorporated into some models, where epicardial potentials are estimated with finite volume method in 3D models (B. M. Johnston and Johnston 2018), (B. M. Burton et al. 2018). With the conclusions drawn from this work, reseachers may pay more attention to conductivity changes due to ischemia in future simulation studies.

8.2. Future Research

The studies accomplished in this dissertation work can be furthered in several aspects in the future.

We have performed a two-dimensional study in this work to deal with a moderate level of computational burden. While we believe that the main conclusion are not going to change drastically, it is possible to repeat this study on a three-dimensional model. Clearly, the computational burden that comes with a three-dimensional simulation is significantly higher than we have encountered in the current study, and a three-dimensional model requires proportionally higher computing resources.

In the solution of the inverse problem, it is possible to add some error (i.e. some noise) to the torso potentials to build a more realistic scenario. Measurement error may have an effect on locating the ischemic region.

The computational setting established in this work can be used to research more clinically relevant problems. For example, it is possible that ischemia occurring on certain parts of the heart can be better diagnosed if torso potentials are measured at a non-standard spot on the chest. A FE based research can be helpful to identify such alternative lead locations.

The sensitivity based approach introduced in this study holds promise for the solution of the inverse ECG problem. We have evaluated the sensitivity matrix numerically in this work, but it may be possible to calculate it analytically or semi-analytically using the FE formulation. It may be also possible to parameterize the ischemic conductivity, and optimize TMP and conductivity parameters simultaneously in an iterative scheme.

REFERENCES

Andrew Pullan, Leo Cheng, and Martin Buist. 2005. *Mathematically Modelling the Electrical Activity of the Heart: From Cell to Body Surface and Back Again*. World Scientific Publishing Company.

Barnes, J. P., and P. R. Johnston. 2012. "How Ischaemic Region Shape Affects ST Potentials in Models of Cardiac Tissue." *Mathematical Biosciences* 239(2): 213–21.

Barr, Roger C., Maynard Ramsey, and Madison S. Spach. 1977. "Relating Epicardial to Body Surface Potential Distributions by Means of Transfer Coefficients Based on Geometry Measurements." *IEEE Transactions on Biomedical Engineering* BME-24(1): 1–11.

Barth, Timothy J, David E Keyes, and Dirk Roose. 2007. Computing the Electrical Activity in the Heart *Computing the Electrical Activity in the Heart*.

Bear, Laura R. et al. 2015. "Forward Problem of Electrocardiography: Is It Solved?" *Circulation: Arrhythmia and Electrophysiology* 8(3): 677–84.

Ben-Shahar, Ohad, and Steven W. Zucker. 2003. "The Perceptual Organization of Texture Flow: A Contextual Inference Approach." *IEEE Transactions on Pattern Analysis and Machine Intelligence* 25(4): 401–17.

Bendahmane, Mostafa, Raimund Bürger, and Ricardo Ruiz-Baier. 2010. "A Finite Volume Scheme for Cardiac Propagation in Media with Isotropic Conductivities." *Mathematics and Computers in Simulation* 80(9): 1821–40.

Berenfeld, Omer, and Shimon Abboud. 1996. "Simulation of Cardiac Activity and the ECG Using a Heart Model with a Reaction-Diffusion Action Potential." *Medical Engineering and Physics* 18(8): 615–25.

Berrier, Keith L, Danny C Sorensen, and Dirar S Khoury. 2004. "Solving the Inverse Problem of Electrocardiography Using a Duncan and Horn Formulation of the Kalman Filter." *IEEE Transactions on biomedical engineering* 51(3): 507–15.

Bradley, C. P., Andrew J. Pullan, and P. J. Hunter. 2000. “Effects of Material Properties and Geometry on Electrocardiographic Forward Simulations.” *Annals of Biomedical Engineering* 28(7): 721–41.

Buist, Martin L., and Andrew J. Pullan. 2003. “The Effect of Torso Impedance on Epicardial and Body Surface Potentials: A Modeling Study.” *IEEE Transactions on Biomedical Engineering* 50(7): 816–24.

Buist, Martin, and Andrew Pullan. 2002. “Torso Coupling Techniques for the Forward Problem of Electrocardiography.” *Annals of Biomedical Engineering* 30(10): 1299–1312.

Burger, Martin, and Stefanie Kälz. “Anisotropic Conduction in Electrocardiology.”

Burton, B. M. et al. 2018. “Image-Based Modeling of Acute Myocardial Ischemia Using Experimentally Derived Ischemic Zone Source Representations.” *Journal of Electrocardiology* 51(4): 725–33.

Burton, Brett M. et al. 2018. “A Framework for Image-Based Modeling of Acute Myocardial Ischemia Using Intramurally Recorded Extracellular Potentials.” *Annals of Biomedical Engineering* 46(9): 1325–36.

Carmeliet, Edward. 2017. “Cardiac Ionic Currents and Acute Ischemia: From Channels to Arrhythmias.” *Physiological Reviews* 79(3): 917–1017.

Chamorro-Servent, Judit, Remi Dubois, and Yves Coudière. 2018. “Exploring Possible Choices of the Tikhonov Regularization Parameter for the Method of Fundamental Solution in Electrocardiography.” *2017 Computing in Cardiology Conference (CinC)* 44: 4–7.

Cheng, Leo K., John M. Bodley, and Andrew J. Pullan. 2003. “Comparison of Potential- and Activation-Based Formulations for the Inverse Problem of Electrocardiology.” *IEEE Transactions on Biomedical Engineering* 50(1): 11–22.

Cimponeriu, A., C. Frank Starmer, and A. Bezerianos. 2001. “A Theoretical Analysis of Acute Ischemia and Infarction Using ECG Reconstruction on a 2-D Model of Myocardium.” *IEEE Transactions on Biomedical Engineering* 48(1): 41–54.

Clayton, R. H., and A. V. Panfilov. 2008. “A Guide to Modelling Cardiac Electrical Activity in Anatomically Detailed Ventricles.” *Progress in Biophysics and Molecular Biology* 96(1–3): 19–43.

Darrell J. Swenson et al. 2011. “Cardiac Position Sensitivity Study in the Electrocardiographic Forward Problem Using Stochastic Collocation and Boundary Element Methods.” *PLoS ONE* 32(7): 736–40.

Denisov, Alexander M., Eugene V. Zakharov, Alexander V. Kalinin, and Vitaliy V. Kalinin. 2012. “Numerical Method for Solving an Inverse Electrocardiography Problem for a Quasi Stationary Case.” *Journal of Inverse and Ill-Posed Problems* 20(4): 501–12.

Dmytro F. 2008. “Forward and Inverse Problems of Electrocardiography : Clinical Investigations.”

Engl, Heinz Werner, Martin Hanke, and Andreas Neubauer. 1996. 375 *Regularization of Inverse Problems*. Springer Science & Business Media.

Farina, Dmytro. 2008a. *Forward and Inverse Problem of Electrocardiography: Clinical Investigations*. PhD thesis. Universität Karlsruhe. digbib.ubka.uni-karlsruhe.de/volltexte/documents/191031.

Farina, Dmytro. 2008b. “Forward and Inverse Problems of Electrocardiography : Clinical Investigations.”

Fischer, Gerald et al. 2000. “Bidomain Model Based BEM-FEM Coupling Formulation for Anisotropic Cardiac Tissue.” *Annals of Biomedical Engineering* 28(10): 1229–43.

Fletcher, Gerald F., Thomas R. Flipse, Paul Kligfield, and Joseph R. Malouf. 1998. “Current Status of ECG Stress Testing.” *Current Problems in Cardiology* 23(7): 353–423.

Le Floch, R. et al. 2011. “Heart Wall Myofibers Are Arranged in Minimal Surfaces to Optimize Organ Function.” *Proceedings of the National Academy of Sciences* 108(40): 16663–68.

Fox, Stuart Ira. 2006. *Human Physiology 9th Editon*. McGraw-Hill press, New York, USA.

Franzone, P. Colli, and E. Magenes. 1979. “On the Inverse Potential Problem of Electrocardiology.” *CALCOLO* 16(4): 459–538.

Geneser, Sarah E., Robert M. Kirby, and Robert S. MacLeod. 2008. “Application of Stochastic Finite Element Methods to Study the Sensitivity of ECG Forward Modeling to Organ Conductivity.” *IEEE Transactions on Biomedical Engineering* 55(1): 31–40.

Geneser, Sarah E, Seungkeol Choe, Robert M Kirby, and Robert S MacLeod. 2006. “The Influence of Stochastic Organ Conductivity in 2D ECG Forward Modeling: A Stochastic Finite Element Study.” In *2005 IEEE Engineering in Medicine and Biology 27th Annual Conference*, IEEE, 5528–31.

Glass, Leon, and Andrew Mcculloch. 1987. 117 Journal of Sound and Vibration *Theory of Heart: Biomechanics, Biophysics, and Nonlinear Dynamics of Cardiac Function*.

Grandin. 1986a. *Linear Operator Equations : Approximation and Regularization*. Macmillan New York.

Grandin, Hartley. 1986b. *Fundamentals of the Finite Element Method*. Macmillan New York.

Groetsch, Charles W, and C W Groetsch. 1993. 52 *Inverse Problems in the Mathematical Sciences*. Springer.

Gulrajani. 1998a. “The Forward and Inverse Problems of Electrocardiography.” *IEEE Engineering in Medicine and Biology Magazine* 17(5): 84–101.

Gulrajani, Ramesh M. 1998b. *Bioelectricity and Biomagnetism*. New York: John Wiley & Sons Inc.

Guofa Shou et al. 2008. “Solving the ECG Forward Problem by Means of Standard H- and h-Hierarchical Adaptive Linear Boundary Element Method: Comparison With Two Refinement Schemes.” *IEEE Transactions on Biomedical Engineering* 56(5): 1454–64.

Henriquez, Craig S. 2014. “A Brief History of Tissue Models for Cardiac Electrophysiology.” *IEEE Transactions on Biomedical Engineering* 61(5): 1457–65.

Hooks, Darren A., and Mark L. Trew. 2008. “Construction and Validation of a Plunge Electrode Array for Three-Dimensional Determination of Conductivity in the Heart.” *IEEE Transactions on Biomedical Engineering* 55(2): 626–35.

Hopenfeld, Bruce, Jeroen G. Stinstra, and Rob S. MacLeod. 2004. “Mechanism for ST Depression Associated with Contiguous Subendocardial Ischemia.” *Journal of Cardiovascular Electrophysiology* 15(10): 1200–1206.

Hou, Zong Yi, and Qi Nian Jin. 1997. “Tikhonov Regularization for Nonlinear Ill-Posed Problems.” *Nonlinear Analysis, Theory, Methods and Applications* 28(11): 1799–1809.

Iaizzo, Paul A. 2009. *Handbook of Cardiac Anatomy, Physiology, and Devices*. Springer Science & Business Media.

Iakovidis, Ilias, and Clyde F. Martin. 1991. “A Model Study of Instability of the Inverse Problem in Electrocardiography.” *Mathematical Biosciences* 107(1): 127–48.

Iakovidis, Ilias, and Clyde F. Martin. 1992. “The Inverse Problem in Electrocardiography on a Spherical Model.” *Applied Mathematics and Computation* 48(2–3): 187–217.

Jamison, Colin et al. 2011. “The Inverse Problem Utilizing the Boundary Element Method for a Nonstandard Female Torso.” *IEEE Transactions on Biomedical Engineering* 58(4): 876–83.

John G., Webster. 2010. “Medical Instrumentation Aplication and Design.” : 675.

Johnson, Christopher R, Robert S MacLeod, and Philip R Ershler. 1992. “A Computer Model for the Study of Electrical Current Flow in the Human Thorax.” *Computers in Biology and Medicine* 22(5): 305–23.

Johnson, Leonard R. 2003. *Essential Medical Physiology*. Elsevier.

Johnson, and R. S. MacLeod. 2012. “Adaptive Local Regularization and Adaptive Methods for the Inverse Problem.” *Biomedical and Life Physics* 69: 223–33.

Johnston. 2005. “The Effect of Simplifying Assumptions in the Bidomain Model of Cardiac Tissue: Application to ST Segment Shifts during Partial Ischaemia.” *Mathematical Biosciences* 198(1): 97–118.

Johnston, Barbara M. et al. 2018. “Quantifying the Effect of Uncertainty in Input Parameters in a Simplified Bidomain Model of Partial Thickness Ischaemia.” *Medical and Biological Engineering and Computing* 56(5): 761–80.

Johnston, Barbara M., and Peter R. Johnston. 2018. “Sensitivity Analysis of ST-Segment Epicardial Potentials Arising from Changes in Ischaemic Region Conductivities in Early and Late Stage Ischaemia.” *Computers in Biology and Medicine*102(June):288–99.

Johnston Peter R. 2018. “How Accurately Can the Method of Fundamental Solutions Solve the Inverse Problem of Electrocardiology?” *2017 Computing in Cardiology Conference (CinC)* 44: 1–4.

Johnston, Peter R., and Ramesh M. Gulrajani. 1997. “A New Method for Regularization Parameter Determination in the Inverse Problem of Electrocardiography.” *IEEE Transactions on Biomedical Engineering* 44(1): 19–39.

Johnston, Peter R., David Kilpatrick, and Chuan Yong Li. 2001. “The Importance of Anisotropy in Modeling ST Segment Shift in Subendocardial Ischaemia.” *IEEE Transactions on Biomedical Engineering* 48(12): 1366–76.

Johnston R. 2011. “A Nondimensional Formulation of the Passive Bidomain Equation.” *Journal of Electrocardiology* 44(2): 184–88.

Johnston R. 2011. “A Sensitivity Study of Conductivity Values in the Passive Bidomain Equation.” *Mathematical Biosciences* 232(2): 142–50.

Kahle, Werner et al. 2004. *Color Atlas and Textbook of Human Anatomy. Vol. 1, Locomotor System*. Thieme.

Katz, Arnold. 2011. *Physiology of the Heart*.

Klepfer, Ruth Nicholson, Christopher R. Johnson, and Robert S. Macleod. 1997. “The Effects of Inhomogeneities and Anisotropies on Electrocardiographic Fields: A 3-D Finite-Element Study.” *IEEE Transactions on Biomedical Engineering* 44(8): 706–19.

Li, Danshi, Chuan Yong Li, Ah Chot Yong, and David Kilpatrick. 1998. “Source of Electrocardiographic ST Changes in Subendocardial Ischemia.” *Circulation Research* 82(9): 957–70.

Lines, G. T. et al. 2003. “Mathematical Models and Numerical Methods for the Forward Problem in Cardiac Electrophysiology.” *Computing and Visualization in Science* 5(4): 215–39.

Lopez-Perez, Alejandro, Rafael Sebastian, and Jose M. Ferrero. 2015. “Three-Dimensional Cardiac Computational Modelling: METHODS, Features and Applications.” *BioMedical Engineering Online* 14(1): 1–31. ???

Macfarlane, Peter W et al. 2010. *Comprehensive Electrocardiology*. Springer Science & Business Media.

MacLachlan, Mary C. et al. 2007. “A Linear System of Partial Differential Equations Modeling the Resting Potential of a Heart with Regional Ischemia.” *Mathematical Biosciences* 210(1): 238–52.

MacLachlan, Mary C., Joakim Sundnes, and Glenn Terje Lines. 2005. “Simulation of ST Segment Changes during Subendocardial Ischemia Using a Realistic 3-D Cardiac Geometry.” *IEEE Transactions on Biomedical Engineering* 52(5): 799–807.

MacLachlan, Mary C, Bjørn Fredrik Nielsen, Marius Lysaker, and Aslak Tveito. 2006. “Computing the Size and Location of Myocardial Ischemia Using

Measurements of ST-Segment Shift." *IEEE Transactions on Biomedical Engineering* 53(6): 1024–31.

MacLeod, Robert S. et al. 2005. "Mechanisms of Ischemia-Induced ST-Segment Changes." *Journal of Electrocardiology* 38(4 SUPPL.): 8–13.

Marieb, EN, and KN Hoehn. 2013. Human Anatomy & Physiology *Human Anatomy and Physiology 9th Edition*.

Mueller, Jennifer L, and Samuli Siltanen. 2012. 10 *Linear and Nonlinear Inverse Problems with Practical Applications*. Siam.

Nielsen, Bjorn Fredrik, Marius Lysaker, and Per Grottum. 2013. "Computing Ischemic Regions in the Heart with the Bidomain Model - First Steps towards Validation." *IEEE Transactions on Medical Imaging* 32(6): 1085–96.

Nielsen, Bjørn Fredrik, Marius Lysaker, and Aslak Tveito. 2007. "On the Use of the Resting Potential and Level Set Methods for Identifying Ischemic Heart Disease: An Inverse Problem." *Journal of Computational Physics* 220(2): 772–90.

Oster, Howard S., and Yoram Rudy. 1992. "The Use of Temporal Information in the Regularization of the Inverse Problem of Electrocardiography." *IEEE Transactions on Biomedical Engineering* 39(1): 65–75.

Ottesen, Johnny T, Mette S Olufsen, and Jesper K Larsen. 2004. *Applied Mathematical Models in Human Physiology*. SIAM.

Plonsey, Robert, and Dennis B. Heppner. 1967. "Considerations of Quasi-Stationarity in Electrophysiological Systems." *The Bulletin of Mathematical Biophysics* 29(4): 657–64.

Potse, Mark et al. 2007. "The Effect of Lesion Size and Tissue Remodeling on ST Deviation in Partial-Thickness Ischemia." *Heart Rhythm* 4(2): 200–206.

Pullan, Andrew. 1996. "A High-Order Coupled Finite Element/Boundary Element Torso Model." *IEEE Transactions on Biomedical Engineering* 43(3): 292–98.

Ramon, Ceon et al. 2002. “The Effect of Volume Currents Due to Myocardial Anisotropy on Body Surface Potentials.” *Physics in Medicine and Biology* 47(7): 1167–84.

Reddy, Junuthula Narasimha. 2014. *An Introduction to Nonlinear Finite Element Analysis: With Applications to Heat Transfer, Fluid Mechanics, and Solid Mechanics*. OUP Oxford.

Rodriguez, Blanca, Natalia Trayanova, and Denis Noble. 2006. “Modeling Cardiac Ischemia.” *Annals of the New York academy of sciences* 1080(1): 395–414.

Rudy, and Howard Oster. 1997. “Regional Regularization of the Electrocardiographic Inverse Problem: A Model Study Using Spherical Geometry.” *IEEE Transactions on Biomedical Engineering* 44(2): 188–99.

Rudy, Y., and R. Plonsey. 1980. “A Comparison of Volume Conductor and Source Geometry Effects on Body Surface and Epicardial Potentials.” *Circulation Research* 46(2): 283–91.

Rudy, Y., R. Plonsey, and J. Liebman. 1979. “The Effects of Variations in Conductivity and Geometrical Parameters on the Electrocardiogram, Using an Eccentric Spheres Model.” *Circulation Research* 44(1): 104–11.

Ruud, Tomas Syrstad, Bjørn Fredrik Nielsen, Marius Lysaker, and Joakim Sundnes. 2009. “A Computationally Efficient Method for Determining the Size and Location of Myocardial Ischemia.” *IEEE Transactions on Biomedical Engineering* 56(2): 263–72.

S. Pezzuto, J.Hake, J. Sundnes. 2010. “Remarks on Some Properties of Conic Yield Restrictions in Limit Analysis.” *International Journal for Numerical Methods in Biomedical Engineering* 26(1): 807–27.

Savadjiev, Peter, Steven W. Zucker, and Kaleem Siddiqi. 2007. “On the Differential Geometry of 3D Flow Patterns: Generalized Helicoids and Diffusion MRI Analysis.” *Proceedings of the IEEE International Conference on Computer Vision*.

Sebastian, Rafael et al. 2008. “Assessing Influence of Conductivity in Heart Modelling with the Aim of Studying Cardiovascular Diseases.” *Medical Imaging 2008: Physiology, Function, and Structure from Medical Images* 6916(JANUARY): 691627.

Shahidi, A. Vahid, Pierre Savard, and Réginald Nadeau. 1994. “Forward and Inverse Problems of Electrocardiography: Modeling and Recovery of Epicardial Potentials in Humans.” *IEEE Transactions on Biomedical Engineering* 41(3): 249–56.

Shaw, R. 2002. “Electrophysiologic Effects of Acute Myocardial Ischemia: A Theoretical Study of Altered Cell Excitability and Action Potential Duration.” *Cardiovascular Research* 35(2): 256–72.

Sherwood, Lauralee. 2012. *Fundamentals of Human Physiology*.

Shou, Guofa et al. 2008. “Truncated Total Least Squares: A New Regularization Method for the Solution of ECG Inverse Problems.” *IEEE Transactions on Biomedical Engineering* 55(4): 1327–35.

Skipa, Oleg. 2004. “Linear Inverse Problem of Electrocardiography :” *Dissertation* (April).

Smith, William M., and Roger C. Barr. 2001. “The Forward and Inverse Problems: What Are They, Why Are They Important, and Where Do We Stand?” *Journal of Cardiovascular Electrophysiology* 12(2): 253–55.

Sovilj, Siniša, Amr Al Abed, Nigel H Lovell, and Socrates Dokos. 2014. “Simplified 2D Bidomain Model of Whole Heart Electrical Activity and ECG Generation.” 14(3): 136–43.

Stenroos, Matti, and Jens Haueisen. 2008. “Boundary Element Computations in the Forward and Inverse Problems of Electrocardiography: Comparison of Collocation and Galerkin Weightings.” *IEEE Transactions on Biomedical Engineering* 55(9): 2124–33.

Stern, Shlomo. 2002. “State of the Art in Stress Testing and Ischaemia Monitoring.” *Cardiac Electrophysiology Review* 6(3): 204–8.

Stinstra, J. G., S. Shome, B. Hopenfeld, and R. S. MacLeod. 2005. “Modelling Passive Cardiac Conductivity during Ischaemia.” *Medical and Biological Engineering and Computing* 43(6): 776–82.

Stinstra, Jeroen G, Bruce Hopenfeld, and Rob S Macleod. 2004. “Using Models of the Passive Cardiac Conductivity and Full Heart Anisotropic Bidomain to Study the Epicardial Potentials in Ischemia.” In *The 26th Annual International Conference of the IEEE Engineering in Medicine and Biology Society*, IEEE, 3555–58.

Sundnes, Joakim et al. 2006. “On the Computational Complexity of the Bidomain and the Monodomain Models of Electrophysiology.” *Annals of Biomedical Engineering* 34(7): 1088–97.

Throne, Robert D., Lorraine G. Olson, and Terry J. Hrabik. 1999. “ A Comparison of Higher-Order Generalized Eigensystem Techniques and Tikhonov Regularization for the Inverse Problem of Electrocardiography * .” *Inverse Problems in Engineering* 7(2): 143–93.

Tuboly, G., G. Kozmann, and I. Maros. 2015. “Computational Aspects of Electrocardiological Inverse Solutions.” *IFAC-PapersOnLine* 28(20): 48–51.

Tung, Leslie A. 1978. “Bidomain Model for Describing Ischemic Myocardial D-C Potential.” : 277.

Tveito, Aslak et al. 2017. “A Cell-Based Framework for Numerical Modeling of Electrical Conduction in Cardiac Tissue.” *Frontiers in Physics* 5(October): 1–18.

Veneroni, Marco. 2006. “Reaction-Diffusion Systems for the Microscopic Cellular Model of the Cardiac Electric Field.” *Mathematical Methods in the Applied Sciences* 29(14): 1631–61.

Volume, I, L Sirovich, and J E Marsden. 8 *Interdisciplinary Applied Mathematics*.

W., L. B., and R. E. White. 2006. “An Introduction to the Finite Element Method with Application to Nonlinear Problems.” *Mathematics of Computation* 50(181): 343.

Wach, P., B. Tilg, G. Lafer, and W. Rucker. 1997. “Magnetic Source Imaging in the Human Heart: Estimating Cardiac Electrical Sources from Simulated and Measured Magnetocardiogram Data.” *Medical & Biological Engineering & Computing* 35(3): 157–66.

Wang. 2012. “Finite Element Solutions to Inverse Electrocardiography.” (December).

Wang, Dafang, Robert M Kirby, and Chris R Johnson. 2009. “Finite Element Refinements for Inverse Electrocardiography : Hybrid-Shaped Elements and High-Order Element Truncation.” *Computers in Cardiology* 0: 193–96. http://ieeexplore.ieee.org/xpls/abs_all.jsp?arnumber=5445436&tag=1.

Wang, Yong, and Yoram Rudy. 2006. “Application of the Method of Fundamental Solutions to Potential-Based Inverse Electrocardiography.” *Annals of Biomedical Engineering* 34(8): 1272–88.

Wei, Chia-Ling et al. 2003. “3D Finite Element Complex Domain Numerical Models of Electric Fields in Blood and Myocardium.” In *Proceedings of the 25th Annual International Conference of the IEEE Engineering in Medicine and Biology Society (IEEE Cat. No. 03CH37439)*, IEEE, 62–65.

Wu, Zemin, Shaofeng Bian, Caibing Xiang, and Yude Tong. 2013. “A New Method for TSVD Regularization Truncated Parameter Selection.” *Mathematical Problems in Engineering* 2013: 1–9.

Yamashita, Yasuo. 1981. “Inverse Solution in Electrocardiography: Determining Epicardial from Body Surface Maps by Using the Finite Element Method: The Basic Problems on the Body Surface Potential Mapping.” *Japanese circulation journal* 45(11): 1312–22.

Young, R. J., and A. V. Panfilov. 2010. “Anisotropy of Wave Propagation in the Heart Can Be Modeled by a Riemannian Electrophysiological Metric.” *Proceedings of the National Academy of Sciences* 107(34): 15063–68.

Zemzemi, Nejib et al. 2015. “Effect of the Torso Conductivity Heterogeneities on the ECGI Inverse Problem Solution.” *Computing in Cardiology*: 233–36.

CURRICULUM VITAE

Hamed KAGHAZCHI was born in Maragheh, IRAN in 1984. He received his B.Sc. degree in Electrical and Electronics Engineering Department from AZAD University of Birjand, Iran in 2007. Then he came Turkey, Adana to keep his education in 2010 and received his M.Sc. degree in Electrical and Electronics Engineering Department from Çukurova university in 2013. His research interests include mathematical modeling of physiological systems, forward and inverse problems in Electrocardiography, biomedical signal processing and computer programming.